STABILITY ANALYSIS OF THE INTERFACES AT COMPRESSIBLE AND INCOMPRESSIBLE FLUIDS

A Thesis Submitted to the
Babasaheb Bhimrao Ambedkar University, Lucknow
in Fulfillment of Requirement for the Award of degree of

Doctor of Philosophy

in

Mathematics

BABASAHEB BHIMRAO AMBEDKAR UNIVERSITY
LUCKNOW
प्रज्ञा शील करूणा
ESTABLISHED 1996

BY

Dharamendra

Enrolment No. 1330/19

SUPERVISOR

Dr. Mukesh Kumar Awasthi

Assistant Professor

DEPARTMENT OF MATHEMATICS
SCHOOL OF PHYSICAL & DECISION SCIENCES
BABASAHEB BHIMRAO AMBEDKAR UNIVERSITY
(A CENTRAL UNIVERSITY)
VIDYA VIHAR, RAEBARELI ROAD,
LUCKNOW-226025
(U.P.) INDIA

2022

DECLARATION

I, **Dharamendra** declare that the thesis entitled **STABILITY ANALYSIS OF THE INTERFACES AT COMPRESSIBLE AND INCOMPRESSIBLE FLUIDS** has been prepared by me under the supervision of Dr. Mukesh Kumar Awasthi, Assistant Professor, Department of Mathematics, Babasaheb Bhimrao Ambedkar Univesity, Lucknow. No part of this thesis has formed the basis for the award of any degree, diploma or fellowship previously.

Further, I declare that the material embodied in the present work is based on original research work and the indebtedness to others has been duly acknowledged at relevant places.

I also declare that the thesis is essentially free from all kinds of plagiarism.

Dharamendra

Department of Mathematics, School of Physical & Decision Sciences,

Babasaheb Bhimrao Ambedkar University

Lucknow, Uttar Pradesh-226025

DATE:- 16.08.2022

CERTIFICATE

This is to certify that the thesis titled **"STABILITY ANALYSIS OF THE INTERFACES AT COMPRESSIBLE AND INCOMPRESSIBLE FLUIDS"** submitted by Mr. **Dharamendra** is an original research work and has not been previously submitted in part or full for the award of any other degree or diploma to this or any other University

The thesis submitted to Babasaheb Bhimrao Ambedkar University, Lucknow satisfies all the requirements as stipulated in the **Doctor of Philosophy (Ph.D.) regulations as amended in 2019** and it is fit for submission and evaluation for the award of the degree of Doctor of Philosophy of the University.

16/08/2022

Supervisor

S. K. Singh
16.08.2022

Head of the Department

Date: 16/08/2022

ACKNOWLEDGEMENTS

First and foremost, I would like to express my gratitude to all who gave me the possibility to complete this thesis. I am deeply indebted to my supervisor **Dr. Mukesh Kumar Awasthi**, Assistant Professor, Department of Mathematics, Babasaheb Bhimrao Ambedkar University, Lucknow, whose help, stimulating suggestions, and encouragement helped me in all the time of research and writing of this thesis. His ideals and concepts have had a remarkable influence on my entire career in the field of stability theory.

I take this opportunity to express my profound respect to **Dr. Sunil Kumar Singh**, Head, Department of Mathematics, Babasaheb Bhimrao Ambedkar University, for providing the basic infrastructural facilities for research work. I further place on record my thanks to **Prof. Surendra Kumar**, Department of Statistics, Babasaheb Bhimrao Ambedkar University, for his invaluable suggestions and support.

I am thankful to **Prof. B. S. Bhadauria**, **Dr. Jagmohan Tanti**, **Dr. Brajesh Kumar Sigh, Dr. Maitri Verma**, and **Dr. Gopal Datt** for their valuable suggestions and guidance on this journey of research work.

I want to acknowledge **Shri Bhoopendra Singh Sachan**, Assistant Professor, Department of Physics, Captain Sukhwasi Singh Smarak Janta Mahavidyalaya, Ghatampur Kanpur Nagar (Uttar Pradesh),who gave a historical turn during my graduation, and **Shri Neeraj Mohan Gupta**, Assistant Professor, Department of Chemistry, Govt PG College Guna (Madhya Pradesh) who helped me a lot in my difficult situations. During this work, I also got support from **Dr. Amit Kumar Misra**, Department of Statistics, Babasaheb Bhimrao Ambedkar University.

I gratefully acknowledge the financial assistance provided by the Council of Science and Industrial Research, New Delhi (India), in the form of a Junior Research Fellowship and Senior Research Fellowship during the research period.

I feel deeply gratitude for my father, **Shri Ram Ratan**, and mother, **Smt. Sada Pyari** formed part of my vision and taught me the good things that matter in life. I have no words to define my sincere thanks to my family members and relatives for their blessings, patience, and moral support.

I warmly thank **Mr. Atul Kumar Shukla**, not only for his valuable advice and friendly help but also for his great efforts during this work. His extensive discussions about my work and interesting explorations in operations have been very helpful for this study. I also wish to thank **Mr. Shivam Agarwal**, for his kind support and guidance during this study.

I also want to acknowledge my friends, **Mr. Arpit Dwivedi**, and **Mr. Anurag Awasthi**, who helped me with my previous study.

The inspiration, support, cooperation, and patience that I have received from my colleagues Dr. Neetu Singh, Mr. Anurag Srivastava, Mr. Awanish Kumar, Ms. Saloni Agrawal, Mr. Mukesh Gupta, Mr. Anil Kumar, Mr. ShobhNath Rai, Mr. Alok Kumar, Mr. Anish Kumar, Mr. Divakar Vikram Singh, Mr. Brijesh Kumar Singh, Mr. Kuldeep Kumar Mr. Ismail, Ms. Shiplee Ms. Cherie Gautam, Mr. Mithlesh Roy, and Ms. Soumya Singh are beyond the scope of any acknowledgment, yet I would express my heartfelt gratitude to them.

Last but not least, I would like to thank the divine force of blessing of Almighty God, who never left me trapped in difficulties.

Lucknow

Date - 16.08.2022

DHARAMENDRA

ABSTRACT

The theory of purely irrotational flows of a viscous fluid is an approximate theory which works well especially in gas-liquid flows of liquids of high viscosity, at low Reynolds numbers. The theory of purely irrotational flows of a viscous fluid can be seen as a very successful competitor to the theory of purely irrotational flows of an inviscid fluid. A free surface in viscous potential flow analysis takes into account viscous stresses through normal stress balance at the surface, but tangential stresses are not considered. The present research work is the study on **"STABILITY ANALYSIS OF THE INTERFACES AT COMPRESSIBLE AND INCOMPRESSIBLE FLUIDS"** through viscous potential flow theory, normal mode technique and computer based MATLAB programming. The stability of the interface of viscous-viscoelastic incompressible, viscous-nanofluid, and viscous-compressible fluids has been investigated theoretically in the cylindrical geometry. The Newton-Raphson approach is used to solve the dispersion relation for the critical wave number and the various graphs are plotted to depict the behavior of flow variables on the perturbations growth rate and wave number.

Chapter 1 presents a brief introduction to the general stability theory, capillary instability, Kelvin-Helmholtz instability along with some definitions and basic equations related to stability analysis. Various related studies are described by various authors in this field and a summary of the thesis is provided.

The stability of the interface between a viscous and a viscoelastic fluid is theoretically investigated in **Chapter 2** when mass and heat transfer between phases is permitted. The viscoelastic liquid and the viscous fluid are contained by two rigid cylinders in an annular area. The research was carried out utilizing the Rivlin-Ericksen model-satisfying potential flow theory for viscoelastic liquid. The findings

indicate that the impact of heat and mass transfer is observed to increase the stability of the interface.

Chapter 3 examines the stability of interface between the viscous incompressible fluid and Walter's B viscoelastic liquid. These liquids are contained in an annular space that is bounded by two rigidly defined cylinders. The interface obeys capillary instability because the surface tension effect is taken into account. It is found that, compared to the Newtonian fluid perturbations grow more slowly at the interface containing Walter's B viscoelastic fluid.

In **Chapter 4**, a region bounded by two rigid cylindrical surfaces is considered to investigate the stability properties of the viscous fluid-viscoelastic fluid interaction. The Walter's B viscoelastic fluid is taken for analysis and the fluid's phases are transferring mass-heat from one phase to another. The surface is unstable the surface forces produced by the surface tension are responsible for the breakup. It is found that as heat is transferred more efficiently, the interface's instability reduces.

The instability at the viscous fluid-viscoelastic fluid interface is studied in **Chapter 5**. The power-law viscoelastic is considered and the interface is transporting heat along with mass from one fluid phase to another. The irrotational flow theory of viscous-viscoelastic fluid is employed to work out the mathematical equations. The algebraic equation of the growth rate parameter is computed and analyzed numerically. The transport of heat is found to stabilize the interface by enlarging the stability range. The power-law index and consistency coefficient have stabilizing character while the density of power-law has an inverse effect.

The instability in a circular cavity occurring at the interface of viscous fluid and nanofluid is investigated in **Chapter 6**. The viscous fluid is considered inside the cavity while nanofluid lies outside the cavity and both the fluids form a circular

interface. The dispersion relationship is quadratic in growth rate and it reduces to the case of plane interface for larger modes of perturbations. The viscosity of the nanofluid has a stabilizing effect. In comparison to smaller-sized nanoparticles, the nanofluid with greater radius nanoparticles forms a more unstable interface.

In **Chapter 7**, the Rayleigh instability has been examined at the interface of two compressible viscous fluids interface. In the cylindrical coordinate system, a viscous compressible fluid surrounds another viscous compressible fluid. The dispersion relationship is quadratic in terms of the growth rate achieved and plotted with the help of MATLAB software for various flow parameters. The interfacial stability increases with an increase in the non-dimensional viscosity ratio parameter of the compressible fluids and while the density ratio of compressible fluids interface has destabilizing character. It is found that inside fluid viscosity slows the growth of disturbance but an increase in outside fluid viscosity makes the interface unstable.

The **last Chapter** of the thesis is related to the conclusions and future scope of the work. In the present work, the stability results are achieved utilizing the linear theory of stability analysis. The nonlinear analysis of interfacial stability problems is very important because the governing equations describing these flows are nonlinear in nature. The same problems can be studied through the nonlinear analysis of stability theory.

PREFACE

Instability of fluid flow is responsible for the turbulence of fluid flow. There are a large number of applications of fluid's instability in engineering and the natural environment. The instability phenomenon is also found in the area of astrophysics, applied mathematics, geophysics, biology, physics, oceanography, etc. Some examples of instabilities are interfacial instability, baroclinic instability, rotational instability, thermal instability etc.

This thesis examines the interfaces of two viscous/viscoelastic fluids when the interface is experiencing capillary instability. The viscous potential flow theory is utilized to solve the constitutive equations. Chapter 1 consists of an introduction to the general stability problems, some definitions, and basic equations related to the stability analysis. The viscous-Rivlin-Ericksen fluids interface is examined in chapter 2. Chapter 3 discusses the viscous-Walter's B viscoelastic fluid interface while the effect of heat and mass transfer is investigated on the viscous-Walter's B viscoelastic fluid interface in chapter 4. The stability of viscous-power law fluid interface is analysed in chapter 5. The instability of nanofluid film in a circular cavity is examined in chapter 6 and viscous compressible fluids are discussed in chapter 7. Finally, in chapter 8, conclusions are drawn and future research work in this direction is suggested.

We wish the readers of a successful study of the material presented, leading to new inspiration, a deepening understanding of the described concepts, and also fruitful applications to the flow instability issues in nature and engineering.

DHARAMENDRA

LIST OF SYMBOLS

$\rho_o \rightarrow$ The density of the outer fluid

$\rho_i \rightarrow$ The density of the inner fluid

$\rho \rightarrow$ The density ratio of two fluids

$\mu_o \rightarrow$ The viscosity of the outer fluid

$\mu_i \rightarrow$ The viscosity of the inner fluid

$\mu \rightarrow$ The viscosity ratio of two fluids

$\mu_o' \rightarrow$ Viscoelasticity of the viscoelastic fluid

$\sigma \rightarrow$ Surface Tension

$g \rightarrow$ Gravitational acceleration

$T_o \rightarrow$ Temperature of outer fluid layer

$T_i \rightarrow$ Temperature of inner fluid layer

$p_o \rightarrow$ Pressure in outer fluid layer

$p_i \rightarrow$ Pressure in inner fluid layer

$\xi \rightarrow$ Surface elevation

$L \rightarrow$ Latent Heat

$n \rightarrow$ Constant integer

$k \rightarrow$ Wave number

$\omega \rightarrow$ Growth rate of disturbance

$\omega_r \rightarrow$ Real part growth rate of disturbance

$\omega_i \rightarrow$ Imaginary part growth rate of disturbance

$\alpha \rightarrow$ Heat Transfer Coefficient

$\hat{\alpha} \rightarrow$ Dimensionless Heat Transfer Coefficient

$Ca \rightarrow$ Capillary Number

$We \rightarrow$ Weber Number

$\mathrm{Re} \rightarrow$ Reynolds Number

$\Phi_o \rightarrow$ Potential function for outer fluid

$\Phi_i \rightarrow$ Potential function for inner fluid

$\tau \rightarrow$ Stress Tensor

$\vec{q}_o \rightarrow$ Velocity of outer fluid

$\vec{q}_i \rightarrow$ Velocity of inner fluid

$\lambda \rightarrow$ Non-dimensional viscoelasticity coefficient

$r_i \rightarrow$ Radius of outer fluid layer

$r_o \rightarrow$ Radius of outer fluid layer

$\vec{F} \rightarrow$ External Force

$\phi \rightarrow$ Nanoparticles Volume fraction

$d \rightarrow$ Fractal Index

$\phi_m \rightarrow$ Maximum Volume fraction

$\phi_{ag} \rightarrow$ Aggregate Volume fraction

$H(\zeta) \rightarrow$ Net Heat Flux

$u_{r,i} \rightarrow$ Radial component of the velocity of the inner fluid

$u_{r,o} \rightarrow$ Radial component of the velocity of the outer fluid

$\kappa \rightarrow$ Ratio of kinematic viscosities

LIST OF TABLES

LIST OF FIGURES

TABLE OF CONTENTS

LIST OF PUBLICATIONS

A. PUBLISHED PAPERS

1. Mukesh Kumar Awasthi, **Dharamendra** and Dhananjay Yadav, **"**Instability of Rivlin-Ericksen fluid film with heat and mass transfer**",** Published in International Comm. Heat and Mass Transfer**. 135 (2022) 106085 (I F- 6.782).**
2. Mukesh Kumar Awasthi, **Dharamendra** and Dhananjay Yadav,"Temporal instability of nanofluid layer in a circular cylindrical cavity", Published in The European Physical Journal Special Topics. (**In Press**) **(I F- 2.891).**
3. Mukesh Kumar Awasthi, **Dharamendra** and Dhananjay Yadav**, "**Instability Characteristics of Walter's B viscoelastic fluid in a cylindrical configuration with heat transfer", Published in Proceedings of the Institution of Mechanical Engineers, Part C: J. Mechanical Engineering Science**. (In Press**) **(I F- 1.758).**
4. **Dharamendra** and Mukesh Kumar Awasthi, **"**Temporal Instability of Walter's B viscoelastic fluid film", published in J. Physics: Conference Series.
5. **Dharamendra** and Mukesh Kumar Awasthi, **"**Magneto-hydrodynamic evaporative Capillary Instability with Swirling", Published in AIP Conference Proceedings.

B. COMMUNICATEDPAPERS

6. Mukesh Kumar Awasthi and **Dharamendra,** "Stability characteristics of the cylindrical power-law viscoelastic fluid interface with heat transfer".
7. **Dharamendra** and Mukesh Kumar Awasthi, "Capillary instability of two compressible viscous fluids".

C. CONFERENCES

8. The paper entitled "Magneto-hydrodynamic Evaporative Capillary Instability with Swirling" is presented virtually at the conference Advance Material and

Radiation Physics (AMRP-2020) held in Punjab-India, during November 9-11, 2020.This paper is published in AIP Proceedings.

9. The paper entitled "Temporal Instability of Walters B viscoelastic Fluid Film" is presented virtually in the conference ''Recent Advancement in physical Sciences'' held at NIT Uttarakhand (India), during December 19-20, 2020. This paper is published in the Journal of Physics: Conference Series.

10. Attended an international conference on "Recent Trends in Mathematics and its applications to Graphs, Networks and Petri Nets", on July, 20-24, 2020, Jointly Organized by the School of Computational and Integrative Sciences Jawaharlal Nehru University, New Delhi India &Vijnana Parishad of India.

11. Attended an international conference on "Advances in Mechanics" on December 18-20, 2020, Organized by the Department of Mathematics & Statistics, Manipal University, Jaipur. India.

D. WORKSHOP ATTENDED

12. Attended Workshop "International workshop on Numerical Methods in Scientific Computing" organized by South Asian University, New Delhi, India, 21-22 February 2020.

13. Attended an international workshop on "Srinivasa Ramanujan: The Man Beyond Infinity", on December 22, 2020, Srinivasa Ramanujan Department of Mathematics, Centre for Vedic Mathematical Studies, Central University of Himachal Pradesh, India.

14. Attended One week National Workshop cum Training Programme on "Scientific Computing with MATLAB" Organized by the Department of mathematics, DIT University, Dehradun, Uttarakhand, during July 11-15, 2022.

E. ONLINECOURSES ATTENDED

15. Attended a course named "An Introductory Course on Fluid Dynamics" organized by the Department of Mathematics, Christ (Deemed to be University), Bangalore-India, during 24-28 August 2020.

16. Attended online lecture series "Recent Advances in Fluid Flow and Heat Transfer" Organized by Department of Mathematics, Indian Institute of Technology Roorkee, India, during 19-25 October 2020.

17. Attended an online Global Initiative For Academic Networks (GIAN) course "Linear and Non-linear Hydrodynamic Stability: Theory and Computation" organized by the Department of Mathematics, National Institute of Technology, Warangal, during 11-24 April 2022.

18. Attended an online Webinar, "An Introductory Course on Fluid Dynamics" organized by the Department of Mathematics, CHRIST (Deemed) to be University, Bangalore during 17-20 August and 24-28 August 2020.

19. Attended two days National Webinar on "Fluid Dynamics and Its Applications", on 28-29, May 2020, Organized by the Department of Mathematics, Govt. College, Vijayanagara, Bengaluru, Karnataka, India.

F. POSTER PRESENTATION

20. Presented a poster and secured the second rank on the Occasion of National Mathematics Day on December 2021, in Poster Presentation Contest, Organized by the Department of Mathematics B B A University Lucknow.

CHAPTER 1

INTRODUCTION

Classical hydrodynamics is based on idealized concept of a perfect or an ideal fluid, fluids of vanishing viscosities. The motion of such fluids is governed by Euler's equations. However, Euler's equations could not explain phenomena like pressure loss in flow through pipes, the drag experienced by a body placed in a uniform stream and flow separation. These discrepancies are due to the result of viscous forces whose effects are significant particularly in the neighbourhood of a solid boundary. During the Nineteenth century Navier, Poisson and Stokes formulated the equation of a viscous fluid's motion, later known as Navier-Stokes equations. The above equations are based on the no-slip condition that the fluid near the solid boundary cannot slip away from it. In other words the velocity of the fluid near the wall is equal to that of the wall (if the wall is moving, otherwise zero). Due to the non-linearity of Navier-Stokes equations the study of viscous flows became complicated except for a few cases for which exact analytical solutions could be obtained.

1.1 Fluid Density

Fluid density is defined as the mass per unit volume that depends on pressure and temperature, as the equation of state shows

$\rho = \rho(p,T)$ or $F(\rho,P,T) = 0$

1.2 Viscosity

Fluid may be defined as a material that continues to deform in the presence of any sheering stress. We refer to the continuous deformation of a fluid as 'flow' and the quantity by which the fluid resists any deformation is called viscosity.

So viscosity is a measure of the reluctance of the fluid to yield to sheer when the fluid is in motion.

The viscosity of fluids usually increases with the pressure at a constant temperature, although water is the exception to this belief i.e., its viscosity decreases with pressure at a constant temperature. It means the pressure effect on viscosity can be ignored.

1.3 NEWTONIAN AND NON-NEWTONIAN FLUIDS

Shear stress and shear strain rate are linearly related in Newtonian fluids. If τ is the shear stress and du/dy is the rate of shear strain, then for the Newtonian fluids, $\tau = \mu du/dy$ where the constant μ is known as the coefficient of viscosity. Most common fluids such as water, air, and gasoline are Newtonian under normal conditions.

In fluid mechanics the ratio of absolute viscosity, μ, to density, ρ, often arises. This ratio is given the name kinematics viscosity and is represented by the symbols ν.

Non-Newtonian fluids are those whose flow curves are not linear, indicating that their "viscosity" does not remain constant at a given temperature and pressure. A nonlinear flow curve for the real fluid can be divided into three major groups.

1. The fluids where the shear rate is a function of the shearing stress at the given point and independent of time.
2. The fluid's time depends on the relationship between shear stress and shear rate.

3. The term "viscoelastic fluids" refers to a system that demonstrates partial elastic recovery after deformation and possesses properties of both solids and fluids.

   An example of a common viscoelastic fluid is egg-white. The linear viscoelastic fluid is Oldroyd B- Type.

1.4 BASIC EQUATIONS OF HYDRODYNAMICS

In this section, we have provided a summary of the corresponding equations utilized in the current thesis.

1.4.1 Equation of Continuity

According to the law of conservation of mass, for a defined region, the amount of fluid is conserved or remains the same, provided it does not contain any source (inlets) or sink (outlets). In other words, fluid mass remains the same for a defined region. The equation of continuity gives us the law of conservation of mass. Let $\vec{q}$ be the velocity of the fluid and ρ be the density of the fluid, then the mathematical form of the general equation of continuity is given as

$$\frac{\partial \rho}{\partial t} + \nabla \rho \bullet \vec{q} + \rho \nabla \bullet \vec{q} = 0 \tag{1.1}$$

This equation can also be written as

$$\frac{d\rho}{dt} + \rho \nabla \bullet \vec{q} = 0 \tag{1.2}$$

Case 1-In the case of steady flow, in which the pattern does not vary with time at any point, then the equation of continuity becomes

$$\nabla \bullet \left(\rho \vec{q} \right) = 0 \tag{1.3}$$

Case 2-For the incompressible fluid density of particle remains the same with time so $\frac{d\rho}{dt} = 0.$ As in the case of non-homogeneous, incompressible fluids there could be a variation of density from particle to particle. But for the case of homogeneous, incompressible fluids density remains the same in the entire fluid, then the equation of continuity reduces to

$$\nabla \bullet \vec{q} = 0 \tag{1.4}$$

Case 3-When the flow of fluid is potential kind, i.e., $\vec{q}$ can be written as in terms of velocity potentials as $\vec{q} = \nabla\Phi$, then the equation of continuity becomes Laplace's equation of form

$$\nabla^2\Phi = 0 \tag{1.5}$$

1.4.2 Continuity equation for cylindrical coordinates having coordinates (r, θ, z)

$$\frac{\partial\rho}{\partial t} + \frac{1}{r}\frac{\partial(\rho v_r r)}{\partial r} + \frac{1}{r}\frac{\partial(\rho v_\theta)}{\partial \theta} + \frac{\partial(\rho v_z)}{\partial z} = 0 \tag{1.6}$$

Here ρ is the density of the fluid and v_r, v_θ and v_z are components of the velocity vector in cylindrical coordinates

Case 1- When fluid is incompressible, the equation of continuity becomes

$$\frac{\partial(v_r r)}{\partial r} + \frac{\partial(v_\theta)}{\partial \theta} + r\frac{\partial(v_z)}{\partial z} = 0 \tag{1.7}$$

Case 2- When fluid is incompressible and potential kind, then the equation of continuity reduces to

$$\frac{\partial}{\partial r}\left(r\frac{\partial\Phi}{\partial r}\right) + \frac{\partial}{\partial \theta}\left(\frac{1}{r}\frac{\partial\Phi}{\partial \theta}\right) + \frac{\partial}{\partial z}\left(\frac{\partial\Phi}{\partial z}\right) = 0 \tag{1.8}$$

Case 3- When there is axial symmetry for cylindrical coordinates in fluid, that means that all quantities are independent of θ, and the equation of continuity becomes

$$\frac{\partial \rho}{\partial t}+\frac{1}{r}\frac{\partial(\rho v_r r)}{\partial r}+\frac{\partial(\rho v_z)}{\partial z}=0 \tag{1.9}$$

1.4.3 Equation of motion or conservation of momentum

The equation which represents the conservation of momentum is given by

$$\rho\left(\frac{\partial \vec{\boldsymbol{q}}}{\partial t}+\vec{\boldsymbol{q}}\cdot\nabla\vec{\boldsymbol{q}}\right)=\vec{F}+\nabla\bullet\boldsymbol{\tau} \tag{1.10}$$

Here $\vec{F}$ represents external force while $\boldsymbol{\tau}$ is stress tensor.

Case 1- If fluids are Newtonian, the expression for $\boldsymbol{\tau}$ is given as

$$\boldsymbol{\tau}=-p\boldsymbol{I}+\mu\boldsymbol{D_1} \tag{1.11}$$

Case 2- In case of Walter's B fluid, normal stress moduli α_1,α_2 and the stress tensor $\boldsymbol{\tau}$ is connected as

$$\boldsymbol{\tau}=-p\boldsymbol{I}+\mu\boldsymbol{D_1}-\alpha_1\boldsymbol{D_2}+\alpha_2\boldsymbol{D_1^2} \tag{1.12}$$

Case 3- The expression stress tensor $\boldsymbol{\tau}$ for Rivlin-Ericksen fluid is given by

$$\boldsymbol{\tau}=-p\boldsymbol{I}+\mu\boldsymbol{D_1}+\alpha_1\boldsymbol{D_2}+\alpha_2\boldsymbol{D_1^2} \tag{1.13}$$

Case 4-The stress tensor $\boldsymbol{\tau}$ for power-law fluid is written as

$$\boldsymbol{\tau}=-p\boldsymbol{I}+\mu(\boldsymbol{D_1})\boldsymbol{D_1} \tag{1.14}$$

where $$\mu(\boldsymbol{D_1})=K\left(\frac{1}{2}\boldsymbol{D_1}\bullet\boldsymbol{D_1}\right)^{\frac{n-1}{2}} \tag{1.15}$$

Here, $\boldsymbol{D_1}$ and $\boldsymbol{D_2}$ are order 1 and 2 tensor, respectively, given by

$$\boldsymbol{D_1}=\nabla\vec{\boldsymbol{q}}+(\nabla\vec{\boldsymbol{q}})^T\,;\,\boldsymbol{D_2}=\frac{D\boldsymbol{D_1}}{Dt}+(\nabla\vec{\boldsymbol{q}})\boldsymbol{D_1}+\boldsymbol{D_1}(\nabla\vec{\boldsymbol{q}})^T \tag{1.16}$$

D/Dt denotes material derivative. The power-law index is denoted by n and K is the consistency coefficient.

1.4.4. Equation of Heat Conduction

The energy equation in each domain is given by

$$\frac{\partial T}{\partial t} + (\vec{q} \bullet \nabla)T = k\nabla^2 T \tag{1.17}$$

One can write the equation of state as

$$\rho = \rho_0[1-\alpha(T-T_0)] \tag{1.18}$$

where α is the volume expansion coefficient. At $T = T_0$, from the equation (1.18) $\rho = \rho_0$.

1.5 NORMAL MODE ANALYSIS

The above section states that stability means stability relating to all possible perturbations. Accordingly, the system's response to all possible disturbances must be checked for the stability check to be complete.

If it represents typical amplitude describing the disturbance, it can be expressed as

$$C(k,t) = \int C_m(k,t)dr \tag{1.19}$$

where m represent the various mode. The equation governing the general perturbation can be specialized for the normal modes. Dependence on time is separated out by considering the solution in the following form

$$C_m(k,t) = C_m(k)e^{p_m t} \tag{1.20}$$

In general p_m is a complex constant, so, p_m can be written as

$$p_m = p_m^{(r)} + ip_m^{(i)} \tag{1.21}$$

where $p_m^{(r)}$ and $p_m^{(i)}$ will depend, apart from m. On the parameters $X_1, X_2, ...X_n$ of the basic flow, the condition for stability is that $p_m^{(r)} < 0$. The state which is neutral stability concerning disturbance belonging to is characterized by $p_m^{(r)} = 0$.

1.6 INCOMPRESSIBLE AND COMPRESSIBLE FLUIDS

The nature of compressibility categorizes compressible and incompressible fluids, the fluids which change their volume by compressing them are known as compressible fluids otherwise, it is incompressible fluids. There are some approximations of this category of fluids we can say the fluids are incompressible if the density of the fluids is constant otherwise it is said to be compressible.

Compressibility is a property of volume change, and a fluid whose volume changes is referred to as a compressible fluid. On the other hand, an incompressible fluid has a fixed volume regardless of compression or expansion. A rigidly incompressible fluid doesn't actually exist.

The Mach number (M) of the flow is one indicator of a gas's level of compressibility. The fluid velocity to sound speed ratio is known as the Mach number. A fluid can be regarded as incompressible at M around 0.3. The speed of sound is roughly 340 m/s for 20 °C air temperature. Therefore, compressibility should be taken into account in the calculations if the fluid velocity is 100 m/s or above. The fluid can be regarded as incompressible for velocities under 100 m/s.

The fluid density will also fluctuate greatly during volume expansion or compression if the fluid temperature changes dramatically (as opposed to the fluid

being at a constant high or low temperature). The fluid may also be handled as a compressible fluid in this situation.

The governing equations of fluid flow for incompressible fluid are solved by Alternating Cell Directions Implicit Method Ba at el [39]. Turkyilmazoglu [213] studied the compressible fluid of a rotating disc in a boundary layer flow; also Turkyilmazoglu et al. [214] studied compressible fluid in a rotating disc in boundary layer flow and saw the convective and absolute instability. The stability of boundary layers was discussed by Brown [47] in which compressibility is considered. The study of Hide [94] is based on incompressible fluid and discussed the hydro-magnetic waves when the fluid is rotating. The compressibility effects were discussed by Hoshoudy [96] by using exponential density distribution when the boundary conditions are fixed. The effect of compressibility has a destabilizing role in this phenomenon. The stability of finitely incompressible plasma layer was done by Hoshoudy [97] in the presence of porous medium, and found that the effect of vertical and horizontal magnetic field has a stabilizing role. The stability of compressible fluid was done by Jeffreys [101], when the compressible fluid is heated from below. Lagerstrom et al. [129] highlight the difficulties in previous theoretical investigations of the impact of compressible fluid viscosity. Le and Koch [130] focused their investigation on the energy transition from natural gas to hydrogen in a porous medium. Lee and Flumerfelt [133] provide numerical results for instability of dynamic as well as stationary cylindrical fluid bodies. The stability limit for laminar boundary layer is theoretically investigated by the Lees [134]. Lessen et al. [135] considered two parallel streams to examine inviscid instability, and they found that a high Mach number has to stabilize the tendency towards the flow. Lifschitz and Hameiri [137] considered three dimensional flows and utilized WKB method to

examine their instability. A review is provided by the Mack [140] for compressible instability. Mitchner and Landshoff [148] considered stability problem of two separating compressible fluids in plane configuration. The fluids are accelerated and found the growth rate reduced, when wave length tends to higher. Morris [161] found asymptotic solution for axisymmetric compressible jet, he found that asymptotic solution in the regions are constant, also he found helical mode which makes more unstable with comparison to the axisymmetric mode. Saad [183] used principle of classical compressible flow in his investigation. Sharma [194] investigated thermal instability considering compressible fluid taking rotation and magnetic field he found that rotation is responsible for oscillatory modes. Shibata and Tanaka [199] considered compressible viscous fluid to investigate instability with the initial disturbance on the steady flow. Spiegel and Veronis [204] considered compressible fluid to apply Boussinesq approximation. Talwar [206] studied capillary instability assuming irrotational and perfectly conducting fluid whereas density is varying also applied horizontal magnetic field. He found that stabilizing character of magnetic fluid. Taylor [208-209] assumed accelerated and directed two superposed fluids. He observed that stability depends upon the direction of acceleration from the heavier dense fluid to lighter dense fluid or vice versa, further, he disintegration of liquid drops in presence of electric field. Valli and Zajaczkowski [218] further studied about global existence of Navier stokes equations for compressible liquid, moreover they gave quantitative properties of the solution in general case.

1.7 HYDRODYNAMIC INSTABILITY

Instability of fluid flow is responsible for the turbulence of fluid flow. There are a large number of applications of fluid's instability in engineering and the natural environment. The instability phenomenon is also found in the area of astrophysics,

applied mathematics, geophysics, biology, physics, oceanography, etc. On applying some perturbation in the fluid system which may in motion or stable, then its flow properties will be different from the original state. The system is called stable if a small perturbation imposed on the system dies and the system comes back in its original state while the system is called unstable if perturbation increases with time and properties of system changes forever. Some examples of instabilities are interfacial instability, baroclinic instability, rotational instability, thermal instability etc.

The hydrodynamic stability theory examines how a laminar flow reacts to a disturbance with modest or moderate amplitude. The flow is considered stable if it returns to its initial laminar state, but unstable if the disturbance intensifies and changes the laminar flow into a new state. In that circumstance, the flow is deemed unstable. Although instabilities frequently cause turbulent fluid motion, they can also change the flow into a different laminar state, which is typically a more complex. The mathematical examination of the evaluation of disturbances superposed on a laminar base flow is the subject of stability theory.

In real-world applications, a perturbation is applied to the field variables before they are re-inserted into the governing equations to assess the stability of a particular flow field concerning minor changes in the system's physical parameters. In the case of linear stability analysis, the perturbations are chosen so that nonlinear term combinations are disregarded from the governing equations, and a subsequent linearization technique reduces the field equations to a mathematical issue. Stability analysis in a slippery pipe was investigated by Chattopadhyay at el [51] in which a double-diffusive system has been covered.

A system is said to be stable with respect to a given disturbance if the disturbance is applied and dissipates over time, but it is said to be unstable with respect to a given disturbance if the disturbance increases in amplitude to the point where the system gradually departs from its initial state and never returns to it. When a system is stable in the face of all potential disturbances, it is considered to be stable, whereas a system is unstable when there is only one disturbance for which it is unstable. The state of marginal stability is used to designate the locus that separates the two states. The hydrodynamic stability between two compressible viscous fluids was done by Feldman [73], in which he considered that the boundary of one surface is bounded and another is unbounded. The incompressible study of it was investigated by Friedlander and Vishik [74]. The linear stability of incompressible fluid was studied by Ding and Kawahara [55], in which they used the finite element method and for compressible fluid the stability of laminar boundary was investigated by Dunn and Lin [58], the study of inviscid fluid was done by Eckhoff and Storesletten [59] on the rotating compressible fluid. The nonlinear analysis of hydrodynamic stability of rotating magnetic was done by El-Dib et al. [62]. Elhefnawy et al [63] considered two fluids which are subjected to uniform electric field, they neglected gravitational effects. They found stability diagrams for various physical flow parameters. Nonlinear stability analysis of superposed semi-infinite viscoelastic fluids with the vertical electric field was studied by El-Sayed [75] and found that the surface tension, kinematic viscosities and porosity of the porous medium has destabilizing nature. The stability between two compressible fluids was done by Fejer [72], he considered inviscid fluids and studied the effect of uniform magnetic fields and concluded that magnetic field has stabilizes the system. Lewis [136] made small number of experiments and observed unstable surface taking to vertical planes. Liu et al [139]

examine analytical solutions considering buckling and wrinkle deformation for stability patterns of slender beam of polymeric gel. Ozen and Narayanan [167, 168] performed linear and weak nonlinear analysis for convective analysis. For weak nonlinear analysis he ignored Marangoni effects. Plesset [172] assumed spherical symmetric configuration and performed the stability analysis taken the interface of two irrotational immiscible fluid interfaces. Raghavan and Marsden [173] investigated the theoretical stability of parallel flow of immiscible fluids, they found that parallel flow of fluids stabilizes the density gradient. Saville [185] considered a cylindrical interface and investigate axial electric field ignoring viscous effects. Shrivastava and Singh [200] took rectilinear oscillation of spherical configuration on conducting dusty viscous fluid. Tauber et al. [207] simulate numerically KH instability in two-dimensional configurations, the generation of fingers happens when surface tension is present for the high Reynold number. Tomotika [211] considered a cylindrical thread of viscous fluid. He analyzed his investigation using Plateau's statical theory. Turkyilmazoglu and Gajjar [212] give the numerical treatment for the linear stability of considered setup. Turkyilmazoglu and Ruban [215] carried numerically calculated the study flow to getting velocity profile over the Joukowskiaerofoil. Yadav et al [232] taken free-free, rigid-rigid and lower rigid and upper free boundaries in their considered setup. They employed linear stability theory and solve the resulting eigen value problem.

1.8 INTERFACIAL INSTABILITY

Interfacial instability occurs at the fluid-fluid or fluid-gas interface. Instability problems can be categorized into two types namely; temporal and spatial. The study of interfacial instability is essential in aerodynamics, aerospace engineering, etc. The concept of multiphase flows was firstly studied for inviscid flows now, people study

viscous and viscoelastic fluids. The study of interfacial instability helps design a car, weather prediction, blood flow in the human body, and many more industrial applications like packed bed reactor. The various types of interfacial instabilities occur in nature.

1.8.1 Rayleigh-Taylor Instability

Rayleigh-Taylor instability arises in the system when a higher-density fluid is positioned over a lower-density fluid in a gravitational field. This instability occurs when the fluids are at rest or in motion. The phenomenon of RTI is discussed by Sharp [198]. The RTI is also mentioned by Kull [118] in the situation of moving surfaces. Rayleigh-Taylor instability (RTI) is studied by various authors and discussed with multiple effects. The RTI in the circular cavity is formed with a Nano fluid layer and viscous studied by Awasthi et al. [38]. The RTI can be seen in many situations in natural as well as industrial applications. The non-linear analysis on RTI was studied by Awasthi at el. [29], and found that the vapor fraction destabilizes of the interface. Awasthi [18] studied the RTI with heat and mass transfer in swirling annular layer.

Usually, heat and mass movement across the interface are not considered while studying the interfacial instability of two fluids separated by an interface. However, the movement of mass and heat across the interface is essential in a variety of situations, including boiling heat transfer, chemical engineering, and geophysical problems. The RTI by VPF theory in cylindrical coordinates was studied by Asthana at el. [10], in this study viscosity enters through normal stresses. The Rayleigh-Taylor instability on another viscoelastic fluid namely Oldroyd B is also considered by Shukla at el. [201], and found that heat and mass transfer has a stabilizing role on it.

Using viscous potential flow theory, the RTI studied by Awasthi and Agrawal [23] in cylindrical geometry. The tangential electric field on RTI was described by Eldabe [61]. Elhefnawy [65] considered interface of two superimposed magnetic fluids to investigate RTI. He did nonlinear analysis supposing mass and heat transferring across the interface. The nonlinear RTI studied by Gill et al. [87] and explains the behaviour of magnetic field in the presence of heat and mass transfer on bubbles. Rayleigh-Taylor instability of Rivlin-Erickson fluid in the presence of porous medium was studied by Kumar [123].The Rayleigh-Taylor instability was investigated by Kumar [124], through porous medium. Kumar [125] considered uniform vertical magnetic field to examine the impact on the thermo-solutal convection. Mohammad et al. [159] took tangential electric field and found Ginzburg-Landau equation for nonlinear electro-hydrodynamic stability analysis. Moreover, for similar consideration Mohammad et al. [160] considered normal electric field. Rudraiah and Chandrashekara [182] used a simple process for fully developed approximation for RTI. Sharma et al. [195] considered porous media to investigate RTI for the viscoelastic interface, also they considered uniform magnetic field for their current problem and found the stabilizing nature of magnetic field.

1.8.2 Capillary instability

If a fluid cylinder collapses in an infinite fluid such as atmospheric air, the instability at the interface is known as capillary instability. The interface becomes unstable due to the presence of capillary forces (capillary force occurs due to surface tension at the free surface). This type of instability arises in various real-life phenomena such as the breakup of the liquid jet, the situation of film boiling and various metallurgical and chemical processes. Capillary instability is also known as Plateau-Rayleigh instability. This instability was first given by Joseph Plateau and

Lord Rayleigh. In around 1873, Plateau saw in nature, that a vertically falling stream of water at the end it breaks up into drops. It happens when its wavelength is approximate to π. Later Rayleigh showed this result theoretically.

In 2004, Ozen and Narayanan [167] studied the evaporation and convection on the Rayleigh instability, after ignoring the Marangoni and gravitional effects, they concluded that in bilayer system, liquid flow destabilizes while vapour flow has stabilizing nature. In 2004, Ozen and Narayanan [168] studied the weak nonlinear theory of phase change instability of a bilayer fluid system. In this study also they ignored the Marangoni and gravity effects. They used the Chebeshev spectral Tau method and found that the system is unstable if heat transfer enhanced.

1.8.3 Kelvin-Helmholtz Instability

Kelvin-Helmholtz instability (KHI) occurs between two superposed fluids of different physical parameters with relative horizontal velocity. Many natural and industrial phenomena encounter these types of flows, such as blowing wind above the ocean; the helical wave movement found in ionized comet tails, meteor toward the inside in the Earth's atmosphere, air blowing above mercury, convection heat transfer, cooling systems, air purifiers etc. The Kelvin-Helmholtz instability was first experienced by Lord Kelvin and Harmann von Helmholtz.

In 2002, Tauber et al. [207] studied KH instability in a sheared fluid interface through numerical simulation, they achieved that at a higher waver number the interfacial behaviour is similar to the non-linear KH instability in the classical case. They also found that if the density ratio is very large the evolution of disturbance wave will not be symmetric. The KH instability of two fluid having non-zero viscosity with porous media was done by Asthana at el. [11]

At the plane geometry, Asthana and Agrawal [9] studied the Kelvin-Helmholtz instability and found that heat and mass transfer stabilize viscous fluids when their viscosity is high and destabilize them when they are low. The KH instability in cylindrical configuration was done by Awasthi et al. [32] and investigated the stability when heat and mass transfer occurs at the interface. The KH instability in cylindrical interface was done by Awasthi and Agrawal [12] in which asymmetric and axisymmetric cases are considered. The linear analysis of KH instability is of parallel flow was covered by Bau [42], where porous medium is also taken into account. Elhefnawy and Radwan [66] considered cylindrical interface to investigate impact of axial as well as radial magnetic fields on accelerated interface. They observed axial magnetic field has stabilizing tendency towards the interface. According to Allah [6], porous media have destabilizing effects on Kelvin- Helmholtz instability and stabilizing effects on Rayleigh-Taylor instability when mass is transferred through them. Awasthi and Agrawal [25] studied the effect of tangential magnetic field on the KH instability. The KH instability with the permeable boundary conditions and constant magnetic field was examined by Awasthi [17]. At the interface between viscoelastic and viscous fluid, the KH instability was studied by Awasthi [20]. KH instability on viscoelastic Oldroyd B fluid was investigated by Fu et al. [75], and discussed the heat and mass transfer effect, and cylindrical study of this problem was done by Fu et al. [76]. The swirling effect of heat and mass transfer gas liquid interface was studied by Fu et al. [77].

1.8.4 Capillary instability of a liquid Jet

Under the influence of gravity, a liquid jet with a constant beginning radius is descending vertically. A crucial length is reached for the liquid as it lengthens. The jet disintegrates into a stream of droplets and loses its cylindrical shape at this critical

point. Surface tension is the main cause of this phenomenon. Building on Savart's research, Joseph Plateau first described this instability in 1873 through experimental observation. He observed the instability developed when the liquid column length was 3.13 times greater than the column diameter. Later, Lord Rayleigh supported Plateau's findings by providing an analytical justification for this physical discovery.

The inviscid fluid was taken by Blumen [44], where compressibility occurs, the stable and neutrally stable waves are considered. A temporal stability case of non-Newtonian fluid in liquid jets is discussed by Brenn et al. [46]. The temporal instability of circular liquid jet was investigated by Funada et al. [82], and found that viscosity reduces the growth rate. The stability of a liquid jet studied by Funada et al. [83], where they taken the incompressible gases and liquids, and effect of irrotational viscous pressure was considered by Funada et al. [81]. Furlani and Hanchak [84] studied the instability of breakup of micro jets of Newtonian and viscous fluid. They used the method of lines in their analysis.

The study of cylindrical jet in a viscoelastic fluid interface was done by Awasthi at el. [30]; another study of Goldin et al. [88] described the stability of non-Newtonian fluid.

The cylindrical analysis of liquid jet was done by Ashgriz and Mashayek [8], mass transfer through porous media was studied by Awasthi [16] in the presence of axial magnetic field.

1.9 VISCOUS POTENTIAL FLOW THEORY

Viscous potential flow theory is an infallible tool to get the solution of Navier-Stokes equations when the flow is irrotational. The evolution of the potential flow theory comes into the picture from the principle of kinematic theory. The kinematic

theory states that for irrotational flow, the curl of the velocity becomes zero and there exists a potential function such as gradient of that function represents the velocity of the flow.

Mathematically,

$$\vec{q} = \nabla\Phi \tag{1.22}$$

The continuity equation for the irrotational/incompressible flow is

$$\nabla \bullet \vec{q} = 0 \tag{1.23}$$

For potential flow, equation (1) turned into the Laplace equation,

$$\nabla^2\Phi = 0 \tag{1.24}$$

Potential flow theory makes the Navier-Stokes equation free of viscous terms, and therefore potential flow theory labeled as inviscid potential flow (IVP) theory. Since flow problem are mainly coalescent with the viscosity, so during utilization of potential flow theory viscosity cannot be taken as zero.

Joseph and Liao [105] utilized the VPF theory first in 1994. Shearing stress for irrotational flow are assumed zero during potential flow analysis while including viscosity in the analysis, the normal stress are utilized. There are no needs of no-slip condition during viscous potential flow analysis at the boundaries. A small group of vorticity and circulation theorems for IPF (inviscid potential flow) are also applicable the viscous potential flow analysis. Many cases revels the excellent physical results of finite Reynolds number (Re) when viscous potential flow theory applied.

Interfacial conditions can be derived for two different phase flow with the help of potential flow theory.

Equations of motion is considered for incompressible non-Newtonian fluid as well as Newtonian fluid are written as:

$$\rho\left(\frac{\partial\vec{\boldsymbol{q}}}{\partial t}+(\vec{\boldsymbol{q}}\bullet\nabla)\vec{\boldsymbol{q}}\right)=-\nabla\Gamma+\nabla\bullet\tau \tag{1.25}$$

$$\text{where}\,\Gamma=-p+\rho gy \tag{1.26}$$

The equation for stress can be written as

$$T_{ij}=-p\delta_{ij}+\tau \tag{1.27}$$

$$\text{where}\ \ \tau=2\mu\boldsymbol{D_1}\qquad\text{and}\qquad\nabla\bullet\tau=\mu\nabla^2\vec{\boldsymbol{q}} \tag{1.28}$$

The mechanical energy balance equation for an incompressible Newtonian fluid can be written as

$$\frac{d}{dt}\int_v\frac{\rho}{2}|\vec{\boldsymbol{q}}|^2\,dV=\int_A[\boldsymbol{n}\bullet\boldsymbol{T}\bullet\boldsymbol{n}]dA-2\mu\int_V\boldsymbol{D_1}\bullet\boldsymbol{D_1}dV \tag{1.29}$$

where A is the boundary of V with outward normal $\boldsymbol{n}$. Let us consider the equation of the free surface is given by

$$y=H(x,z) \tag{1.30}$$

If $\boldsymbol{e_s}$ is any vector tangent to the free surface A_f, the shear stress is given as

$$\boldsymbol{n}\bullet\boldsymbol{T}\bullet\boldsymbol{e_s}=0 \tag{1.31}$$

If σ represents surface tension, one can write

$$\boldsymbol{n}\bullet\boldsymbol{T}\bullet\boldsymbol{n}=-\rho gH+\sigma\,\nabla\bullet\boldsymbol{n} \tag{1.32}$$

Putting the values from equation (1.32) in equation (1.29), we get

$$\frac{d}{dt}\int_v\frac{\rho}{2}|\vec{\boldsymbol{q}}|^2\,dV=-\int_A(\rho g\eta+\sigma\nabla\bullet\boldsymbol{n})v_n dA-2\mu\int_V\boldsymbol{D_1}\bullet\boldsymbol{D_1}dV \tag{1.33}$$

The last term in the above equation represents viscous dissipation term. This equation holds for viscous fluids satisfying the Navier–Stokes equations subject to the vanishing shear stress condition.

Now, for potential flow, the viscous dissipation term reduces to

$$\begin{aligned} 2\mu\int_V \boldsymbol{D_1}\bullet\boldsymbol{D_1}dV &= 2\mu\int_V \frac{\partial^2\Phi}{\partial x_i\partial x_j}\frac{\partial^2\Phi}{\partial x_i\partial x_j}dV \\ &= 2\mu\int_A n_j\frac{\partial^2\Phi}{\partial x_i\partial x_j}v_i dV \\ &= 2\mu\int_A \boldsymbol{n}\bullet\boldsymbol{D_1}\bullet\vec{\boldsymbol{q}}\,dA = 2\mu\int_A \boldsymbol{n}\bullet\boldsymbol{D_1}\bullet\left(v_n\boldsymbol{n}+v_s\boldsymbol{e_s}\right)dA \\ &= \int_A\left(2\mu\frac{\partial^2\Phi}{\partial n^2}v_n+\tau_s v_s\right)dA \end{aligned} \tag{1.34}$$

where τ_s represents irrotational shear stresses.

$$\tau_s = 2\mu\boldsymbol{n}\bullet\boldsymbol{D_1}\bullet\boldsymbol{e_s} \tag{1.35}$$

and $v_s = \vec{\boldsymbol{q}}\bullet\boldsymbol{e_s}$

As $$\left(\vec{\boldsymbol{q}}\bullet\nabla\right)\vec{\boldsymbol{q}} = \nabla\frac{\left|\vec{\boldsymbol{q}}\right|^2}{2}$$

The inertia term becomes

$$\begin{aligned} &\frac{d}{dt}\int_v\frac{\rho}{2}\left|\vec{\boldsymbol{q}}\right|^2 dV = \int_v\frac{\rho}{2}\left(\vec{\boldsymbol{q}}\bullet\frac{\partial\vec{\boldsymbol{q}}}{\partial t}+\vec{\boldsymbol{q}}\bullet\nabla\frac{\left|\vec{\boldsymbol{q}}\right|^2}{2}\right)dV \\ &= \int_v\frac{\rho}{2}\left(\frac{\partial\Phi}{\partial x_i}\frac{\partial}{\partial x_i}\frac{\partial\Phi}{\partial t}+\nabla\bullet\left|\vec{\boldsymbol{q}}\frac{\left|\vec{\boldsymbol{q}}\right|^2}{2}\right|\right)dV \\ &= \int_A\rho v_n\left(\frac{\partial\Phi}{\partial t}+\frac{\left|\nabla\Phi\right|^2}{2}\right)dA \end{aligned} \tag{1.36}$$

Putting values form equations (1.34) and (1.36) into the equation (1.29), the expression for mechanical energy balance equation can be written as:

$$\int_A v_n \left[\rho \left(\frac{\partial \Phi}{\partial t} + \frac{|\nabla \Phi|^2}{2} + gH \right) + 2\mu \frac{\partial^2 \Phi}{\partial n^2} + \sigma \nabla \bullet \boldsymbol{n} \right] dA = -\int_A \tau_s v_s dA \tag{1.37}$$

Also, the Bernoulli's equation for unsteady potential flow can be written as;

$$p' + \rho \left(\frac{\partial \Phi}{\partial t} + \frac{|\nabla \Phi|}{2} + gH \right) = C \tag{1.38}$$

Here, p' represents the irrotational pressure.

Using divergence theorem, we can write

$$C \int_A \vec{\boldsymbol{q}} \bullet \boldsymbol{n} dA = C \int_A \nabla \bullet \vec{\boldsymbol{q}} dV = 0 \tag{1.39}$$

If we use equations (1.38) and (1.39), the equation (1.37) reduces to

$$\int_A v_n \left[-p' + 2\mu \frac{\partial^2 \Phi}{\partial n^2} + \sigma \nabla \bullet \boldsymbol{n} \right] dA = -\int_A \tau_s v_s dA \tag{1.40}$$

As we know, viscous potential flow analysis requires vanishing irrotational shearing stresses at the free surface i.e. $\tau_s = 0$. Therefore, the conservation of momentum at the free surface A_f can be derived as

$$-p' + 2\mu \frac{\partial^2 \Phi}{\partial n^2} = -\sigma \nabla \bullet \boldsymbol{n} \tag{1.41}$$

Since, $\boldsymbol{n} = \frac{\nabla \boldsymbol{f}}{|\nabla \boldsymbol{f}|}$ and $\nabla \bullet \boldsymbol{n} = \nabla \bullet \left(\frac{\nabla \boldsymbol{f}}{|\nabla \boldsymbol{f}|} \right) = \left(\frac{1}{R_1} + \frac{1}{R_2} \right)$, R_1, R_2 stands for principal radii of curvatures of the interface and always positive value taken, therefore, equation (1.41) takes form as

$$p' - 2\mu \frac{\partial^2 \Phi}{\partial n^2} = \sigma \left(\frac{1}{R_1} + \frac{1}{R_2} \right) \tag{1.42}$$

The viscous potential flow theory in which, the viscosity enters through normal stresses studied by Awasthi and Agrawal [23]. The pressure correction on incompressible fluid interfaces was investigated by Awasthi et al. [32] and Awasthi et al. [33] studied heat and mass transfer on it and found a destabilizing configuration. The KH instability by using VPF theory in a channel was discussed by Funada and Joseph [78] and found a critical value of a relative velocity, when viscosity ratio is equal to the density ratio then the critical value of the critical relative velocity is high.

1.10 MASS TRANSFER CONDITIONS

The relative motion of species in mixture due to concentration gradients is termed as mass transfer. The erratic movement of the molecule origins a net transport of heat from an area of higher concentration to the area of lower concentration. The processes of transportation of mass can be understand by some massive examples like mass evaporation of water from a water tank into atmosphere, chemical impurities diffusion in oceans, rivers and lakes.

If we take the transfer of mass from an interface into a well-mixed solution, it is expected that the transferred amount of mass is proportional to the product of interfacial area and concentration difference i.e.

$$\left.\begin{array}{l}\text{mass tranfer rate } \propto \text{ area of interface} \times \text{concentration difference} \\ \text{e.i. mass tranfer rate per unit area } (N) \propto \text{concentration difference } (C_1 - C_2)\end{array}\right\} \quad (1.43)$$

$$\text{i.e. } N_1 = k(C_1 - C_2)$$

The proportionality constant k, is known as mass transfer coefficient and C_1, C_2 are the concentrations at the interface and in the mixture, respectively. The mass per unit area N_1 is also termed as interfacial flux which includes both convection as

well as diffusion. From equation (24), it can be easily seen that flux will become double if the concentration difference gets doubled. It can also be seen that the total amount of transferred mass will become double but the flux per area will not change if taking area is double.

Now, we derive the interfacial mass transfer condition using potential flow theory. In the systems of fluid flows, the conservation of mass is represented by the equation of continuity.

$$\frac{\partial \rho}{\partial t} + \nabla \bullet (\rho \vec{q}) = 0 \tag{1.44}$$

Let us consider, the interfacial equation between two fluids is given by

$$f(\vec{x}, t) = 0 \tag{1.45}$$

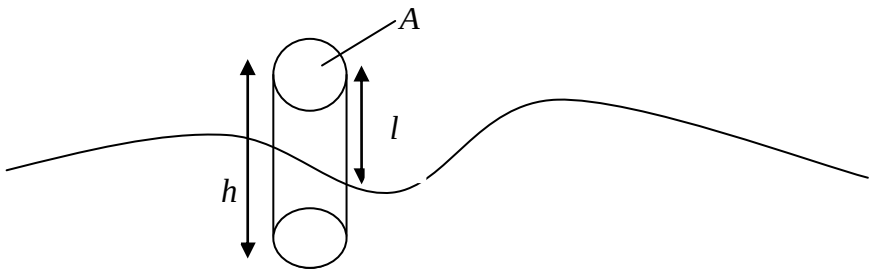

Figure 1.1: The configuration of fluid system

We assume that $f(x,t) > 0$ is the region occupied by the fluid 1 above the interface having density ρ_1 viscosity μ_1 and the fluid 2 having density ρ_2, viscosity μ_2 occupies the region $f(x,t) < 0$ above the interface. We also consider a right small cylinder of height h and base area A situated at the interface and its space coordinates are fixed. We consider that part of right cylinder of height l is situated in fluid 1 and remaining part situated in fluid 2. The cylinder is fixed but interface is changing with time

therefore the value of l is also changing with time. Now integrating equation (1.44) over the boundary *B* of any region of volume *V*, we get

$$\frac{d}{dt}\int_V \rho dx^3 + \int_B (\rho\vec{\boldsymbol{q}}) \bullet \hat{\boldsymbol{n}} \mathrm{d}x^2 = 0 \tag{1.46}$$

If we take, inside cylindrical region *V*, the above equation takes form as

$$\frac{d}{dt}\left[\rho_1 lB + \rho_2 (l-1)B\right] + \left[(\rho q)_1 \bullet \frac{\nabla f}{|\nabla f|} - (\rho q)_2 \bullet \frac{\nabla f}{|\nabla f|} \right] B = 0 \tag{1.47}$$

Simplifying,

$$\left[\rho_1 + \rho_2\right]\frac{dl}{dt} + \left[(\rho q)_1 - (\rho q)_2\right]\frac{\nabla f}{|\nabla f|} = 0 \tag{1.48}$$

As we know the equation of interface between two fluids is represented as $f(\vec{\boldsymbol{x}}, t) = 0$ and therefore, we can write

$$\frac{dl}{dt} = -\boldsymbol{n} \bullet \frac{d\vec{\boldsymbol{x}}}{dt} = \frac{\nabla f}{|\nabla f|} \bullet \frac{d\vec{\boldsymbol{x}}}{dt} \tag{1.49}$$

At the interface $df = \frac{\partial f}{\partial t} dt + \nabla f \bullet d\vec{\boldsymbol{x}}$ (1.50)

From equations (1.49) and (1.50), one can conclude that

$$\frac{dl}{dt} = \frac{\partial f / \partial t}{|\nabla f|} \tag{1.51}$$

Using (1.51) in equation (1.48), we get

$$\rho_1\left(\frac{df}{dt} + \vec{\boldsymbol{q}}_1 \bullet \nabla f\right) = \rho_2\left(\frac{df}{dt} + \vec{\boldsymbol{q}}_2 \bullet \nabla f\right) \tag{1.52}$$

In case of potential flow analysis, $\vec{\boldsymbol{q}}_i = \nabla\Phi_i$, equation (1.52) takes form as

$$\rho_1\left(\frac{df}{dt}+\nabla\Phi_1\bullet\nabla f\right)=\rho_2\left(\frac{df}{dt}+\nabla\Phi_2\bullet\nabla f\right) \tag{1.53}$$

If fluids are immiscible, there will not any transfer of mass across the interface and therefore equation (1.53) changes into

$$\begin{cases}\rho_1\left(\frac{df}{dt}+\nabla\Phi_1\bullet\nabla f\right)=0\\ \rho_2\left(\frac{df}{dt}+\nabla\Phi_2\bullet\nabla f\right)=0\end{cases} \tag{1.54}$$

Equation (1.54) shows that the normal velocities of fluid particles at the interface are zero. i.e. every particle which is on the interface currently, will remain on the interface throughout the analysis. There conditions are known as kinematic conditions.

1.11 HEAT TRANSFER CONDITIONS

If the fluids are thermally conducting with thermal diffusivity α, the equation of diffusion can be written as,

$$\frac{\partial T}{\partial t}+\vec{\boldsymbol{q}}\cdot\nabla T=\alpha\nabla^2 T \tag{1.55}$$

We assume that fluid 1 has temperature T_1 and fluid 2 has temperature T_2 and also the fluids are in thermodynamics equilibrium in the basic state and the saturation temperature is equal to the interface temperature T_0. Here we assume heat transfer across the interface is dominated by the latent heat, the conservation of energy (1.55) across the interface takes the form as follows;

$$L\rho_1\left(\frac{df}{dt}+\nabla\Phi_1\cdot\nabla f\right)=H(\varsigma) \tag{1.56}$$

where L denotes the latent heat and $H(\varsigma)$ represents the total heat flux across the boundary. Here we neglect the kinetic energy terms which are very less in comparison to the latent heat and terms of heat flux are replaced using equilibrium conditions. The equation for total heat flux $H(\varsigma)$ can be represented as

$$H(\varsigma) = \frac{K_2(T_0 - T_2)}{h_2 - \varsigma} - \frac{K_1(T_1 - T_0)}{h_1 + \varsigma} \tag{1.57}$$

Expand the heat flux term using the Taylor series and only consider the linear term, the heat flux can be represented by Eq. (1.57).

$$H(\varsigma) = H(0) + \varsigma H'(0) + \ldots\ldots\ldots \tag{1.58}$$

As we know $H(0) = 0$ from the symmetry condition, we get from equation (1.57)

$$\frac{K_2(T_0 - T_2)}{h_2 - \varsigma} = \frac{K_1(T_1 - T_0)}{h_1 + \varsigma} = Q\,, \quad \text{where } Q \text{ is constant}$$

1.12 HEAT AND MASS TRANSFER

Usually, heat and mass movement across the interface are not taken into account while studying the interfacial instability of two fluids separated by an interface. Contrarily, a range of situations, such as boiling heat transfer in chemical engineering and geophysical problems, depend on the transport of mass and heat across an interface.

Heat transfer occurs whenever there is inhomogeneous temperature distribution within system or between the system and its surrounding environment. There are four basic modes of heat transfer: conduction, convection, phase change, and radiation. The process by which heat diffuses through a solid or a stationary fluid is termed as heat conduction. The transfer of heat from a wetted surface is assisted by the motion of the fluid, which is known as heat convection. However, when the fluid

undergoes a phase change at or near the wetted surface, it is called phase-change heat transfer. The thermal radiation is by electromagnetic wave propagation. There is no medium needed for thermal radiation, although the electromagnetic waves can be transferred through gases.

The relative migration of species in a mixture caused by concentration gradients is explicitly referred to as mass transfer. A net mass transfer from a region of high concentration to a region of low concentration results from the molecule's random mobility. The diffusion of chemical contaminants from point sources, whether natural or manufactured, into lakes, rivers, and oceans are two typical instances of mass transfer processes.

Interfacial instability, which happens when two fluids are divided by an interface, is typically discussed without taking heat and mass transport across the interface into account. On the other hand, many scenarios, such as boiling heat transfer in chemical engineering and geophysical difficulties, depend greatly on the transmission of mass and heat over a contact.

The heat and mass transfer are studied by several researchers in Rayleigh- Taylor, Kelvin Helmholtz and capillary instabilities etc, where researchers considered inviscid, viscous and many viscoelastic fluids. Awasthi [14] studied capillary instability with heat and mass transfer on viscoelastic fluid and Rayleigh-Taylor and Kelvin-Helmholtz instabilities in planar geometry were addressed by Hsieh [99], who also developed a generic formulation for the interfacial flow problem with heat mass and transport. The heat transfer and magnetic effects on viscoelastic field was analyzed by Khan et al. [113] in the presence of porous medium. In Hsieh's [100] study, heat and mass transfer inhibit the development of instability when the vapor region is hotter than the liquid region, as is usually the case.

An equilibrium dispersion relationship was derived by Ho [95] for two viscous fluids of equal kinematic viscosity and linear Rayleigh-Taylor stability in the presence of heat and mass transfer. Taking heat and mass transfer into account, Lee [131, 132] studied the nonlinear behavior of various stability problems of inviscid fluids and found that it plays an important role in the nonlinear behavior. Using Kelvin-Helmholtz instability with heat and mass transfer, Nayak and Chakraborty [164] observed a more stable configuration with plane geometry than cylindrical geometry. Khan et al. [112] studied the heat and mass transfer effect on Maxwell viscoelastic fluid and checked the behavior of Deborah number. The extension of heat in hybrid micro polar Nano fluid was analyzed by Ahmad et al. [3]. The vaporization with heat and mass transfer was studied by Asthana and Agrawal [9].

According to Khodaparast et al. [114], the liquid-vapor interface is stable for Rayleigh-Taylor and Kelvin- Helmholtz heat and mass transfer because liquid is viscous and motionless while vapor moves horizontally, A coupled viscosity-phase change could stabilize Rayleigh-Taylor stability, but can destabilize Kelvin-Helmholtz stability. The numerical study of mass transfer flow was done by Reddy et al. [178]; Reddy et al. [177] investigated the Darcy-Forchheimer two-dimensional carbon nanotubes. The study of Reddy et al. [179] explores the Blasius-Rayleigh-Stokes flow on the stretching surface and the effect of magnetic dipole is discussed. The heat and mass transfer was studied by Jia et al. [102] on the swirling annular fluid layers. Kumar [119] studied the heat transfer where he taken the viscous incompressible fluid and concluded that the Nusselt number shifts in the same direction as the heat source, but the existence of the heat source causes the recovery factor to decrease. Awasthi and Agrawal [23] examine the impact of heat and mass transfer on the viscous interface utilizing viscous potential flow theory. Moatimid

[151] assumed two rotating magnetic fluids to investigating impact of rotation and magnetic effects on the cylindrical interface. Wang et al. [226] investigated power law liquid jet when heat is transferred across the interface.

1.13 INSTABILITY IN VISCOELASTIC FLUIDS

Due to the enormous importance of viscoelastic liquids the field of chemical industries, engineering and technology several workers have been attracted to work on various aspects of viscoelastic liquids in different models. The fluids having the nature of viscosity and elasticity are known as viscoelastic fluids. There are so many types of viscoelastic fluids. The work of power law viscoelastic fluid in a nanofluid layer was done by Awasthi et al. [38] the study of Barik et al. [41] is based on porous medium.

The study of Joseph et al. [106] was based on viscoelastic fluid. The study of Joseph [104] was first explained the potential flow of viscous and viscoelastic fluids, and dissipations approximation and viscous potential flow were explored by Joseph and Wang [103]. The Rayleigh-Taylor instability of viscoelastic fluids was studied by Joseph et al [106]. Joseph et al [108] compared the breakup of purely viscous and viscoelastic fluids. The study of Kango and Singh [110] was based on a Rivlin-Erickson viscoelastic fluid in which porous medium is considered and found that for stationary convection, Rivlin-Erickson elastic-viscous fluid reacts a Newtonian fluid. Stability of viscoelastic fluid interfaces was discussed by Kumar and Singh [127], where Walter's B viscoelastic fluid is considered and Kumar [122] investigated the stability of Walter's B fluid interfaces with porous medium. Kumar [123-125] considered viscoelastic interface and investigated stability in plane geometry. Marshall and Metzner [141] considered high Deborah number to analyzing its influence upon the distribution in the porous medium. The numerical as well as

theoretical investigation has been done by Megahed and Reddy [142] for Walter's B fluid flow. Metzner and Park [145] examine characteristic of turbulent flow considering viscoelastic fluids. Middleman [146] considered viscoelastic jet and compared stability to the Newtonian jet, he found that less stability of viscoelastic jet. Moatimid and Zekry [156] performed nonlinear analysis considering Walter's B fluid interface with axial electric field, further Moatimid et al. [158] considered periodic electric field for nonlinear stability analysis. Moatimid and Hassan [153] found a dispersion relation of order three solving governing equations for the interface of viscoelastic nanofluid layer. They utilized Routh-Hurwitz criteria. Park and Lee [169] considered a viscoelastic flow system which is heated from below performing nonlinear analysis, he considered two types of boundary conditions i.e. rigid-rigid and rigid-free boundaries. Rivlin and Ericksen [181] derived the stress-deformation relation considering isotropic materials. Sharma and Chand [187, 188] considered different types of viscous fluids to investigate the instability. They ignored the perturbation streaming direction and analyzed stability criteria. Further Sharma and Kango [189] considered Rivlin Ericksen interface to investigate thermal convection in porous medium. They found over stability for the nonexistence as a sufficient condition. Sharma et al. [157] considered viscoelastic interface under porous media and they found that surface forces were able to overcome the KH instability. Sharma and Kumar [190-193] investigated the impact of rotation on the Rivlin-Ericksen and Walter's B viscoelastic fluid interface on thermal instability, further, they considered magnetic conducting fluids for the same problem, they also introduce oscillatory modes. Sharma et al. [195] considered a viscoelastic stratified interface assuming horizontal magnetic field together with rotation and porous media. An unsteady flow considered by Srivastava and Singh [205] for the Rivlin-Ericksen fluid when pressure

gradient is time dependent. Tiwari et al. [210] examine the impact of axial electric field on the capillary viscoelastic instability. They found a critical point of wave number and observed system is unstable for less than the critical value of wave number. Walters [222-223] characterized the viscoelastic liquid during a small shear rate viscoelastic liquids demonstrate, further he found the solution of the flow problem in the case of materials with memory. Yerushalmi et al. [235] examined initial data of small perturbation for stability of steady shear flow under viscoelastic fluids.

1.14 INSTABILITY IN NANOFLUIDS

A nanofluid is a fluid containing particles that are less than a nano-meter in size, called nanoparticles, suspended in a base fluid. In nanofluids, nanoparticles are frequently formed of metals, oxides, carbides, or carbon nano tubes. Oil, water, and ethylene glycol are typical base fluids. The use of nanofluid in industrial settings is very beneficial.

The first crucial stage in experimental research using nanofluids is the preparation of the nanofluids. Nanofluids are not merely combinations of liquid and solid. Certain unique conditions are necessary, such as even and stable suspension, long-lasting suspension, little particle agglomeration, no chemical change of the fluid, etc. By scattering solid particles with a size of a few nano-meters into common base liquids like water, ethylene glycol (EG), oils, etc., one can create nanofluids. A key issue with nanofluid production is agglomeration.

The thermo-physical properties, synthesis and stability of nanofluid was examined by Sezer et al. [186], in nanofluid the Rayleigh-Benard convection was described by Dhananjay et al [54]. The stability of nanofluid studied by Chakraborty

and Panigrahi [49], Yadav et al. [229] studied the Rayleigh Benard Convection on nanofluids. Electro hydrodynamics study through porous media was done by Moatimid and Amer [153], the study of heat and mass transfer in nanofluid studied by Ahmad et al. [1, 3, and 4], they saw the magnetic effect on a stretched cylinder and double and triple stratification. Another study was done by Ahmad et al. [5] is based on hybrid nanofluid. A temporal analysis of nanofluid layer of power law viscoelastic fluid was done by Awasthi et al. [36]. The stability characteristics of nanofluid in stationary situation was given by Ghadimi et al. [85] another study of nanofluid with heat and mass transfer effects in Marangoni convection is given by Han [91]. The numerical study of Hassan [93] explored the effect of electric and magnetic field on viscoelastic nanofluid. The characteristic of nanofluid by dispersion method was studied by Nasiri et al. [163]. Heat and mass transfer investigation on hybrid nanofluid was done by Xia et al. [228] by using multiple slip boundary conditions. Yadav et al. [229, 230] considered thermal instability in a rotating nanofluid and onset of convection in porous layer. Heat and mass transfer in a rotating nanofluid and magnetic effect was also studied by Yadav et al. [231, 232].

The study of Ghadimi et al. [85] is explains the stability property on nano fluid and discussed the stationary conditions on it. Analytical and Numerical study was done by Hassan [93], he explores the linear stability of viscoelastic nanofluid layer and studied the effect of electric and magnetic fields. Moatimid et al. [157] examine temporal instability of nano gas-liquid layers. They added the effect of Marangoni convection in their analysis. Nadeem et al. [162] utilized Thomson and Troian slip conditions to investigate convection flow assuming hybrid nanoparticles. Thermal conductivity and instability of nanofluid have been investigated by Nasiri et al. [163] using dispersion method. Saffman and Taylor [184] considered a system in which

viscous fluid penetrated in porous media. They found that fluids are fully separated to the definite interface. According to Yu et al. [236], the dispersion stability of thermal nanofluids is poor, thus restricting their further development and application.

1.15 ORGANIZATION OF THE THESIS

The aim of the present thesis is to analyze the interface of two viscous/viscoelastic fluids when the interface is experiencing capillary instability. The viscous potential flow theory is utilized to solve the constitutive equations. Various types of viscous-viscoelastic fluid combinations are considered to examine the instability behavior of the interface. The instability behavior is discussed when there is heat and mass transfer across the interface. The normal mode analysis has been used and the stability conditions are achieved. The interface of two compressible fluids is also examined in a cylindrical coordinate system using viscous potential flow theory. The chapter wise summary of the thesis is as follows

Chapter 1 consists of an introduction to the general stability problems, Rayleigh-Taylor instability, capillary instability, Kelvin-Helmholtz instability, instability of liquid jet, viscous potential theory, some definitions, and basic equations related to the stability analysis. A brief summary of the related studies made by various authors in the field of stability has been presented. Lastly, chapter wise brief summary of other chapters of the thesis is also presented.

In **chapter 2,** the normal mode approach is used to investigate the instability of the interface formed by a Rivlin-Ericksen viscoelastic fluid- viscous liquid interface. The irrotational potential theory of viscous/viscoelastic fluids is used to solve the formulated mathematical equations. Viscoelastic liquid and

viscous fluids are contained within an annular region surrounded by rigid cylinders. The interface formed is capable to transportation of heat-mass across the interface. It is assumed as the viscoelastic liquid occupies the outer zone; the viscous fluid occupies the interior zone.

Chapter 3 examines the instability of the interface shaped by a Walter's B viscoelastic fluid and a Newtonian viscous liquid through the normal mode procedure. The formulated mathematical equations are solved by the potential function hypothesis of viscous/viscoelastic fluids. The polynomial equation of degree two is achieved to discuss the stability/instability of the interface.

Within a region confined by rigid cylindrical surfaces, the stability characteristics of viscous fluid-viscoelastic fluid interfaces are examined in **chapter 4.** Considering Walter's B viscoelastic fluid, it is also analyzed the impact of heat transport on the interface. Using a viscous incompressible fluid-Walter' B viscoelastic liquid, it is examined the stability of a fluid-liquid interface. In this case, the fluids are confined within an annular region between two rigid boundaries of cylindrical shapes.

In **chapter 5**, the irrotational flow theory is applied to the analytical study of heat- mass transfer in viscous-viscoelastic fluids interface. Capillary instability, considering power-law fluid/viscoelastic fluid is studied both for asymmetric and axisymmetric disturbances under two rigid concentric cylinders surround the fluids in an annular region.

The circular cavity containing nanofluid layer is presented in **chapter 6.** A two-dimensional flow is taken in the cavity, which is represented by an infinite circular cylinder. Newtonian viscous fluid fills the cavity, while Newtonian nanofluid fills the outside.

The linear instability analysis of capillary stability has been performed in **chapter 7** at the interface of a viscous compressible fluid. In the cylindrical coordinate system, a compressible viscous fluid was surrounded by another compressible viscous fluid. In order to investigate the flow of fluid satisfying the compressible flow model, the potential flow theory of the fluid was used.

Finally, in **chapter 8,** based on the present study, conclusions are drawn and future research work in this direction is suggested.

A list of references is appended at the end of thesis.

CHAPTER 2
CAPILLARY INSTABILITY OF RIVLIN-ERICKSEN FLUID FILM WITH HEAT AND MASS TRANSFER

The stability of the viscous- viscoelastic fluid interface is theoretically examined when the heat and mass transfer is allowed from one phase to another phase. The viscoelastic liquid and viscous fluids lie in an annular region and are enclosed by two rigid cylinders. The viscoelastic liquid is taken in the outer region while viscous fluid lies in the inner region. The analysis was performed by using the potential flow theory for viscoelastic liquid satisfying the Rivlin-Ericksen model. In potential flow theory, the tangential stresses are not considered, the viscosity enters through normal stress balance and the no-slip condition at the two cylindrical rigid boundaries is not enforced. A second-order polynomial in terms of growth rate is achieved and analyzed numerically using the well-known Newton-Raphson method. The results show that the impact of the transfer of heat/mass is found to boost the stability of the interface.

2.1 BACKGROUND

The non-Newtonian liquids are very important fluids as they are used heavily in the bio-medical appliances, communication devices, and agriculture industry. Specific examples of these fluids include pulps, molten metal, crude and slurries materials in a liquid state, polymers, etc. Rivlin and Ericksen [181] presented a theoretical model for a fluid known as Rivlin-Ericksen fluid. Rivlin-Ericksen (R-E) fluid is one of the non-Newtonian fluids used in the insulation system, tyres, seat foams, oil filtration process, ceramic processing, etc.

Although, various studies are available in the literature on the thermal instability/Natural convection of Rivlin-Ericksen fluid but no study has been made on the interfacial instability with heat transfer involving Rivlin-Ericksen fluid. Srivastava and Singh [205] considered the unsteady pressure-dependent flow of Rivlin-Ericksen fluid in a variable cross-section channel. Shrivastava and Singh [200] studied the magnetic field effect on the Rivlin-Ericksen fluid flowing in a sphere with oscillations. Sharma et al. [190-193] employed normal mode theory to study the thermal instability in a layer of Rivlin-Ericksen fluid with various effects such as rotation, magnetic field, porous medium, Hall Effect, etc. Gupta and Sharma [90] extended the study of thermal instability of Rivlin-Ericksen fluid by adding concentration, compressibility, Hall effects, and rotation. The magnetic field and porous effects are added by Kango and Singh [110].

The elastic effects play a crucial role in the stability of superposed fluids. Kumar [122-123] presented the stability of superposed fluids involving Rivlin-Ericksen fluid. The porous effect on the stability of viscous-Rivlin-Ericksen fluid was investigated by Sharma et al. [195]. Sharma et al. [197] extended the work of Sharma et al. [195] by adding the streaming effect. The effective interfacial tension in the instability of superposed Rivlin-Ericksen fluid was included by Kumar and Mohan [121]. In the above studies, interfacial instability was discussed but heat transfer was not taking place.

The convective and absolute stability analysis for 2-D wakes formed in a wedge-shaped thin aerofoil was made by Turkyilmazoglu et al. [214]. Turkyilmazoglu et al. [215] applied the Chebyshev-collocation method along with the fourth-order Runge-Kutta integrator to study the stability of the inviscid compressible boundary layer formed over a disk when the disk was rotating. The spatial resonance that

occurs in the boundary layer due to the rotation of the disk was numerically analyzed by Turkyilmazoglu and Gajjar [212]. The lower branch marginal stability of a compressible boundary layer on a rotating disk was investigated by Turkyilmazoglu [213].

The investigation of stratification effects and thermophoretic on the Maxwell fluid was analyzed by Khan et al. [112] using Cattaneo-Christov theory and found that flow velocity decreases when Deborah number is high. Ahmad et al. [1] analyzed a similar problem by taking double stratification into the account. The triple stratification effect on the unsteady flow of hybridized bio-convective micropolar nanofluid was investigated by Ahmad et al. [3]. The impact of double stratification and magnetic dipole on the transfer of heat/mass in the hybrid Casson nanofluid flowing over the spreading cylinder was considered by Ahmad et al. [2]. Xia et al. [228] analyzed the heat/mass transport in the mixed convection of hybrid micropolar nanofluid boundary layer flow with multiple slip conditions. The study of Ahmad et al. [4] reported the heat transfer study of micropolar nanofluid in the thin moving needle. The bio-convective micropolar hybrid nanofluid in steady-state was analyzed by Ahmad et al. [5]. Nadeem et al. [162] examined the mixed convection in the hybrid nanofluid over a Riga surface with Trion and Thompson conditions.

The transport of mass and heat from one fluid to another fluid always makes a great impact on interfacial stability and has numerous applications such as film boiling, heat exchangers, etc. Hsieh [99] formulated the heat transfer conditions along with mass transfer for the interface phenomenon. These conditions are extensively used by various authors (Nayak and Chakraborty [164], Lee [132]) for the study of interfaces involving heat transfer. These studies are based on inviscid fluids.

The potential flow theory of viscous fluids (Joseph and Liao [105]) is a theory where flow is irrotational but viscosity is not zero. This theory has been applied to study the various interfacial stability problems. Funada and Joseph [79-80] studied capillary instability using the potential flow theory. Kim et al. [115] included the heat transfer effect to the stability of viscous-viscous fluids in an annular configuration. The interfacial instability with heat transport is studied by various authors in the literature ([19, 20, 75, and 102]) but these studies include viscous-viscous fluid interface or an Oldroyd B type viscoelastic fluid. Some authors [36, 226] considered the power-law viscoelastic fluid but in these cases second fluid was inviscid.

To the best of the author's knowledge, there is no study available in the literature for interfacial instability involving Rivlin-Ericksen fluid and heat transfer. This is an attempt to study the stability of the interface in an annular region along with heat transport. The fluid in the internal part is taken as a viscous fluid and the external part is filled with Rivlin-Ericksen viscoelastic fluid. The potential flow theory of viscous-viscoelastic fluids is applied and a relationship in terms of perturbation's growth is established. The mathematical modeling is presented in section 2 and conditions at the boundary and interface are written. The normal mode theory and linear perturbed equations are achieved in section 3 and section 4 contains a dispersion relationship. The obtained results are discussed in section 5. The key results are concluded in section 6.

2.2 MATHEMATICAL MODEL AND BOUNDARY CONDITIONS

As shown in figure 2.1, we consider a layer of viscous incompressible fluid of density ρ_i and viscosity μ_i surrounded by a Rivlin-Ericksen incompressible viscoelastic fluid layer of density ρ_o, viscosity μ_o , and viscoelasticity μ_o'. These

layers are confined in an annular region enclosed by two concentric cylinders of radii r_i and $r_o (r_i < r_o)$. The viscous fluid layer is at the temperature T_i, and the temperature of the viscoelastic fluid layer is T_o. The cylindrical surface $r = R$ separates the viscoelastic and viscous fluids. Initially, the fluid phases are in thermal equilibrium and the interfacial tension is denoted by σ.

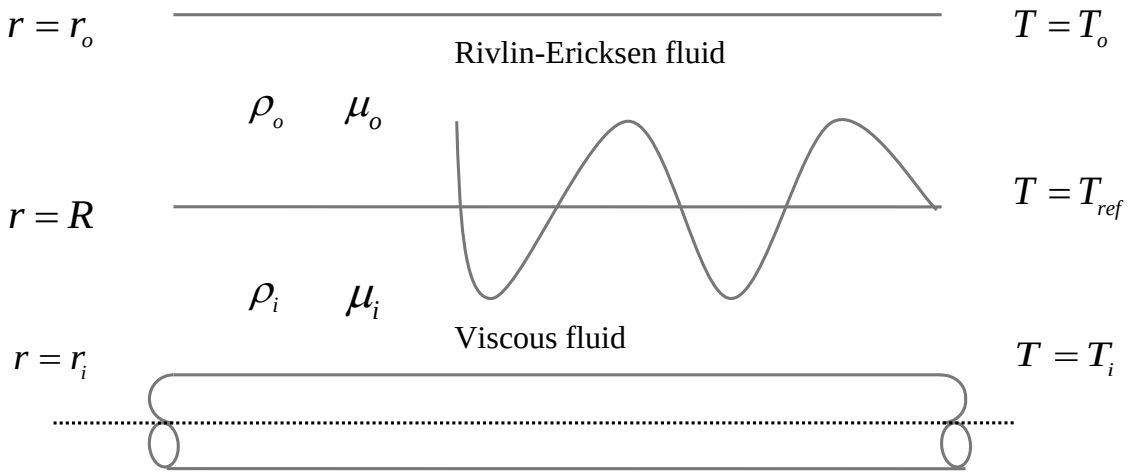

Figure 2.1: Flow diagram

If $\vec{q}_i = (u_{r,i}, u_{\theta,i}, u_{z,i})$ and $\vec{q}_o = (u_{r,o}, u_{\theta,o}, u_{z,o})$ are the velocities in the fluid phases, the mathematical equations describing fluid motion in these phases can be expressed as (Kim et al. [115])

$$\left.\begin{aligned} &\nabla \bullet \vec{q}_i = 0 \\ &\rho_i \left(\frac{\partial \vec{q}_i}{\partial t} + (\vec{q}_i \bullet \nabla)\vec{q}_i \right) = -\nabla p_i + \mu_i \nabla^2 \vec{q}_i \end{aligned}\right\} \tag{2.1}$$

$$\left.\begin{aligned} &\nabla \bullet \vec{q}_o = 0 \\ &\rho_o \left(\frac{\partial \vec{q}_o}{\partial t} + (\vec{q}_o \bullet \nabla)\vec{q}_o \right) = \nabla \bullet \boldsymbol{\tau} \end{aligned}\right\} \tag{2.2}$$

If pressure is denoted by p, μ is the dynamic viscosity and the normal stress moduli are α_1, α_2, the Cauchy stress tensor $\boldsymbol{\tau}$ for a Rivlin-Ericksen fluid can be written as (Rivlin and Ericksen [181])

$$\boldsymbol{\tau} = -p\boldsymbol{I} + \mu\boldsymbol{D_1} + \alpha_1\boldsymbol{D_2} + \alpha_2\boldsymbol{D_1^2} \tag{2.3}$$

Here, $\boldsymbol{D_1}$ and $\boldsymbol{D_2}$ are order 1 and 2 Rivlin-Ericksen tensor, respectively, given by

$$\boldsymbol{D_1} = \nabla\vec{\boldsymbol{q}} + (\nabla\vec{\boldsymbol{q}})^T \; ; \; \boldsymbol{D_2} = \frac{D\boldsymbol{D_1}}{Dt} + (\nabla\vec{\boldsymbol{q}})\boldsymbol{D_1} + \boldsymbol{D_1}(\nabla\vec{\boldsymbol{q}})^T \tag{2.4}$$

D/Dt denotes material derivative and $\vec{\boldsymbol{q}}$ is the velocity of the Rivlin-Ericksen fluid.

There will be no radial flow across the cylindrical surfaces as these boundaries are rigid, and therefore (Awasthi [19]),

$$\left.\begin{aligned} u_{r,i} &= 0 \quad \text{at} \quad r = r_i \\ u_{r,o} &= 0 \quad \text{at} \quad r = r_o \end{aligned}\right\} \tag{2.5}$$

It is assumed that the interface is transferring heat along with mass from the viscoelastic fluid phase to the viscous fluid phase and vice versa. There is no source or sink available at the interface and therefore mass transferred from the inner phase to the outer phase is the same as the mass transferred from the outer to inner phase. The mathematical equation for mass transport is given by (Hsieh [99])

$$\rho_i\left(\frac{df}{dt} + \vec{\boldsymbol{q}}_i \cdot \nabla f\right) = \rho_o\left(\frac{df}{dt} + \vec{\boldsymbol{q}}_o \cdot \nabla f\right) \tag{2.6}$$

here $f = f(r,\theta,z,t)$ represents the interfacial equation.

For the heat transport equation at the interface, the model accepted by Awasthi [19] is followed.

The heat transport equation is mathematically written as

$$L\rho_o\left(\frac{df}{dt} + \vec{\boldsymbol{q}}_o \cdot \nabla f\right) = H(r) = \frac{\kappa_o(T_{ref} - T_o)}{r[\ln r_o - \ln r]} - \frac{\kappa_i(T_i - T_{ref})}{r[\ln r - \ln r_i]} \tag{2.7}$$

At the interface, the forces exerted by interfacial tension neutralize the normal viscous stresses (Awasthi et al. [36]). Mathematically, we can write

$$\left(p_o - 2\left(\mu_o + \mu_o' \frac{\partial}{\partial t}\right)\frac{\partial u_{r,o}}{\partial r}\right) - \left(p_i - 2\mu_i \frac{\partial u_{r,i}}{\partial r}\right) = \sigma\left(\frac{1}{R_1} + \frac{1}{R_2}\right) \tag{2.8}$$

2.3 STABILITY INVESTIGATION

2.3.1 Basic state

Initially (at $r = R$), the fluids are at rest i.e. $\vec{q}_i = (0,0,0)$ and $\vec{q}_o = (0,0,0)$. Hence, there is no transfer of heat and mass in the basic state. Also, from equation (8), $p_o = p_i = c$.

2.3.2 Perturbed state

For the investigation of the stability of the interface, a small disturbance is employed and the interfacial equation changes to $r - R - \xi(\theta, z, t) = 0$. The pressures and velocities in the inner and outer phases are $p_i + p_i'$, $p_o + p_o'$ and $\vec{q}_i = (u_{r,i}', u_{\theta,i}', u_{z,i}')$, $\vec{q}_o = (u_{r,o}', u_{\theta,o}', u_{z,o}')$, respectively. The mathematical perturbed equations in the linear form will be

$$\left.\begin{aligned}
&\frac{1}{r}\frac{\partial\left(ru_{r,i}'\right)}{\partial r} + \frac{1}{r}\frac{\partial u_{\theta,i}'}{\partial \theta} + \frac{\partial u_{z,i}'}{\partial z} = 0 \\
&\rho_i \frac{\partial u_{r,i}'}{\partial t} = -\frac{\partial p_i'}{\partial r} + \mu_i \nabla^2 u_{r,i}' \\
&\rho_i \frac{\partial u_{\theta,i}'}{\partial t} = -\frac{1}{r}\frac{\partial p_i'}{\partial \theta} + \mu_i \nabla^2 u_{\theta,i}' \\
&\rho_i \frac{\partial u_{z,i}'}{\partial t} = -\frac{\partial p_i'}{\partial z} + \mu_i \nabla^2 u_{z,i}'
\end{aligned}\right\} \tag{2.9}$$

$$\left.\begin{aligned}
&\frac{1}{r}\frac{\partial\left(ru_{r,o}'\right)}{\partial r} + \frac{1}{r}\frac{\partial u_{\theta,o}'}{\partial \theta} + \frac{\partial u_{z,o}'}{\partial z} = 0 \\
&\rho_o \frac{\partial u_{r,o}'}{\partial t} = -\frac{\partial p_o'}{\partial r} + \left(\mu_o + \mu_o' \frac{\partial}{\partial t}\right)\nabla^2 u_{r,o}' \\
&\rho_o \frac{\partial u_{\theta,o}'}{\partial t} = -\frac{1}{r}\frac{\partial p_o'}{\partial \theta} + \left(\mu_o + \mu_o' \frac{\partial}{\partial t}\right)\nabla^2 u_{\theta,o}' \\
&\rho_o \frac{\partial u_{z,o}'}{\partial t} = -\frac{\partial p_o'}{\partial z} + \left(\mu_o + \mu_o' \frac{\partial}{\partial t}\right)\nabla^2 u_{z,o}'
\end{aligned}\right\} \tag{2.10}$$

The boundary conditions in the perturbed state can be expressed as follows

$$\left.\begin{array}{lll} u'_{r,i} = 0 & \text{at} & r = r_i \\ u'_{r,o} = 0 & \text{at} & r = r_o \end{array}\right\} \tag{2.11}$$

The linear form of mass transport, and heat transport conditions in the perturbed state, are described as

$$\rho_i\left(u'_{r,i} - \frac{\partial \xi}{\partial t}\right) = \rho_o\left(u'_{r,o} - \frac{\partial \xi}{\partial t}\right) \tag{2.12}$$

$$\rho_o\left(u'_{r,o} - \frac{\partial \xi}{\partial t}\right) = \alpha\xi \tag{2.13}$$

where $\alpha = H'(R)/L$

The viscous normal stress balance at $r = R$ in linear form is written as

$$\left(p'_o - 2\left(\mu_o + \mu'_o \frac{\partial}{\partial t}\right)\frac{\partial u'_{r,o}}{\partial r}\right) - \left(p'_i - 2\mu_i \frac{\partial u'_{r,i}}{\partial r}\right) = \sigma\left(\frac{\partial^2 \xi}{\partial z^2} + \frac{1}{R^2}\frac{\partial^2 \xi}{\partial \theta^2} + \frac{\xi}{R^2}\right) \tag{2.14}$$

2.4 DISPERSION RELATIONSHIP

To get the analytical solutions to the above equations, we use the concept of potential flow. In the perturbed state, the perturbed velocities will be expressed as the gradient of potential functions i.e. $\vec{q}_i = \nabla\Phi_i$ and $\vec{q}_o = \nabla\Phi_o$.

Introducing the potential functions in the equations (2.9) and (2.10), it can be easily verified that these potential functions are harmonic i.e.

$$\nabla^2\Phi_i = 0; \quad \nabla^2\Phi_o = 0 \tag{2.15}$$

The well-known normal mode theory is used to study the instability of the interface. Hence, the perturbed state function $\mathrm{E}'(r,\theta,z,t)$ will be

$\mathrm{E}'(r,\theta,z,t) = E(r)\exp(-i\omega t + in\theta + ikz)$ and $\xi(\theta,z,t) = \mathrm{P}\ \exp(-i\omega t + in\theta + ikz)$

The expressions of Φ_i and Φ_o can be achieved using boundary conditions (2.11) and interfacial conditions (2.12) and (2.13). These expressions are given as follows;

$$\Phi_i = \frac{1}{k}\left(-i\omega + \frac{\alpha}{\rho_i}\right) A_i(kr)\ \mathrm{P}\ \exp(-i\omega t + in\theta + ikz) \tag{2.16}$$

$$\Phi_o = \frac{1}{k}\left(-i\omega + \frac{\alpha}{\rho_g}\right) A_o(kr)\ \mathrm{P}\ \exp(-i\omega t + in\theta + ikz) \tag{2.17}$$

$$A_i(kr) = \frac{I_n(kr)K_n'(kr_i) - I_n'(kr_i)K_n(kr)}{I_n'(kR)K_n'(kr_i) - I_n'(kr_i)K_n'(kR)},\quad A_o(kr) = \frac{I_n(kr)K_n'(kr_o) - I_n'(kr_o)K_n(kr)}{I_n'(kR)K_n'(kr_o) - I_n'(kr_o)K_n'(kR)}$$

As the flow is irrotational, the pressure in equation (2.14) can be achieved using Bernoulli's equation. Also, $u_{r,i} = \partial\Phi_i/\partial r$ and $u_{r,o} = \partial\Phi_o/\partial r$. Retaining linear terms in the Bernoulli's equation, equation (14) can be expressed as;

$$\left(\rho_o \frac{\partial\Phi_o}{\partial t} + 2\left(\mu_o + \mu_o' \frac{\partial}{\partial t}\right)\frac{\partial^2\Phi_o}{\partial r^2}\right) - \left(\rho_i \frac{\partial\Phi_i}{\partial t} + 2\mu_i \frac{\partial^2\Phi_i}{\partial r^2}\right) = -\sigma\left(\frac{\partial^2\xi}{\partial z^2} + \frac{1}{R^2}\frac{\partial^2\xi}{\partial\theta^2} + \frac{\xi}{R^2}\right) \tag{2.18}$$

The values of Φ_i and Φ_o will be inserted in the above equation and the dispersion relationship can be achieved. The relationship can be expressed as

$$q_1\omega^2 + iq_2\omega - q_3 = 0 \tag{2.19}$$

where $q_1 = \rho_i A_i(kR) - \rho_o A_o(kR) - 2\mu_o' k^2 B_o(kR)$

$$q_2 = \alpha\left(A_i(kR) - A_o(kR)\right) + 2k^2\left(\mu_i B_i(kR) - \mu_o B_o(kR)\right) - 2\frac{\mu_o'}{\rho_o}\alpha k^2 B_o(kR)$$

$$q_3 = 2\alpha k^2\left(\frac{\mu_i}{\rho_i}B_i(kR) - \frac{\mu_o}{\rho_o}B_o(kR)\right) + \frac{\sigma k}{R^2}\left(k^2R^2 + n^2 - 1\right)$$

$$B_i(kR) = \left(1 + \frac{n^2}{k^2R^2}\right)A_i(kR) - \frac{1}{kR},\quad B_o(kR) = \left(1 + \frac{n^2}{k^2R^2}\right)A_o(kR) - \frac{1}{kR}$$

The dispersion relationship presented by Kim et al. [115] can be recovered by setting viscoelasticity $\mu_o' = 0$ in equation (2.19) as they have studied the effect of heat transport on the viscous-viscous fluid interface.

If V is assumed as characteristic velocity and $H = r_o - r_i$ is taken as characteristic length, the dimensionless form of equation (2.19) is achieved as

$$\hat{q}_1\hat{\omega}^2 + i\hat{q}_2\hat{\omega} - \hat{q}_3 = 0 \tag{2.20}$$

where $\hat{q}_1 = \rho A_i(\hat{k}\hat{R}) - A_o(\hat{k}\hat{R}) - 2\lambda_o\hat{k}^2 B_o(\hat{k}\hat{R})$

$$\hat{q}_2 = \hat{\alpha}\left(A_i(\hat{k}\hat{R}) - A_o(\hat{k}\hat{R})\right) + 2\hat{k}^2\frac{Ca}{We}\left(\mu B_i(\hat{k}\hat{R}) - B_o(\hat{k}\hat{R})\right) - 2\lambda_o\hat{\alpha}\hat{k}^2 B_o(\hat{k}\hat{R})$$

$$\hat{q}_3 = 2\hat{\alpha}\hat{k}^2\frac{Ca}{We}\left(\kappa B_i(\hat{k}\hat{R}) - B_o(\hat{k}\hat{R})\right) + \frac{\hat{k}}{\hat{R}^2}\frac{1}{We}\left(\hat{k}^2\hat{R}^2 + n^2 - 1\right)$$

The capillary number is defined as $Ca = \frac{\mu_o V}{\sigma}$, the Weber number $We = \frac{\rho_o V^2 H}{\sigma}$, density ratio $\rho = \frac{\rho_i}{\rho_o}$, viscosity ratio $\mu = \frac{\mu_i}{\mu_o}$, $\kappa = \frac{\mu}{\rho}$, and non-dimensional heat transfer coefficient $\hat{\alpha} = \frac{\alpha H}{V\rho_o}$.

Here, $\hat{\omega}$ is a complex quantity i.e. $\hat{\omega} = \hat{\omega}_r + i\hat{\omega}_i$ and the interface will be unstable only when $\hat{\omega}_i > 0$. Equation (2.19) can be separated as

$$\hat{q}_1\left(\hat{\omega}_r^2 - \hat{\omega}_i^2\right) - \hat{q}_2\hat{\omega}_i - \hat{q}_3 = 0 \tag{2.21}$$

$$2\hat{q}_1\hat{\omega}_r\hat{\omega}_i + \hat{q}_2\hat{\omega}_r = 0 \tag{2.22}$$

It must be noted from equation (2.22) that $\hat{\omega}_i = -\hat{q}_2/2\hat{q}_1$ or $\hat{\omega}_r = 0$. As densities and viscosities are always positive and the properties of modified Bessel's functions tell us that $\hat{q}_1, \hat{q}_2$ both will be positive, and therefore if we take $\hat{\omega}_i = -\hat{q}_2/2\hat{q}_1$, the system will always be stable. Here, we are discussing the instability of the interface and therefore we take $\hat{\omega}_r = 0$. Hence, equation (2.21) takes the form as

$$\hat{q}_1\hat{\omega}_i^2 + \hat{q}_2\hat{\omega}_i + \hat{q}_3 = 0 \tag{2.23}$$

Now, from equation (2.22), it should be noted that ω_i is positive only when $\hat{q}_3 > 0$. The neutral stability criterion can be expressed as $\hat{q}_3 = 0$ i.e.

$$2\hat{\alpha}\hat{k}\hat{R}^2 Ca\left(\kappa B_i(\hat{k}\hat{R}) - B_o(\hat{k}\hat{R})\right) + \left(\hat{k}^2\hat{R}^2 + n^2 - 1\right) = 0 \tag{2.24}$$

As $\hat{k}$ is wave number and it should be positive but if $n \geq 1$, equation (2.24) does not possess positive solutions. Hence, for numerical computation, axisymmetric perturbations $(n = 0)$ are considered.

2.5 Results and Discussions

The numerical computation based on equations (2.23) and (2.24) for symmetric perturbations $(n = 0)$ is presented here. Equation (2.23) is a second-order algebraic equation and for a particular set of values, we will get two values of $\hat{\omega}_I$. The highest value is plotted here for the growth rate. Equation (2.24) is an implicit equation and the Newton-Raphson procedure is employed to compute the wave number. The region above the wave number curve is the stable region while the below region is unstable. The values are considered for the numerical calculation is given in Table 2.1.

The growth of perturbations on the viscous-viscous fluid interface and Rivlin-Ericksen (R-E)-viscous fluid interface are shown in figure 2.2. The maximum growth rate for non-dimensional heat transfer coefficient $\hat{\alpha}$ is displayed for viscoelasticity $\lambda_o = 0.0$ and $\lambda_o = 0.2$. The values of perturbations maximum growth is given in Table 2.2. If viscoelasticity is zero i.e. $\lambda_o = 0.0$, the RE fluid will behave like a Newtonian viscous fluid. It should be noted that the perturbation's maximum growth for the viscous-viscous fluid interface is higher than the interface involving RE fluid and therefore, one can say the viscoelasticity of the RE fluid slows the movement of perturbations at the interface. The force due to the elasticity of the fluid produces acceleration which slows the speed of the perturbation at the interface. It can also be seen that as $\hat{\alpha}$ increases, the perturbation's growth decreases indicating that heat transfer has stabilizing character. The growth rate behavior is similar for both interfaces but for higher values of heat transfer, the perturbation's growth coincides.

The viscoelasticity effect on the R-E-viscous fluid interface is shown in figure 2.3. Here, the perturbation's maximum growth for the viscoelasticity of R-E fluid is plotted for heat transfer coefficient $\hat{\alpha} = 0.0$ and $\hat{\alpha} = 0.1$. The values of perturbations maximum growth is given in Table 2.3. As the viscoelasticity λ_o increases, the perturbation's growth decreases and remains the same whether the interface transfers heat or not. This also proves that heat transfer does not change the nature of viscoelasticity, but in the presence of heat transfer, the flow of perturbation decreases, which shows that the transfer of heat prevents the interface from becoming unstable. Viscoelasticity is the root cause of the temporary connections between particles such as fibers. Many polymers have long molecules and those molecules make temporary connections with their neighbors, hence polymers show viscoelastic behavior. As the

viscoelasticity increases, the connection between the molecules becomes stronger so that the disturbance cannot travel easily, and hence the behavior of the viscoelasticity is stabilizing.

The marginal stability curves of wave number for various values of capillary number Ca are shown in figure 2.4. The region below the curve shows the unstable region while the above region is stable. The stable region increases on increasing the capillary number Ca showing the stabilizing nature of capillary number. As capillary number depends directly on the viscosity of R-E fluid and inversely on surface tension and therefore, R-E fluid viscosity has to stabilize nature while surface tension will make the free surface unstable. As the viscosity of R-E fluid increases, the flow impedes, and therefore, the instability delays. The surface tension produces surface forces that are responsible for the breakup. The increment in surface tension increases the magnitude of such forces and therefore, instability occurs early.

The transport of heat through the interface makes a strong impact on the instability of the interface. Figure 2.5 depicts the behavior of wave-number curves for various values of non-dimensional heat transfer coefficient $\hat{\alpha}$. It is found that the stable region enlarges if the transfer of heat increases through the interface. Hence, $\hat{\alpha}$ has stabilizing nature. Kim et al. [115] and Awasthi [19, 36] also found the same character of heat transport on the interface in an annular region. Hence, one can say that viscoelasticity has no impact on the character of heat transport i.e. heat transport has stabilizing character. The theory of evaporation and condensation can explain this effect. The R-E fluid is at high temperature than the viscous fluid and therefore, there will evaporation in the outer region and condensation will take place in the inner region. When transport will start, the R-E vapor condenses in the inner region and

viscous fluid evaporates in the outer region. This evaporation/condensation will create a hindrance for perturbations and instability delays.

In figure 2.6, the influence of the thickness of R-E fluid on the neutral curves of wave numbers is shown. The configuration is taken in such a way that the R-E fluid lies in the outer region and the viscous fluid is in the inner region. As the R-E fluid thickness increases, the stable region decreases indicating that the thickness of R-E fluid induces instability in the system. On increasing the R-E fluid thickness, evaporation will increase but as the viscous fluid layer is fixed, condensation will remain the same. This one-sided evaporation will increase the amplitude of perturbations and they will travel faster. Hence, an interface with a thin R-E fluid layer is more stable than a thick R-E fluid layer.

Weber number is one of the important non-dimensional numbers for the capillary flow. The variation of Weber's number is shown in figure 2.7. Here, the perturbation's maximum growth is displayed. As the Weber number increases, the perturbation's growth decreases suggesting the stabilizing character of the Weber number. The ratio of inertia force to the surface tension force is known as the Weber number and therefore, one can say that inertia force makes stabilizing impact on the interface while surface tension has destabilizing nature. Generally, inertia force produces by the density of the fluid and therefore, the density of the R-E fluid induces stability to the system. The perturbations take more time to travel in a more dense fluid than the less dense fluid and instability delays. Hence, the interface involving high dense R-E fluid is more stable.

2.6 Conclusions

The stability of the Rivlin-Ericksen fluid-viscous fluid interface is investigated theoretically when the interface is transporting heat and mass. The investigation is based on the potential flow theory of viscoelastic/viscous fluids and the normal mode theory is applied to compute the stability of the interface. The two-degree equation in terms of perturbation's growth rate is established and analyzed. The results expose that the stability of the arrangement is enhanced with the increasing transfer of heat, while a reverse accomplish is detected with surface tension. The viscoelasticity of the R-E fluid shows stabilizing character, whether the heat is transferring or not. The density and viscosity of R-E fluid induce stability in the system. It has also been shown that the transfer of heat does not change the nature of viscoelasticity.

Table 2.1: Parameters values for numerical computation

Parameter	values
ρ	0.01
μ	0.001
Ca	0.07
We	0.7
$\hat{\alpha}$	0.01
λ_o	0.2
ϕ	0.5

Table 2.2: Variation of perturbations growth with heat transfer coefficient $\hat{\alpha}$

heat transfer coefficient $\hat{\alpha}$	Maximum growth $(\hat{\omega}_1)_{max}$ when $\lambda_0 = 0.0$	Maximum growth $(\hat{\omega}_1)_{max}$ when $\lambda_0 = 0.2$
0.001	0.1952	0.1850
0.002	0.1941	0.1839
0.003	0.1929	0.1828
0.004	0.1917	0.1818
0.005	0.1906	0.1807
0.006	0.1895	0.1796
0.007	0.1883	0.1785
0.008	0.1872	0.1775
0.009	0.1861	0.1764
0.010	0.1850	0.1754

Table 2.3: Variation of perturbations maximum growth with viscoelasticity λ_0

viscoelasticity λ_0	Maximum growth $(\hat{\omega}_1)_{\max}$ when $\hat{\alpha} = 0.0$	Maximum growth $(\hat{\omega}_1)_{\max}$ when $\hat{\alpha} = 0.10$
0.1	0.1910	0.1080
0.2	0.1862	0.1054
0.3	0.1817	0.1030
0.4	0.1777	0.1007
0.5	0.1740	0.0986
0.6	0.1706	0.0966
0.7	0.1674	0.0947
0.8	0.1644	0.0929
0.9	0.1616	0.0912
1.0	0.1590	0.0897

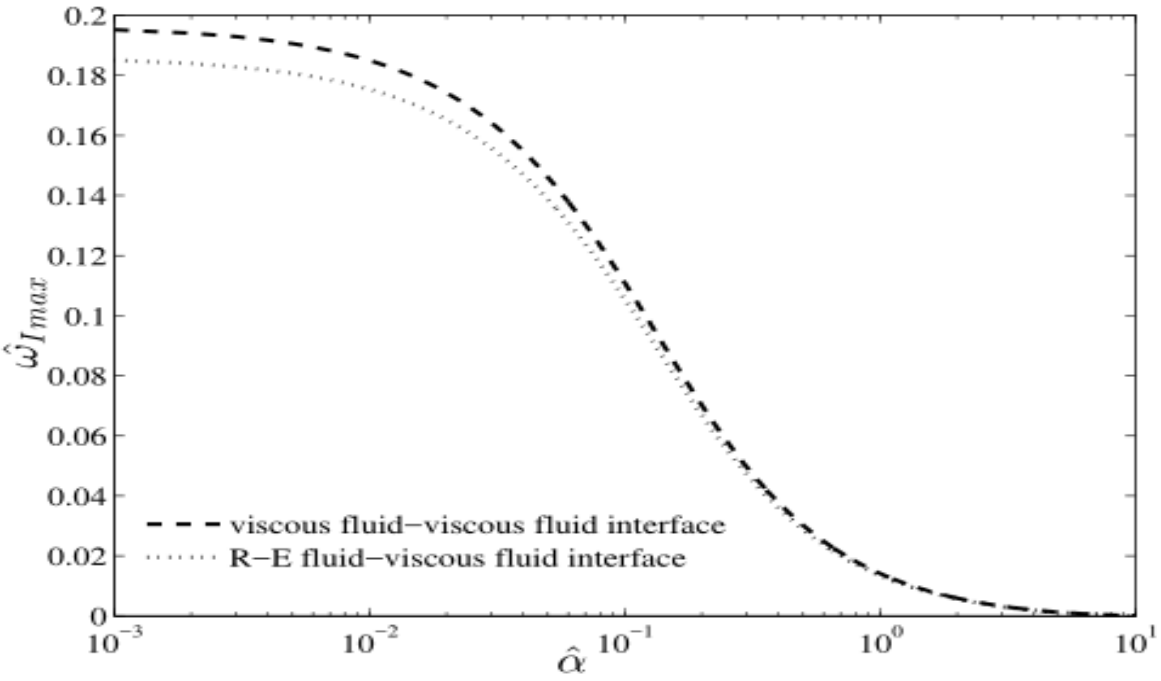

Figure 2.2: Comparison of perturbation's maximum growth for $\lambda_o = 0.0$ and $\lambda_0 = 0.2$. $(\phi = 0.5, Ca = 0.007, We = 0.7, \rho = 0.01, \mu = 0.001)$

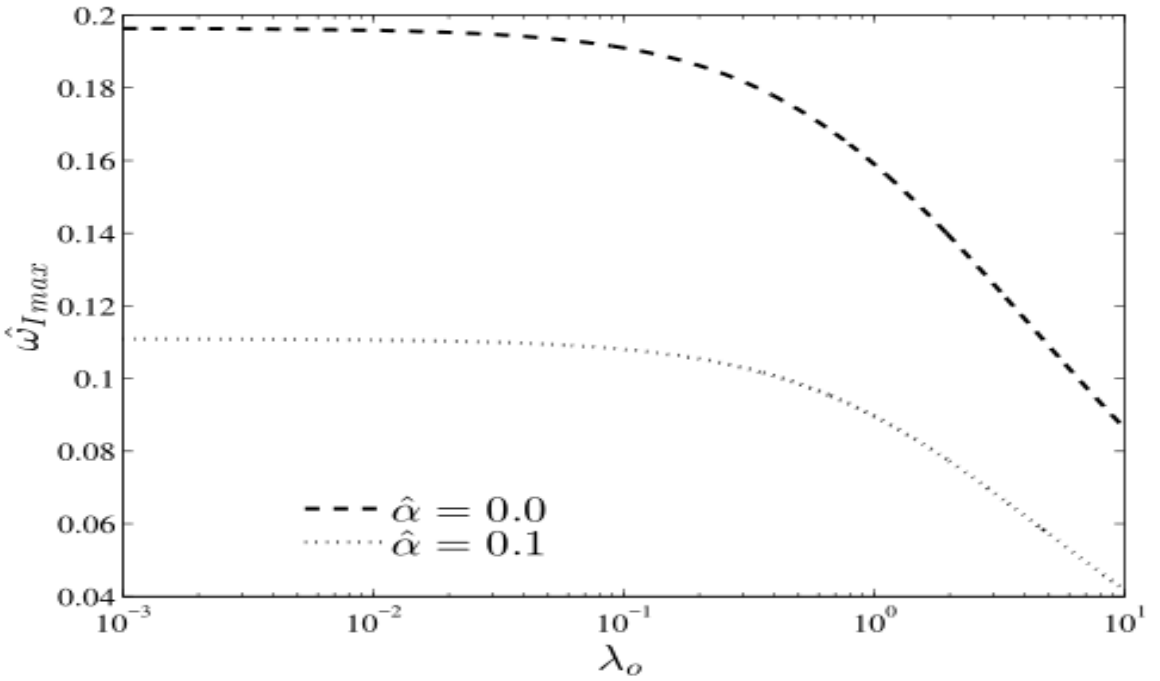

Figure 2.3: Effect of viscoelasticity for $\hat{\alpha} = 0.0$ and $\hat{\alpha} = 0.1$.
$(\phi = 0.5, Ca = 0.007, We = 0.7, \rho = 0.01, \mu = 0.001)$

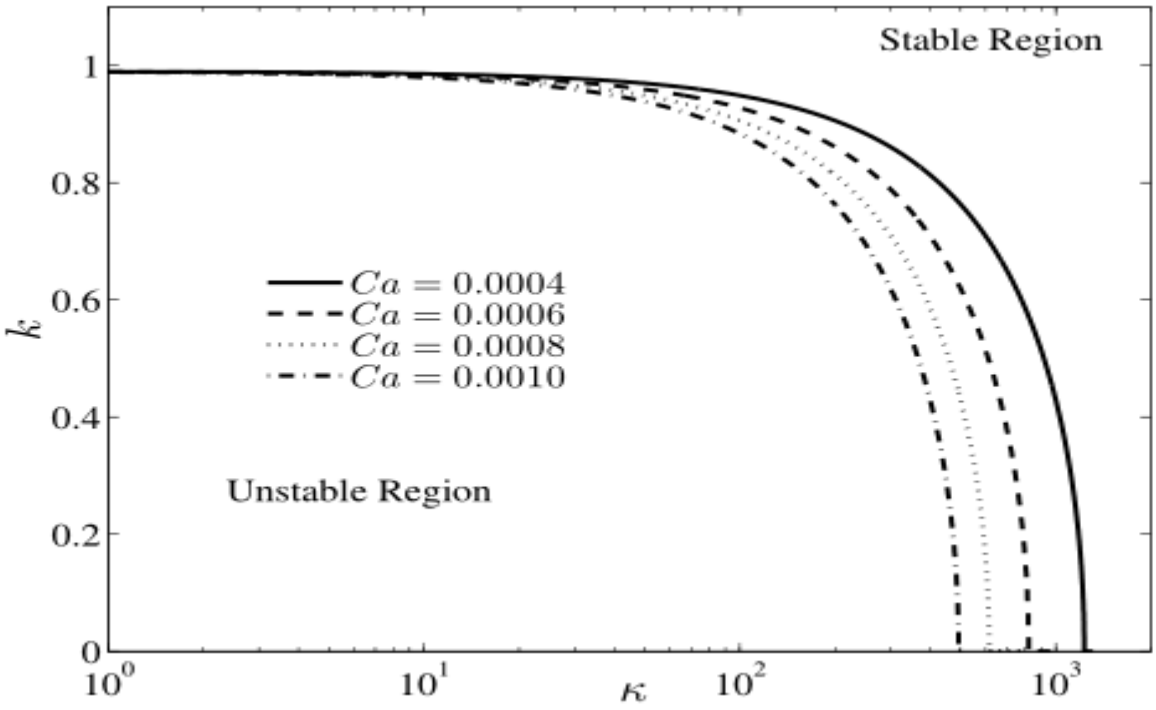

Figure 2.4: Effect of Capillary number $Ca.(\phi = 0.01, \hat{\alpha} = 0.01)$

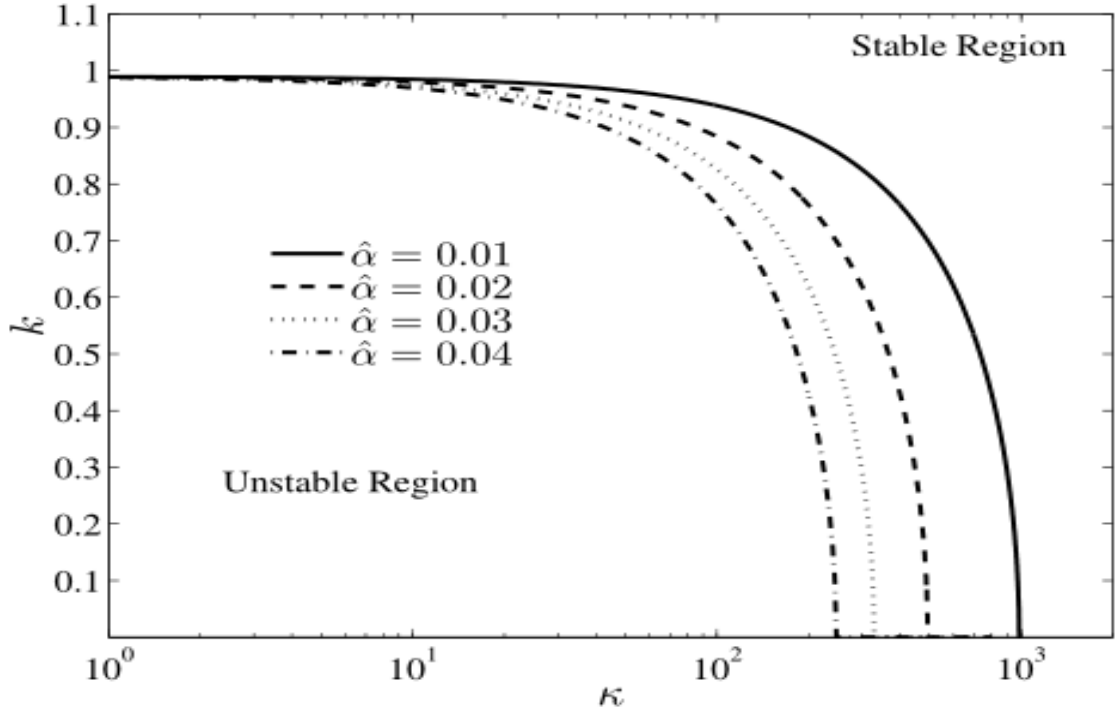

Figure 2.5: Effect of heat transfer $\hat{\alpha}.(\phi = 0.01, Ca = 0.0005)$

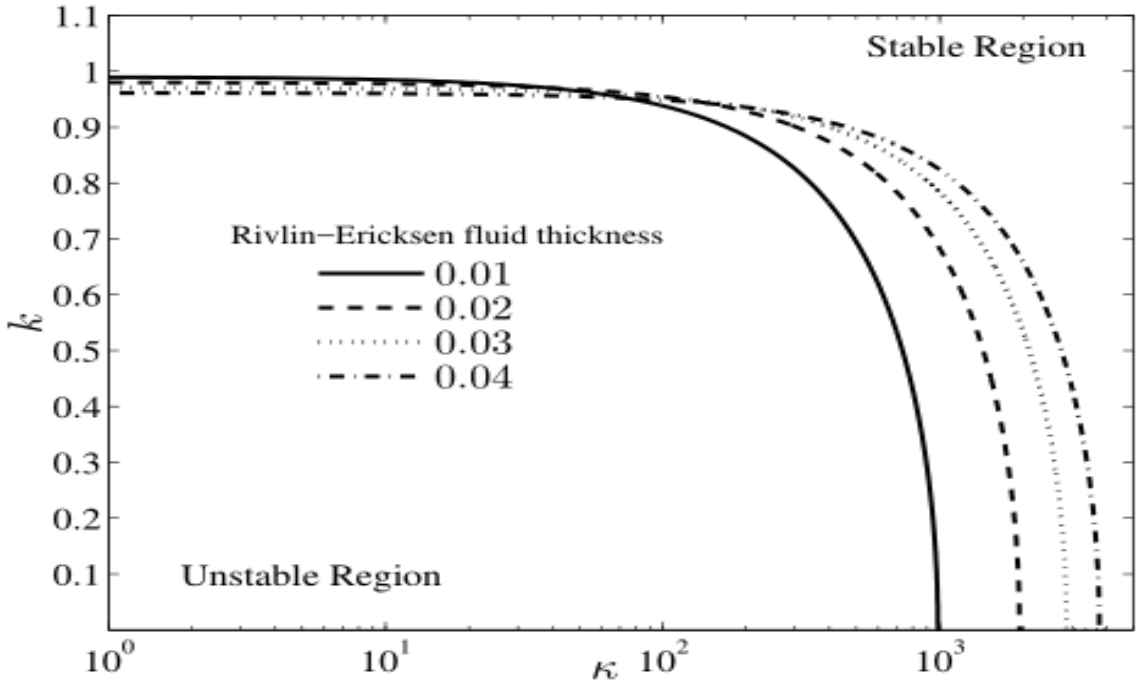

Figure 2.6: Effect of R-E fluid thickness. ($\hat{\alpha} = 0.01, Ca = 0.0005$)

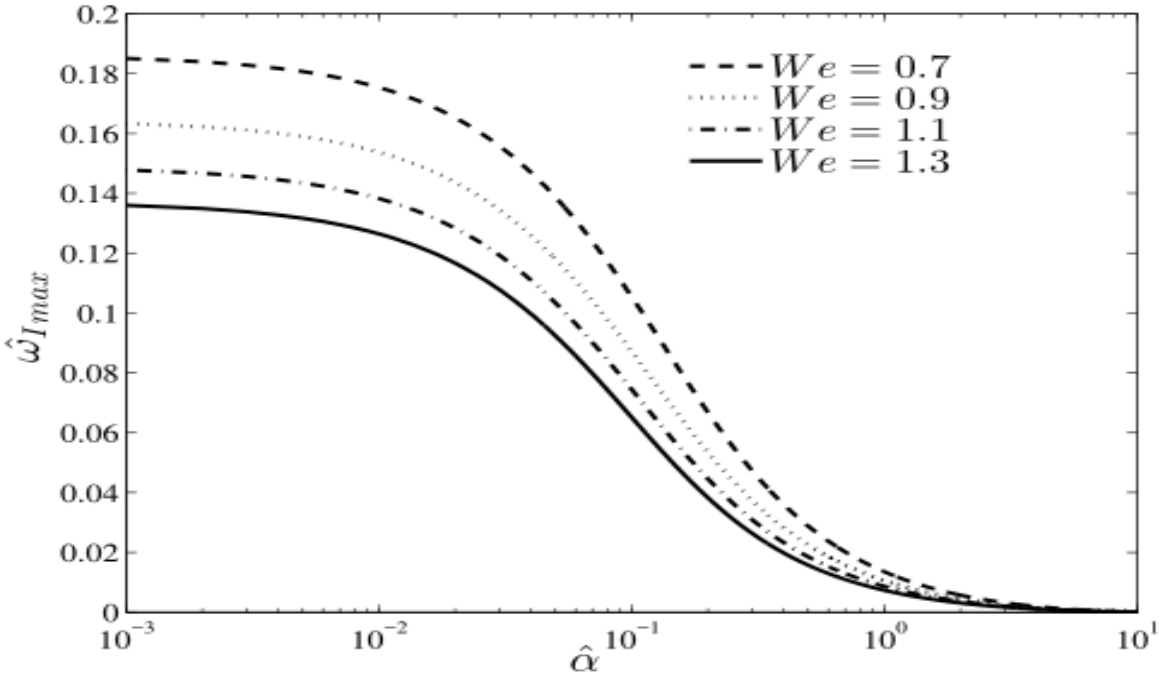

Figure 2.7: Effect of Weber number *We.*

($\phi = 0.5, Ca = 0.007, \rho = 0.01, \mu = 0.001, \lambda_o = 0.2$)

CHAPTER 3

CAPILLARY INSTABILITY OF WALTER'S B VISCOELASTIC FLUID FILM

The stability of an interface formed by Walter' B viscoelastic liquid and viscous incompressible fluid is examined. These fluids lie in an annular region enclosed by two cylindrical shapes rigid boundaries. The surface tension effect is considered at the interface and therefore, the interface obeys capillary instability. The potential flow theory of viscoelastic-viscous fluids is utilized to compute the solution of modeled equations and the normal mode technique is enforced for the calculation of perturbation's growth. A two-degree algebraic equation is established to obtain the stability/instability criterion. We found that the perturbations grow slower at the interface containing Walter's B viscoelastic fluid than the corresponding Newtonian fluid.

3.1 BACKGROUND

When a liquid cylinder falls into another fluid, the capillary forces arise due to surface tension make the interface of the fluids unstable. This type of instability is called capillary instability and this instability can be seen in the liquid jet breakup, film boiling, etc.

The first study of instability of a liquid cylindrical column of the radius R with the effect of capillary forces was done by Plateau [171]. He showed that the liquid cylinder is unstable for those perturbations who have wavelengths more than $2\pi R$. Rayleigh [174] also studied the stability of the liquid cylinder using potential flow theory but he ignores the effect of outside liquid. Rayleigh [176] added the viscous effect into his previous analysis but he again neglected the outside fluid

effect. The effect of outside fluid on the instability of a liquid cylinder was included by Weber [227]. Tomotika [211] studied the stability of a viscous liquid cylinder into another viscous fluid. He achieved the dispersion relation for fully viscous fluids in the case of axisymmetric perturbations.

The Navier-Stokes equation reduces to Euler's equation of motion when the flow is potential but viscosity is not zero. Joseph and Liao [105] presented a potential flow theory that includes viscosity into the free surface problems. Funada and Joseph [79] studied instability of viscous liquid cylinder surrounded by a viscous fluid utilizing potential flow theory. They found that the potential flow theory gives very good agreement with fully viscous results.

The capillary instability of an Oldroyd B viscoelastic fluid surrounded by a viscous fluid was investigated by Funada and Joseph [80]. They applied the potential flow theory and achieved a cubic equation for the perturbation growth. Awasthi et al. [30] examined the breakup of the viscoelastic jet of Oldroyd B fluid with the help of potential flow theory. They found that the growth of perturbations for viscoelastic fluids is larger than the Newtonian fluids but smaller than the inviscid fluids.

The instability of the interface containing Walter's B viscoelastic fluid was examined by Kumar and Singh [127]. They formulated Rayleigh-Taylor instability and established a certain condition for stability. The Kelvin-Helmholtz instability of Walter's B fluid was carried out by El-Sayed et al. [71]. They considered the flow region porous and the normal electric field was applied. The effect of porous media, elasticity, suction/injection, in the flow of Walters' B visco-elastic fluids was studied by Barik et al. [41]. These studies are limited to inviscid fluids. The only study was

done by Moatimid and Zekry [156] for Walters' B visco-elastic fluids includes viscosity into the analysis along with viscoelasticity.

In this chapter, we attempted to study the instability of Walter's B viscoelastic fluid surrounded by a viscous fluid. The potential flow theory is used and interfacial condition includes the viscosity of both the fluids. The fluids are confined in an annular region bounded by rigid cylindrical boundaries. The effect of gravity is neglected at the interface while the interface is experiencing a surface tension effect. The well-known normal mode technique is applied and an algebraic equation for the growth of perturbations is obtained. The instability is discussed through various plots.

3.2 MATHEMATICAL STATEMENT OF THE PROBLEM

As shown in figure 3.1, we consider a cylindrical layer of Walter's B viscoelastic fluid of viscosity μ_i, viscoelasticity μ_i', and density ρ_i surrounded by a viscous fluid of viscosity μ_o and density ρ_o. The surface tension at the interface is σ. The viscous fluid is bounded by the outer cylinder of radius $r = r_o$ and the inner cylinder $r = r_i$ bounds viscoelastic fluid. The Walter's B viscoelastic fluid and viscous fluid are separated by the cylindrical boundary $r = R$, initially.

If the velocity in the Walter's B viscoelastic fluid phase is $\vec{\boldsymbol{q}}_i$, the governing equations for the viscoelastic fluid phase can be written as

$$\left.\begin{aligned} &\nabla \cdot \vec{\boldsymbol{q}}_i = 0 \\ &\rho_i \left(\frac{\partial \vec{\boldsymbol{q}}_i}{\partial t} + \left(\vec{\boldsymbol{q}}_i \cdot \nabla \right) \vec{\boldsymbol{q}}_i \right) = -\nabla p_i + \nabla \cdot \boldsymbol{\tau}_i \end{aligned}\right\} \tag{3.1}$$

The stress $\boldsymbol{\tau}_i$ for Walter's B viscoelastic is given by the expression

$$\boldsymbol{\tau_i} = 2\left(\mu_i - \mu_i' \frac{\partial}{\partial t}\right)\boldsymbol{D_i} \tag{3.2}$$

where $\boldsymbol{D_i} = \left((\nabla \vec{\boldsymbol{q}}_i) + (\nabla \vec{\boldsymbol{q}}_i)^T\right)$

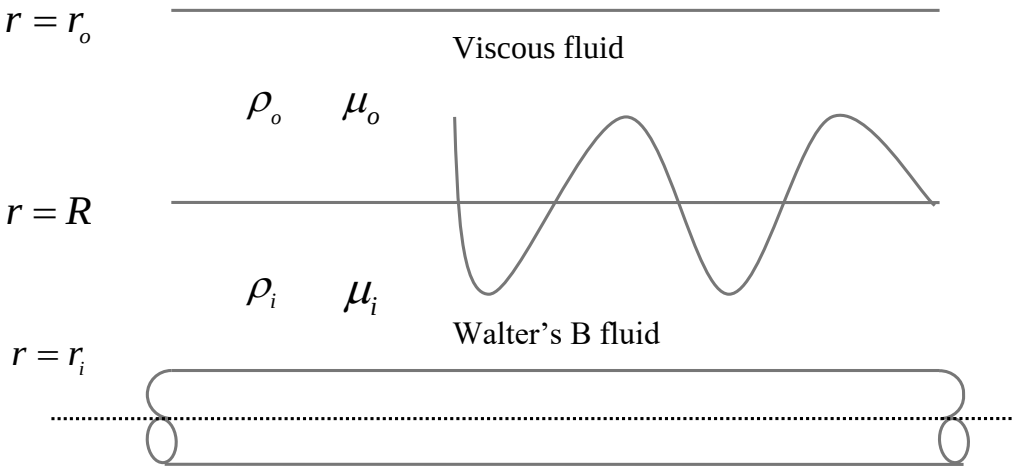

Figure 3.1: Flow diagram

If the viscous fluid has velocity $\vec{\boldsymbol{q}}_o$, the governing equations can be written as

$$\left.\begin{aligned} &\nabla \cdot \vec{\boldsymbol{q}}_o = 0 \\ &\rho_o\left(\frac{\partial \vec{\boldsymbol{q}}_o}{\partial t} + (\vec{\boldsymbol{q}}_o \cdot \nabla)\vec{\boldsymbol{q}}_o\right) = -\nabla p_o + \mu_o \nabla^2 \vec{\boldsymbol{q}}_o \end{aligned}\right\} \tag{3.3}$$

3.3 Stability Analysis

3.3.1 Basic state

Initially, the fluids are at rest in both the phases i.e. $\vec{\boldsymbol{q}}_o = (0,0,0)$ and $\vec{\boldsymbol{q}}_i = (0,0,0)$. Also, the interface is cylindrically flat in an equilibrium state and hence, $p_o = \text{constant} = p_i$.

3.3.2 Perturbed state

A small perturbation is introduced to the basic state and therefore interface is located at $r - R - \xi(\theta, z, t) = 0$. In the perturbed state, the velocities and pressures become

$\vec{q}_o = 0 + \vec{q}'_o$, $\vec{q}_i = 0 + \vec{q}'_i$ and $p_o + p'_o$, $p_i + p'_i$, respectively. The linearized perturbations equations for both the phases can be written as;

$$\left.\begin{aligned} &\nabla \cdot \vec{q}'_i = 0 \\ &\rho_i \frac{\partial \vec{q}'_i}{\partial t} = -\nabla p'_i + \nabla \cdot \boldsymbol{\tau}'_i \end{aligned}\right\} \tag{3.4}$$

$$\left.\begin{aligned} &\nabla \cdot \vec{q}'_o = 0 \\ &\rho_o \frac{\partial \vec{q}'_o}{\partial t} = -\nabla p'_o + \mu_o \nabla^2 \vec{q}'_o \end{aligned}\right\} \tag{3.5}$$

The potential flow theory of viscous fluids is used here and therefore, $\vec{q}'_o = \nabla\Phi_o$; $\vec{q}'_i = \nabla\Phi_i$. Hence form continuity equations from (3.4) and (3.5), we have

$$\nabla^2\Phi_o = 0;\ \nabla^2\Phi_i = 0 \tag{3.6}$$

3.3.3 Boundary and Interfacial Conditions

There is no flow in the perturbed state across the rigid cylindrical boundary and therefore,

$$\left.\begin{aligned} &\frac{\partial \Phi_o}{\partial r} = 0 \quad \text{at} \quad r = r_o \\ &\frac{\partial \Phi_i}{\partial r} = 0 \quad \text{at} \quad r = r_i \end{aligned}\right\} \tag{3.7}$$

Also, the normal velocity of the interface is zero. Hence,

$$\left.\begin{aligned} &\frac{\partial \Phi_o}{\partial z} = \frac{\partial \xi}{\partial t} \\ &\frac{\partial \Phi_i}{\partial z} = \frac{\partial \xi}{\partial t} \end{aligned}\right\} \quad \text{at} \quad r = R \tag{3.8}$$

3.4 Dispersion Relationship

The conventional normal mode technique is imposed to examine the stability of the interface. The interface distortion can be expressed as

$\xi(\theta,z,t)=\mathrm{P}\ \exp(ikz+in\theta-i\omega t)$ and other quantities $E(r,z,t)$ are depicted as $E(r,\theta,z,t)=f(r)\ \exp(ikz+in\theta-i\omega t)$.

The potential functions Φ_o,Φ_i satisfying conditions (3.7) and (3.8) can be expressed as

$$\Phi_i=-\frac{i\omega}{k}A_i(kr)\xi+c.c. \tag{3.9}$$

$$\Phi_o=-\frac{i\omega}{k}A_o(kr)\xi+c.c. \tag{3.10}$$

$$A_i(kr)=\frac{I_n(kr)K_n'(kr_i)-I_n'(kr_i)K_n(kr)}{I_n'(kR)K_n'(kr_i)-I_n'(kr_i)K_n'(kR)},\ A_o(kr)=\frac{I_n(kr)K_n'(kr_o)-I_n'(kr_o)K_n(kr)}{I_n'(kR)K_n'(kr_o)-I_n'(kr_o)K_n'(kR)}$$

The linearized stress balance equation at the interface containing viscosity can be expressed as

$$\left[\rho_o\left(\frac{\partial\Phi_o}{\partial t}\right)+2\mu_o\frac{\partial^2\Phi_o}{\partial r^2}\right]-\left[\rho_i\left(\frac{\partial\Phi_i}{\partial t}\right)+2\left(\mu_i-\mu_i'\frac{\partial}{\partial t}\right)\frac{\partial^2\Phi_i}{\partial r^2}\right]=-\sigma\left(\frac{\partial^2\xi}{\partial z^2}+\frac{1}{R^2}\frac{\partial^2\xi}{\partial\theta^2}+\frac{\xi}{R^2}\right) \tag{3.11}$$

The dispersion relationship can be obtained by using equations (3.9) and (3.10) into (3.11). This expression is given as

$$q_1\omega^2+q_2i\omega+q_3=0 \tag{3.12}$$

$$q_1=\rho_iA_i(kr)-\rho_oA_o(kr)+2\mu_i'k^2B_i(kr)$$
$$q_2=2k^2\left(\mu_iB_i(kr)-\mu_oB_o(kr)\right)$$
$$q_3=-\sigma k\left(k^2-\frac{1}{R^2}\right)$$

The capillary instability of two viscous fluids was considered by Funada and Joseph [79]. Their relation can be recovered by taking μ_i'. Joseph et al. [106] have also discussed the Rayleigh-Taylor instability exists in viscoelastic flows but in their study, the viscoelastic fluid was Oldroyd B fluid.

If V is assumed as characteristic velocity and $h = r_o - r_i$ is taken as characteristic length, the dimensionless form of equation (3.12) can be written as

$$\hat{q}_1 N^2 + i\hat{q}_2 N - \hat{q}_3 = 0 \tag{3.13}$$

where $\hat{q}_1 = \rho A_i(\hat{k}\hat{R}) - A_o(\hat{k}\hat{R}) + 2\lambda\hat{k}^2 B_i(\hat{k}\hat{R})$

$$\hat{q}_2 = 2\hat{k}^2 \frac{Ca}{We}\left(\mu B_i(\hat{k}\hat{R}) - B_o(\hat{k}\hat{R})\right)$$

$$\hat{q}_3 = \frac{\hat{k}}{\hat{R}^2}\frac{1}{We}\left(\hat{k}^2\hat{R}^2 + n^2 - 1\right)$$

Here, $Ca = \dfrac{\mu_o V}{\sigma}$ is the capillary number, $We = \dfrac{\rho_o V^2 H}{\sigma}$ which denotes the Weber number, $\rho = \dfrac{\rho_i}{\rho_o}$ denotes the fluid's density ratio, $\mu = \dfrac{\mu_i}{\mu_o}$ is the fluid's viscosity ratio.

Here, N is a complex variable i.e. $N = N_r + iN_i$ and the interface will be unstable only when $N_i > 0$. Equation (3.13) can be separated as

$$\hat{q}_1\left(N_r^2 - N_i^2\right) - \hat{q}_2 N_i - \hat{q}_3 = 0 \tag{3.14}$$

$$2\hat{q}_1 N_r N_i + \hat{q}_2 N_r = 0 \tag{3.15}$$

It must be noted from equation (3.15) that $N_i = -\hat{q}_2/2\hat{q}_1$ or $N_r = 0$.

If we take it $N_i = -\hat{q}_2/2\hat{q}_1$, the system will always be stable as $\hat{q}_1$ and $\hat{q}_2$ both are positive.

As we are discussing the instability characteristics of the viscous-viscoelastic fluid interface, we take $N_r = 0$. Hence, equation (3.14) takes the form as

$$\hat{q}_1 N_i^2 + \hat{q}_2 N_i + \hat{q}_3 = 0 \tag{3.16}$$

It should be noted from equation (3.16) that $N_i > 0$ only when $\hat{q}_3 < 0$. The neutral stability criterion can be expressed as $\hat{q}_3 = 0$ i.e.

$$\frac{1}{We}\left(\hat{k}^2\hat{R}^2 + n^2 - 1\right) = 0 \tag{3.17}$$

Equation (3.17) shows that viscosity and viscoelasticity do not affect the marginal stability criterion. This result is inconsistent with the Funada and Joseph [79, 80].

As $\hat{k}$ is wave number and it should be positive but if $n \geq 1$, equation (3.17) does not possess positive solutions. Hence, for numerical computation, axisymmetric perturbations $(n = 0)$ are considered.

3.5 Results and Discussions

In this section, we compute growth rates from the equation (3.16). The equation (3.16) has two roots and will plot the maximum of those two values. The effects of various flow parameters such as viscosity, viscoelasticity, etc. have been illustrated through plotted figures of growth rate curves. The non-dimensional parameters are given in Table 3.1.

In figure 3.2, we have plotted the growth rate for interfaces containing Walter's B viscoelastic fluid and viscous fluid interface. The outside fluid is taken as a viscous fluid which is the same for both cases. The third curve is plotted when both inside and outside fluids are inviscid fluid. The figure shows that the growth of Walter's B viscoelastic fluid is higher than the growth of viscous interface while the growth of inviscid fluids is highest. Funada and Joseph [79] found that the growth rate for

Oldroyd B viscoelastic fluid lies above the viscous fluid. The growth for inviscid fluids always lies on the top. Hence, our result is inconsistent from Funada and Joseph [79]. Actually, in both the cases of viscoelastic fluids (Oldroyd B and Walter's B), the elastic property of fluid supports the perturbed flow, and therefore, the system move towards instability. The viscoelasticity works as a stabilizing parameter for Rivlin-Ericksen fluid as the perturbation energy decreases on increasing the viscoelasticity. This result was shown in chapter 2.

The variation of growth rate curves for the various values of viscoelasticity is shown in figure 3.3. It is clear from the constitutive equation (3.2) of Walter's B viscoelastic fluid that if the viscoelasticity of the fluid increases, higher energy is transferred to the interface. Accordingly, as viscoelasticity decreases, energy dissipation increases due to the negative sign present in equation (3.2). High energy is obtained by the interface, so perturbations will have a high amplitude and travel faster, i.e. perturbations travel faster. The same observation has been obtained from figure 3.3 that viscoelasticity has a destabilizing character. It can be verify from Table 3.2.

The behavior of growth rate curves concerning the Weber number is shown in figure 3.4. As the Weber number increases, perturbations grow slower and the system gets stabilized. To justify this result, Table 3.3 is presented. The surface tension force is opposite of the Weber number, which refers to the destabilizing character of the surface force. Since the higher surface tension acts as a facilitator for perturbation to reach between the fluid layers, it takes less time for disturbance growth to progress. Thus, surface tension helps the interface to be unstable.

The effect of the density ratio of two fluids is studied in figure 3.5. The growth of perturbations decreases with the increment of density ratio and therefore, density ratio has a stabilizing effect and this result can be justified by Table 3.4. The density ratio depends directly on inside fluid density and inversely on outside fluid density. Hence, inside fluid density shows stabilizing character while outside fluid destabilizes the interface. As the inside fluid density increase, the inertia force increases which opposes the development of perturbations, and the system gets stabilized.

Figure 3.6 shows the effect of the viscosity ratio on the growth of perturbations. The perturbation growth is slow on increasing the viscosity ratio of two fluids. Therefore, the viscosity of viscoelastic fluid has a stabilizing nature. If viscosity is high, more resistance to the flow will be high, and therefore, flow moves towards stability.

The viscoelastic fluid thickness has a considerable impact on the interface. Figure 3.7 is the plot of the growth curve for the diverse values of thickness of Walter's B fluid. The growth curves increases with an increase in the thickness of the Walter's B fluid, revealing the instability of the interface due to an increase in the thickness of the outer fluid. Table 3.5 is presented in the favor of this result.

3.6 Conclusions

The linear temporal instability of the interface of Walter's B viscoelastic fluid and viscous fluid is studied. The surface tension is present in the analysis while gravity is absent and hence, instability is modeled as capillary instability. The potential flow theory of viscous fluids is utilized to solve the mathematical equations. We achieve a second-order polynomial in the growth rate parameter and the imaginary part of the growth rate parameter is plotted to examine the effect of physical parameters like

viscoelasticity, viscosity, etc. We found that viscosity of inside fluid promotes stability at the interface while the density of outside fluid has destabilizing nature. The viscoelasticity and surface tension both induce instability. The inside fluid density has a stabilizing character. We also observe that Walter's B viscoelastic fluid is unstable than the Newtonian fluid.

Table 3.1: Parameters values for numerical computation

Parameter	values
ρ	0.01
μ	0.001
Ca	0.07
We	0.7
λ	0.2

Table 3.2: Variation of perturbations maximum growth with viscoelasticity λ

viscoelasticity λ	Maximum grow rate $(N_i)_{\max}$	Maximum wave number $k_{\max}$
0.1	0.2057	0.476
0.2	0.2130	0.485
0.3	0.2215	0.496
0.4	0.2316	0.506
0.5	0.2442	0.521

Table 3.3: Variation of perturbations maximum growth with Weber number *We*

Weber number *We*	Maximum grow rate $(N_i)_{\max}$	Maximum wave number $k_{\max}$
0.5	0.2520	0.487
0.6	0.2301	0.484
0.7	0.2130	0.483
0.8	0.1992	0.481
0.9	0.1878	0.481
1.0	0.1782	0.481

Table 3.4: Variation of perturbations maximum growth with density ratio ρ

density ratio ρ	Maximum grow rate $(N_i)_{\max}$	Maximum wave number $k_{\max}$
0.01	0.2130	0.483
0.02	0.2113	0.483
0.03	0.2097	0.483
0.04	0.2081	0.483
0.05	0.2066	0.483

Table 3.5: Variation of perturbations maximum growth with Walter's B fluid thickness

Walter's B fluid thickness	Maximum grow rate $(N_i)_{\max}$	Maximum wave number $k_{\max}$
0.01	0.4839	0.732
0.02	0.5815	0.737
0.03	0.6214	0.738
0.050	0.6370	0.733
0.060	0.6401	0.730

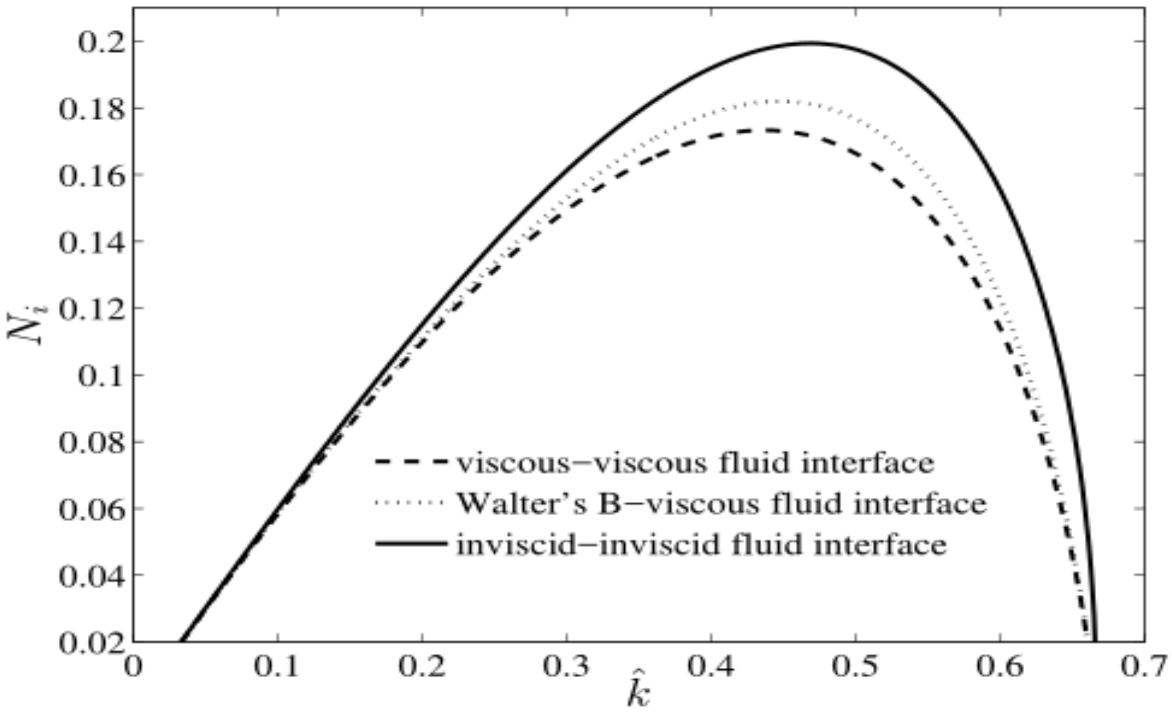

Figure 3.2: Comparisons of various interface combinations.

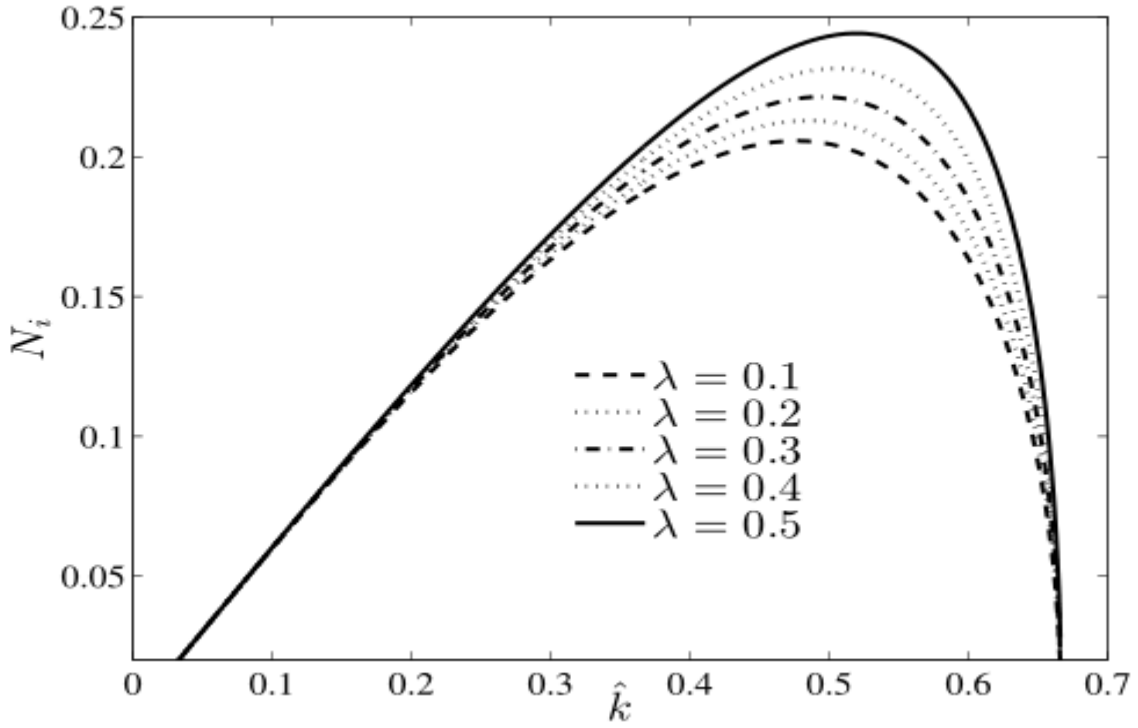

Figure 3.3: Effect of viscoelasticity.

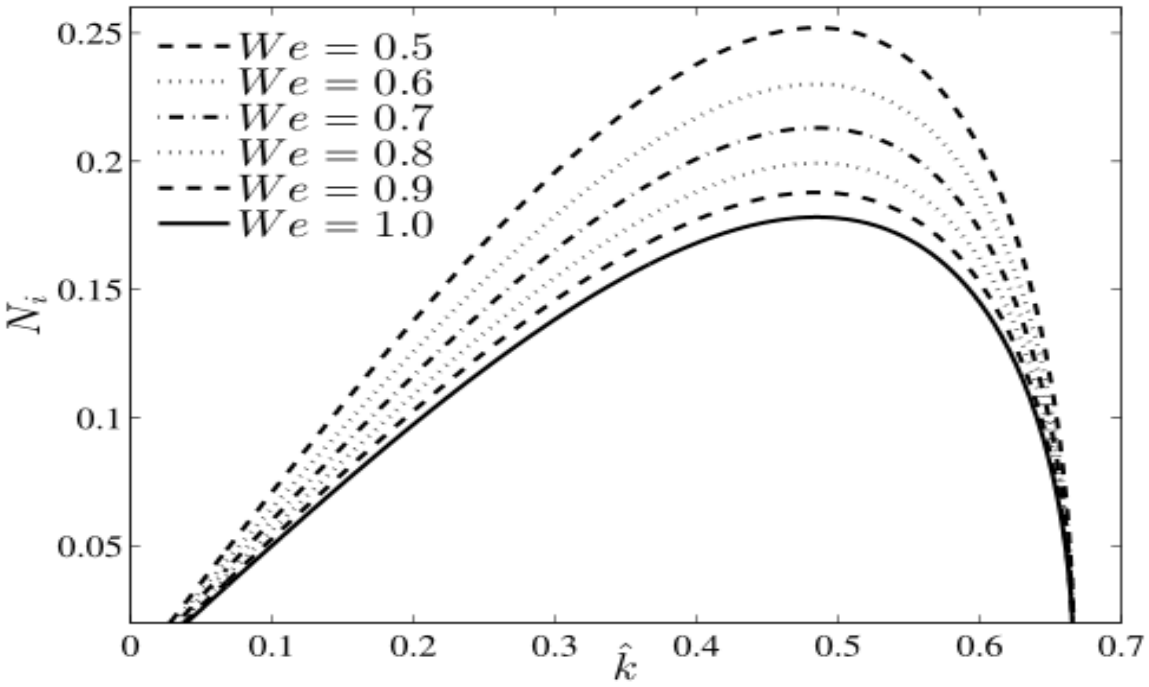

Figure 3.4: Effect of Weber number.

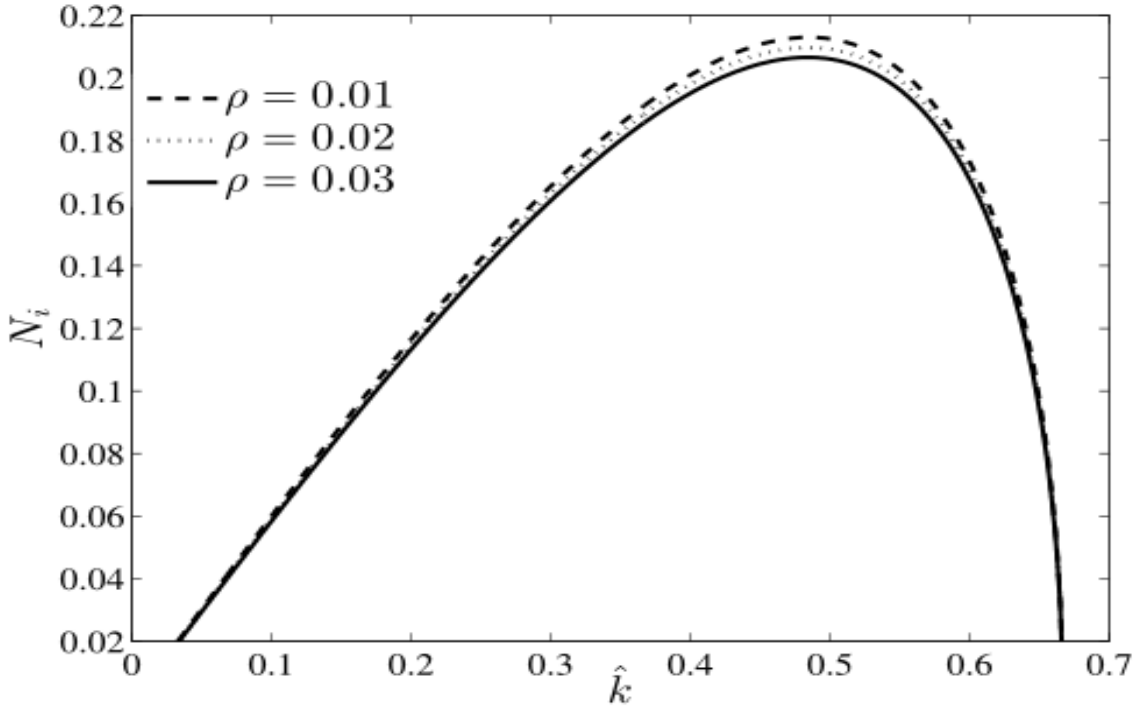

Figure 3.5: Effect of density ratio of fluids.

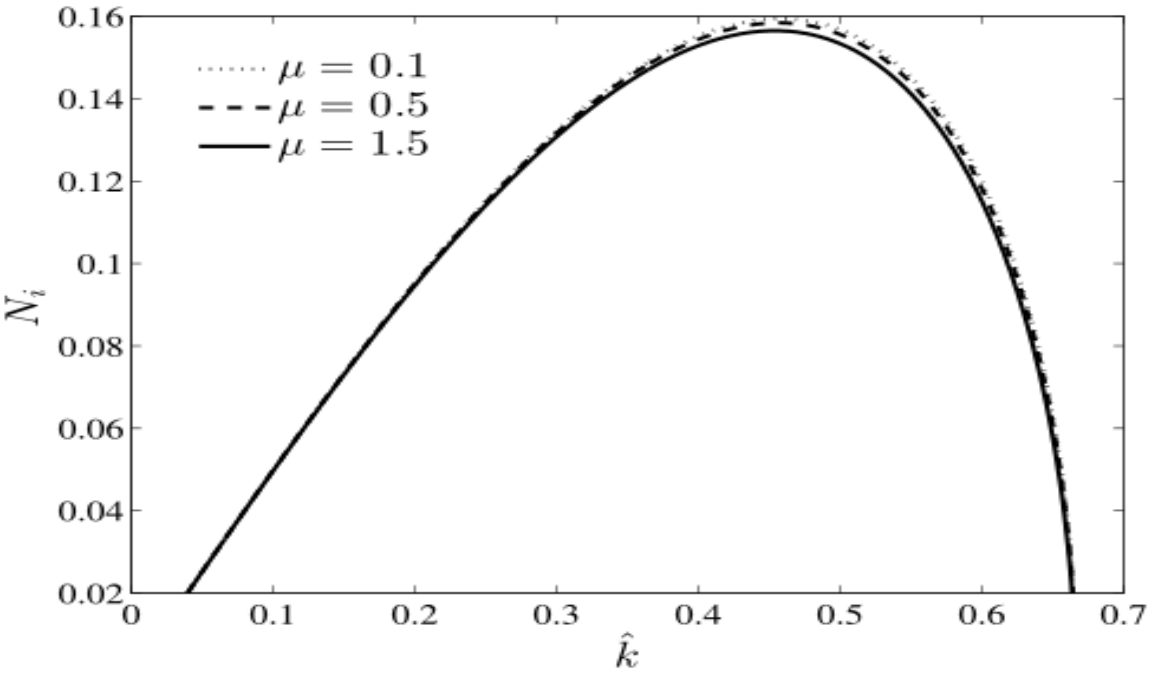

Figure 3.6: Effect of viscosity ratio of fluids.

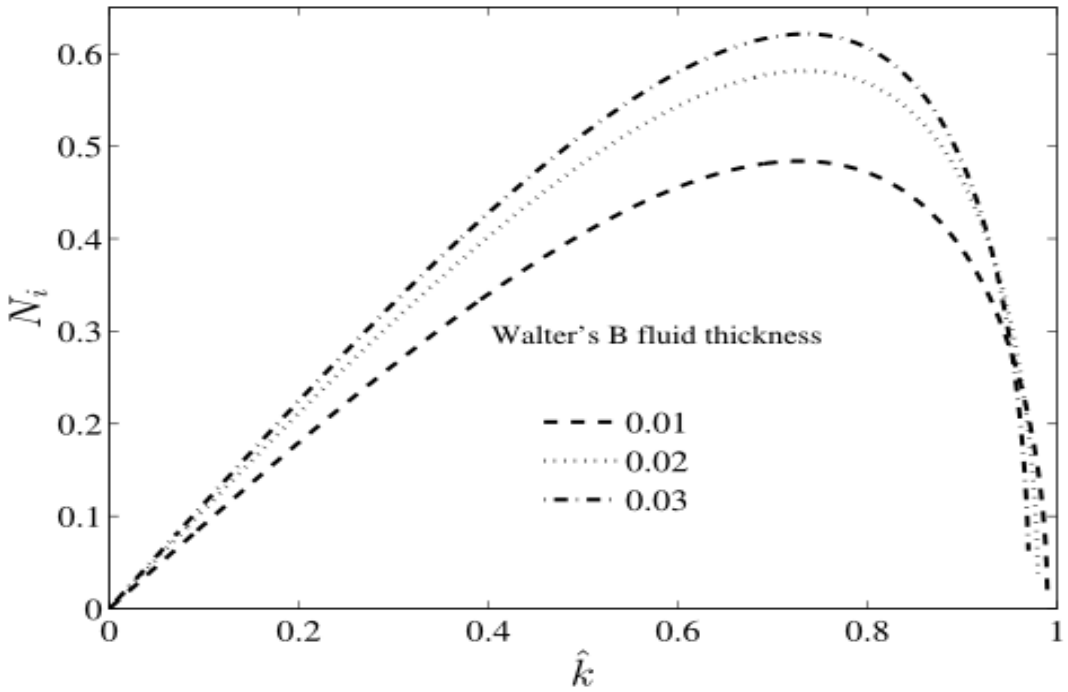

Figure 3.7: Effect of Walter's B fluid Thickness.

CHAPTER 4

CAPILLARY INSTABILITY OF WALTER'S B VISCOELASTIC FLUID WITH MASS AND HEAT TRANSFER

The stability characteristics of the viscous fluid-viscoelastic fluid interface are investigated in a region confined by two rigid cylindrical surfaces. Walter's B viscoelastic fluid is taken for the analysis and the fluid phases are transferring heat along with mass from one phase to the other. The gravitational acceleration effect is neglected and therefore, the interface is unstable due to surface tension. Using the linear stability analysis, the implicit expression for the critical wave number is derived analytically in terms of associated physical parameters and solved through the Newton-Raphson method. The various plots are made in terms of perturbations growth rate and critical wave number showing the behavior of flow variables. It is found that the instability of the interface decreases if the transfer of heat is increased. Walter's B viscoelastic fluid interface is more unstable than the equivalent Newtonian fluid interface. The density of Walter's B fluid resists the perturbation's growth while viscoelasticity has an inverse effect.

4.1 BACKGROUND

The viscoelastic fluids which show the linear stress-strain rate relationship at the small shear rate are referred to as Walter's B viscoelastic fluids. Walters [222] proposed the constitutive equations in terms of pressure p, dynamic viscosity μ, normal stress moduli α_1, α_2, the Cauchy stress tensor $\boldsymbol{\tau}$ as

$$\boldsymbol{\tau} = -p\boldsymbol{I} + \mu\boldsymbol{D_1} - \alpha_1\boldsymbol{D_2} + \alpha_2\boldsymbol{D_1^2} \tag{4.1}$$

Here, $\boldsymbol{D_1}$ and $\boldsymbol{D_2}$ are order 1 and 2 tensor, respectively, given by

$$\boldsymbol{D_1} = \nabla\vec{\boldsymbol{q}} + (\nabla\vec{\boldsymbol{q}})^T \; ; \; \boldsymbol{D_2} = \frac{D\boldsymbol{D_1}}{Dt} + (\nabla\vec{\boldsymbol{q}})\boldsymbol{D_1} + \boldsymbol{D_1}(\nabla\vec{\boldsymbol{q}})^T \tag{4.2}$$

D/Dt denotes material derivative.

The mixture of pyridine and polymethyl methacrylate (density of 0.98 gm/liter) at $25^0 C$ behaves almost like Walter's B viscoelastic fluid [223]. A variety of industrial liquids can be simulated accurately using the above-proposed model and therefore, this model has been extensively analyzed by various researchers in the literature. The stability of two superposed Walter's B fluids was inspected by Sharma and Kumar [192]. The effect of various external variables on the stability of Walter's B fluid was analyzed by Sharma et al. [187], Kumar [122], and El-Sayed [69]. The rotation effect on the thermal instability of Walter's B fluid was studied by Kumar [125]. Sharma et al. [196] analyzed the stratified Walter's B fluid in a porous medium along with the coupled effect of rotation and magnetic field. The suspended particle effect on the stability of superposed Walter's B fluid was discussed by Kumar et al. [128]. The Rayleigh-Taylor (R-T) instability at Newtonian-Walter's B fluid interface is studied by Kumar and Lal [120].

The solution of Navier-Stokes equations for an incompressible fluid for quadrilateral unstructured grids was computed by Ba et al. [39] using Alternating Cell Direction Implicit (ACDI) Method. The impact of thermal radiation on the MHD flow through extending cylinder of hyperbolic fluid was numerically analyzed by Reddy et al. [178]. Megahed et al. [142] discussed the viscous dissipation phenomenon on the Walter's B viscoelastic fluid flowing over a stretching sheet analytically as well as numerically. The study of the Darcy-Forcheimer carbon nanotubes flow in light of similarity transformation was done by Reddy et al. [177] on a two-dimensional melting surface. Babu et al. [40] examined the combined effect

of activation energy and Cattaneo-Christov diffusion on Eyring-Powell fluid flowing over a stretching surface. Reddy et al. [179] Studied Blasius–Rayleigh–Stokes flow over an extending surface in the presence of variable thermal conductivity and a magnetic dipole.

The interface of two fluids in cylindrical configuration was examined by several authors as it has various applications in liquid jets, inkjet printers, petroleum refineries, etc. Govindarajan and Sahu [89] presented a comprehensive review of the viscosity stratification effect on flow instability. They have considered both Newtonian and non-Newtonian fluids. The effect of double-diffusion on the core-annular flow with wall slip was investigated by Chattopadhyay et al. [51] using direct numerical simulation. In this analysis, they found elliptical-shaped stability patterns and wall slip has stabilizing nature. The stability of core-annular flow of Newtonian and a Herschel–Bulkley non-Newtonian fluid was examined by Usha and Sahu [217]. They observed that the core fluid thickness increases the unstable wavenumber's bandwidth and destabilizes the short waves.

An irrotational theory, in which flow velocity is represented by a gradient of the potential function, is generally used in cylindrical flow stability examination. It was proposed by Joseph and Liao [105] that for irrotational analysis, it is not necessary to take viscosity as zero rather we can include viscosity in dynamic interfacial conditions. The stability investigation at the cylindrical interface between two viscous fluids was done by Funada and Joseph [79]. The interface of viscous-viscoelastic fluid was analyzed by Funada and Joseph [80] for Oldroyd B fluid. Awasthi and his coauthors [16, 37, and 210] examined cylindrical interfaces with electro-magnetic effects. The instability of an interface involving Walter's B fluid was analyzed by Moatimid et al. [156, 158].

If one fluid transfers heat/mass to the other fluid, the stability of the interface affects. This type of phenomenon has numerous applications such as film boiling, heat exchangers, etc. The interfacial conditions for heat and mass transport were derived by Hsieh [99]. These conditions were extensively used by Nayak and Chakraborty [164], Lee [131], Fu et al. [77] for inviscid fluids and Kim et al. [115], Awasthi [15, 19-20], Jia et al. [102], Fu et al. [75] for viscous/viscoelastic fluids. Some authors [36, 226] considered the power-law viscoelastic fluid but in these cases second fluid was inviscid.

To the best of the author's knowledge, there is no study available in the literature for interfacial instability involving Walter's B viscoelastic fluid and heat transfer. This is an attempt to study the stability of the interface in an annular region along with heat transport. The fluid in the internal part is taken as a viscous fluid and the external part is filled with Walter's B viscoelastic fluid. The potential flow theory of viscous-viscoelastic fluids is applied and a relationship in terms of perturbation's growth is established. The mathematical modeling is presented in section 4.2 and conditions at the boundary and interface are written. The normal mode theory and linear perturbed equations are achieved in section 4.3 and section 4.4 contains a dispersion relationship. The obtained results are discussed in section 4.5. The key results are concluded in section 4.6.

4.2 MATHEMATICAL STATEMENT

In the current investigation, a cylindrical viscous fluid column of density ρ_i and μ_i is enveloped by a Walter's B viscoelastic fluid of viscosity μ_o, viscoelasticity μ_o', and density ρ_o (figure 4.1). The cylindrical surfaces $r = r_i$ and $r = r_o$ are rigid and both

the fluids lie within these surfaces. The cylindrical surface $r = R$, where $r_i < R < r_o$ forms the interface between the viscous fluid and the viscoelastic fluid. Hence, viscous fluid lies in the $r_i < r < R$ while the region $R < r < r_o$ belongs to the viscoelastic fluid. The viscous fluid phase is at temperature T_i while T_o is the temperature of the viscoelastic fluid phase. The interfacial tension and temperature are denoted by σ and T_{ref} respectively.

If $\vec{q}_o = (u_{r,o}, v_{r,o}, w_{r,o})$ is the outer phase velocity, the mathematical equations for Walter's B fluid phase can be written as (Kim et al. [115])

$$\left.\begin{aligned} &\nabla \cdot \vec{q}_o = 0 \\ &\rho_o \left(\frac{\partial \vec{q}_o}{\partial t} + (\vec{q}_o \cdot \nabla)\vec{q}_o \right) = \nabla \cdot \boldsymbol{\tau}_o \end{aligned}\right\} \tag{4.3}$$

The expression for $\boldsymbol{\tau}_o$ is displayed in equation (4.1).

If $\vec{q}_i = (u_{r,i}, v_{r,i}, w_{r,i})$ is the inner phase velocity, the equations can be written as

$$\left.\begin{aligned} &\nabla \cdot \vec{q}_i = 0 \\ &\rho_i \left(\frac{\partial \vec{q}_i}{\partial t} + (\vec{q}_i \cdot \nabla)\vec{q}_i \right) = -\nabla p_i + \mu_i \nabla^2 \vec{q}_i \end{aligned}\right\}, \qquad \nabla^2 = \frac{\partial^2}{\partial r^2} + \frac{1}{r^2}\frac{\partial}{\partial \theta^2} + \frac{1}{r}\frac{\partial}{\partial r} + \frac{\partial^2}{\partial z^2} \tag{4.4}$$

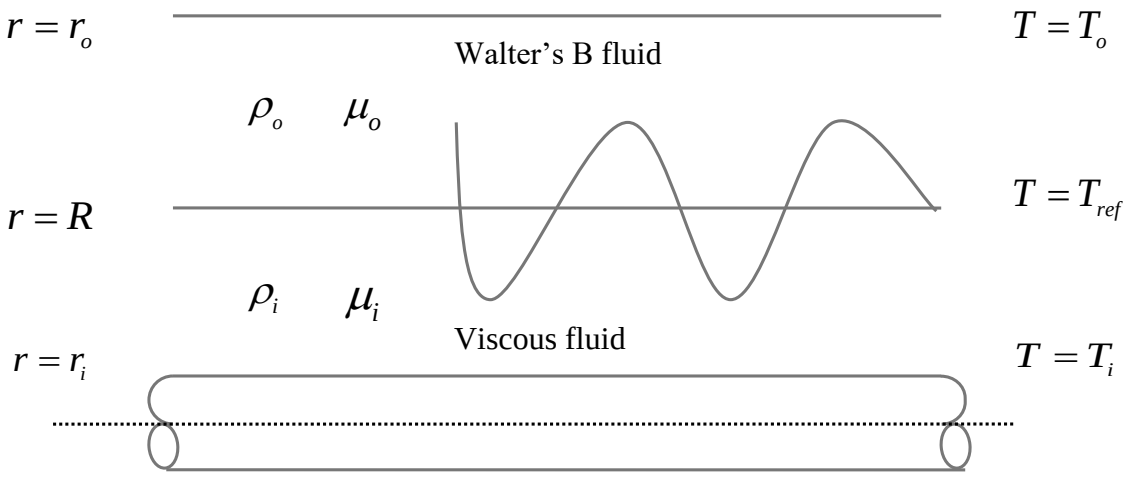

Figure 4.1: Flow diagram

The radial velocity at the cylindrical surfaces will be zero (Awasthi et al. [36]) and therefore,

$$\left.\begin{aligned} u_{r,i} &= 0 \quad \text{at} \quad r = r_i \\ u_{r,o} &= 0 \quad \text{at} \quad r = r_o \end{aligned}\right\} \tag{4.5}$$

The mass transport condition (proposed by Hsieh [99]) can be expressed as

$$\rho_i\left(\frac{\partial f}{\partial t} + \vec{\boldsymbol{q}}_{\boldsymbol{i}} \cdot \nabla f\right) = \rho_o\left(\frac{\partial f}{\partial t} + \vec{\boldsymbol{q}}_{\boldsymbol{o}} \cdot \nabla f\right) \tag{4.6}$$

Here $f = f(r,\theta,z,t)$ is the free-surface expression.

The heat transport at the interface is studied in terms of net heat flux and latent heat. The condition can be expressed as

$$L\rho_i\left(\frac{\partial f}{\partial t} + \vec{\boldsymbol{q}}_{\boldsymbol{i}} \cdot \nabla f\right) = H(r) = \frac{\kappa_o(T_{ref} - T_o)}{r[\ln r_o - \ln r]} - \frac{\kappa_i(T_i - T_{ref})}{r[\ln r - \ln r_i]} \tag{4.7}$$

where L and $H(r)$ represent latent heat and total heat flux, respectively. Here κ_i, κ_o denote the thermal conductivities.

The dynamical equation at the interface will include the viscous effects in the analysis. Mathematically (Awasthi et al. [30]),

$$\left(p_o - 2\left(\mu_o - \mu_o'\frac{\partial}{\partial t}\right)\frac{\partial u_{r,o}}{\partial r}\right) - \left(p_i - 2\mu_i\frac{\partial u_{r,i}}{\partial r}\right) = \sigma\left(\frac{1}{R_1} + \frac{1}{R_2}\right) \tag{4.8}$$

4.3 PERTURBATION ANALYSIS

When the cylindrical interface is in an equilibrium state ($r = R$), the fluids are at rest i.e. $\vec{\boldsymbol{q}}_{\boldsymbol{i}} = \vec{\boldsymbol{q}}_{\boldsymbol{o}} = 0$ and therefore, the pressures in both the phases are constants and there will be no heat/mass transfer at the interface. If an infinitesimal disturbance is employed to the interface, the interface takes the form as $r = R + \xi(\theta,z,t)$. In this state, the velocities and pressures become $0 + \vec{\boldsymbol{q}}_{\boldsymbol{i}}'$, $0 + \vec{\boldsymbol{q}}_{\boldsymbol{o}}'$, $c + p_i'$ and $c + p_o'$.

The linearized form of equations (4.3) and (4.4) with perturbed quantities can be written as

$$\left.\begin{aligned} \nabla \bullet \vec{\boldsymbol{q}}_{\boldsymbol{o}}^{'} &= 0 \\ \rho_o \frac{\partial \vec{\boldsymbol{q}}_{\boldsymbol{o}}^{'}}{\partial t} &= \nabla \bullet \boldsymbol{\tau}_{\boldsymbol{o}}' \end{aligned}\right\} \tag{4.9}$$

$$\left.\begin{aligned} \nabla \bullet \vec{\boldsymbol{q}}_{\boldsymbol{i}}^{'} &= 0 \\ \rho_i \frac{\partial \vec{\boldsymbol{q}}_{\boldsymbol{i}}^{'}}{\partial t} &= -\nabla p_i' + \mu_i \nabla^2 \vec{\boldsymbol{q}}_{\boldsymbol{i}}^{'} \end{aligned}\right\}, \tag{4.10}$$

The conditions at the rigid surfaces reduce to

$$\left.\begin{aligned} u_{r,i}' &= 0 \quad \text{at} \quad r = r_i \\ u_{r,o}' &= 0 \quad \text{at} \quad r = r_o \end{aligned}\right\} \tag{4.11}$$

The perturbed form of linear heat and mass transport conditions are written as follows;

$$\rho_i \left(u_{r,i}' - \frac{\partial \xi}{\partial t} \right) = \rho_o \left(u_{r,o}' - \frac{\partial \xi}{\partial t} \right) \tag{4.12}$$

$$\rho_i \left(u_{r,i}' - \frac{\partial \xi}{\partial t} \right) = \alpha \xi \tag{4.13}$$

The linear dynamical equation takes the form as

$$\left(p_o' - 2\left(\mu_o - \mu_o' \frac{\partial}{\partial t} \right) \frac{\partial u_{r,o}'}{\partial r} \right) - \left(p_i' - 2\mu_i \frac{\partial u_{r,i}'}{\partial r} \right) = \sigma \left(\frac{1}{R_1} + \frac{1}{R_2} \right) \tag{4.14}$$

4.4 DISPERSION RELATIONSHIP

The irrotational flow theory of viscous fluids is utilized to solve the perturbed equations presented in the previous section. The perturbed velocities are expressed in terms of potential functions as $\vec{\boldsymbol{q}}_{\boldsymbol{i}}^{'} = \nabla \Phi_{\boldsymbol{i}}$, $\vec{\boldsymbol{q}}_{\boldsymbol{o}}^{'} = \nabla \Phi_{\boldsymbol{o}}$ and these potential functions are harmonic, as fluids are incompressible i.e.

$$\nabla^2\Phi_i = \nabla^2\Phi_o = 0 \tag{4.15}$$

To examine the stability, we use the normal mode procedure. Hence, the perturbed state function $\beta(r,\theta,z,t)$ will take the form of $\beta(r,\theta,z,t) = \eta(r)\exp(-i\omega t + in\theta + ikz)$ and $\xi(\theta,z,t) = \mathrm{P}\ \exp(-i\omega t + in\theta + ikz)$.

The expressions of Φ_i and Φ_o can be achieved using the conditions (4.11)-(4.13) as follows

$$\Phi_i = \frac{1}{k}\left(-i\omega + \frac{\alpha}{\rho_i}\right)A_i(kr)\ \mathrm{P}\ \exp(-i\omega t + in\theta + ikz) \tag{4.16}$$

$$\Phi_o = \frac{1}{k}\left(-i\omega + \frac{\alpha}{\rho_o}\right)A_o(kr)\ \mathrm{P}\ \exp(-i\omega t + in\theta + ikz) \tag{4.17}$$

$$A_i(kr) = \frac{I_n(kr)K_n'(kr_i) - I_n'(kr_i)K_n(kr)}{I_n'(kR)K_n'(kr_i) - I_n'(kr_i)K_n'(kR)},\quad A_o(kr) = \frac{I_n(kr)K_n'(kr_o) - I_n'(kr_o)K_n(kr)}{I_n'(kR)K_n'(kr_o) - I_n'(kr_o)K_n'(kR)}$$

The pressures in equation (4.14) can be computed using Bernoulli's equation. At the same the radii of curvature can be obtained at the perturbed interface as

$$\left(\frac{1}{R_1} + \frac{1}{R_2}\right) = \left(\frac{\partial^2\xi}{\partial z^2} + \frac{1}{R^2}\frac{\partial^2\xi}{\partial\theta^2} + \frac{\xi}{R^2}\right) \tag{4.18}$$

Equation (4.14) in linear form can be written as

$$\left(\rho_o\frac{\partial\Phi_o}{\partial t} + 2\left(\mu_o - \mu_o'\frac{\partial}{\partial t}\right)\frac{\partial^2\Phi_o}{\partial r^2}\right) - \left(\rho_i\frac{\partial\Phi_i}{\partial t} + 2\mu_i\frac{\partial^2\Phi_i}{\partial r^2}\right) = -\sigma\left(\frac{\partial^2\xi}{\partial z^2} + \frac{1}{R^2}\frac{\partial^2\xi}{\partial\theta^2} + \frac{\xi}{R^2}\right)$$

(4.19)

Inserting the values of Φ_i and Φ_o to the above equation, we have

$$q_1\omega^2 + iq_2\omega - q_3 = 0 \tag{4.20}$$

where $q_1 = \rho_i A_i(kR) - \rho_o A_o(kR) + 2\mu_o' k^2 B_o(kR)$

$$q_2 = \alpha\left(A_i(kR) - A_o(kR)\right) + 2k^2\left(\mu_i B_i(kR) - \mu_o B_o(kR)\right) + 2\frac{\mu_o'}{\rho_o}\alpha k^2 B_o(kR)$$

$$q_3 = 2\alpha k^2\left(\frac{\mu_i}{\rho_i}B_i(kR) - \frac{\mu_o}{\rho_o}B_o(kR)\right) + \frac{\sigma k}{R^2}\left(k^2R^2 + n^2 - 1\right)$$

$$B_i(kR) = \left(1 + \frac{n^2}{k^2R^2}\right)A_i(kR) - \frac{1}{kR}, \quad B_o(kR) = \left(1 + \frac{n^2}{k^2R^2}\right)A_o(kR) - \frac{1}{kR}$$

One can achieve the relationship presented by Kim et al. [115] by setting viscoelasticity $\mu_o' = 0$ in equation (4.20).

If U is assumed as characteristic velocity and $h = r_o - r_i$ is taken as characteristic length, the dimensionless form of equation (4.20) can be written as

$$\hat{q}_1 N^2 + i\hat{q}_2 N - \hat{q}_3 = 0 \tag{4.21}$$

where $\hat{q}_1 = \rho A_i(\hat{k}\hat{R}) - A_o(\hat{k}\hat{R}) + 2\lambda_o \hat{k}^2 B_o(\hat{k}\hat{R})$

$$\hat{q}_2 = \hat{\alpha}\left(A_i(\hat{k}\hat{R}) - A_o(\hat{k}\hat{R})\right) + 2\hat{k}^2\frac{Ca}{We}\left(\mu B_i(\hat{k}\hat{R}) - B_o(\hat{k}\hat{R})\right) + 2\lambda_o\hat{\alpha}\hat{k}^2 B_o(\hat{k}\hat{R})$$

$$\hat{q}_3 = 2\hat{\alpha}\hat{k}^2\frac{Ca}{We}\left(\kappa B_i(\hat{k}\hat{R}) - B_o(\hat{k}\hat{R})\right) + \frac{\hat{k}}{\hat{R}^2}\frac{1}{We}\left(\hat{k}^2\hat{R}^2 + n^2 - 1\right)$$

Here, $Ca = \frac{\mu_o V}{\sigma}$ is the capillary number, $We = \frac{\rho_o V^2 H}{\sigma}$ which denotes the Weber number, $\rho = \frac{\rho_i}{\rho_o}$ denotes the fluid's density ratio, $\mu = \frac{\mu_i}{\mu_o}$ is the fluid's viscosity ratio, $\kappa = \frac{\mu}{\rho}$, and the non-dimensional heat transfer coefficient $\hat{\alpha} = \frac{\alpha h}{U\rho_o}$.

Here, N is a complex variable i.e. $N = N_r + iN_i$ and the interface will be unstable only when $N_i > 0$. Equation (20) can be separated as

$$\hat{q}_1\left(N_r^2 - N_i^2\right) - \hat{q}_2 N_i - \hat{q}_3 = 0 \tag{4.22}$$

$$2\hat{q}_1 N_r N_i + \hat{q}_2 N_r = 0 \tag{4.23}$$

It must be noted from equation (4.23) that $N_i = -\hat{q}_2/2\hat{q}_1$ or $N_r = 0$.

If we take it $N_i = -\hat{q}_2/2\hat{q}_1$, the system will always be stable as $\hat{q}_1$ and $\hat{q}_2$ both are positive.

As we are discussing the instability characteristics of the viscous-viscoelastic fluid interface, we take $N_r = 0$. Hence, equation (4.22) takes the form as

$$\hat{q}_1 N_i^2 + \hat{q}_2 N_i + \hat{q}_3 = 0 \tag{4.24}$$

It should be noted from equation (4.24) that $N_i > 0$ only when $\hat{q}_3 < 0$. The neutral stability criterion can be expressed as $\hat{q}_3 = 0$ i.e.

$$2\hat{\alpha}\hat{k}\hat{R}^2 Ca\left(\kappa B_i(\hat{k}\hat{R}) - B_o(\hat{k}\hat{R})\right) + \left(\hat{k}^2\hat{R}^2 + n^2 - 1\right) = 0 \tag{4.25}$$

As $\hat{k}$ is wave number and it should be positive but if $n \geq 1$, equation (4.25) does not possess positive solutions. Hence, for numerical computation, axisymmetric perturbations $(n = 0)$ are considered.

4.5 RESULTS AND DISCUSSIONS

The perturbation's growth is analyzed numerically in this section. Equation (4.24) is a polynomial of degree 2 and therefore, one can get two roots for a particular set of flow parameters. The maximum value between these two roots has been displayed in the figures. It should be noted that equation (4.25) is an implicit equation and the well-known Newton-Raphson method has been utilized to solve the equation. The region above the wave number curve is the stable region while the below region is unstable. The non-dimensional parameters are given in Table 4.1.

The comparison of the perturbation's growth on the viscous-viscous fluid interface and Walter's B-viscous fluid interface are shown in figure 4.2. The maximum growth rate for non-dimensional heat transfer coefficient $\hat{\alpha}$ is displayed for viscoelasticity $\lambda_o = 0.0$ and $\lambda_o = 0.2$. The values of perturbations maximum growth is given in Table 4.2. Walter's B fluid will behave like a Newtonian fluid if viscoelasticity is zero i.e. $\lambda_o = 0.0$. Kim et al. [115] analyzed the interface of viscous-viscous fluid with heat transfer. It should be noted that the perturbation's maximum growth for Walter's B-viscous fluid interface is higher than the interface of viscous fluids and therefore, it can be concluded that the viscoelasticity of Walter's B fluid grows the perturbations at the interface. The elastic force (due to the elasticity of the fluid) produces acceleration (as per Newton's second law) which increases the speed of the perturbation at the interface and the interface gets more destabilized. One can also note that as the heat transfer coefficient $\hat{\alpha}$ increases, the growth of perturbations declines for both the viscous-viscous interface and viscous-viscoelastic interface. Therefore, heat transport has a stabilizing impact on the stability of the interface. When the heat transport is high at the interface, perturbation's growth coincides.

In figure 4.3, the behavior of maximum growth of perturbations for the elasticity of the fluid is shown for heat transfer coefficient $\hat{\alpha} = 0.0$ and $\hat{\alpha} = 0.01$. The maximum values of growth rate are shown in Table 4.3. It can be easily seen that the impact of viscoelasticity λ_o is not affected by the presence of heat transfer at the interface. This also proves that heat transfer does not change the nature of viscoelasticity, but in the presence of heat transfer, the flow of perturbation decreases, which shows that the transfer of heat prevents the interface from becoming unstable. The maximum growth of perturbations increases with the increase in viscoelasticity λ_o indicating that the viscoelasticity has destabilizing nature at the cylindrical interface. As we know that viscoelasticity is the main reason for the temporary connections between particles within the viscoelastic fluid. Many polymers have long molecules and those molecules make temporary connections with their neighbors, hence polymers show viscoelastic behavior. As the viscoelasticity increases, the connections between the particles begin to weaken, allowing the perturbations to travel through the layers, and as a result, the interface becomes unstable.

We have already stated that equation (4.25) is an implicit equation and using the Newton-Raphson method, the neutral stability curves can be achieved. Figure 4.4 shows the neutral stability curves based on wave-number for various values of capillary number Ca. The neutral stability curves separate the stable region (above the curve) and the unstable region (below the curve) for the stability analysis. The capillary number depends inversely on the surface tension and directly on the viscosity of Walter's B fluid therefore, Walter's B fluid viscosity has stabilizing nature while surface tension will make the free surface unstable. On increasing the viscosity of Walter's B fluid, the flow impedes, and therefore, the instability delays. The surface forces produced by the surface tension are responsible for the breakup.

The increment in surface tension increases the magnitude of such forces and therefore, instability occurs early.

The region of stability with various values of heat transfer coefficient $\hat{\alpha}$ is displayed in figure 4.5. It is found that the stable region enlarges if the transfer of heat increases through the interface. Hence, $\hat{\alpha}$ has stabilizing nature. Kim et al. [115] and Awasthi et al. [19, 36] also found the same character of heat transport on the interface in an annular region. Hence, one can say that viscoelasticity has no impact on the character of heat transport i.e. heat transport has stabilizing character. The effect of the transport of heat along with mass at the interface can be ascribed to relative evaporation and condensation. Walter's B fluid is at high temperature than the viscous fluid and therefore, there will evaporation in the outer region and condensation will take place in the inner region. When transport will start, Walter's B fluid vapor condenses in the inner region and viscous fluid evaporates in the outer region. This evaporation/condensation will prevent the increase of perturbation and the interface will acquire instability late.

The variation of Walter's B fluid thickness on the neutral stability curves of wave number is displayed in figure 4.6. On increasing Walter's B fluid thickness, the evaporation rate in the outer region increases but the condensation rate decreases because the viscous fluid thickness decreases (needless to say that the annular region is fixed). This one-sided evaporation will increase the amplitude of perturbations and they will travel faster. Hence, an interface with a thin Walter's B fluid layer is more stable than a thick Walter's B fluid layer as observed in figure 4.6. We also notice that at the lower values of κ, the stable region slightly decreases. When κ is low, the viscosity of the inner fluid is low and therefore flow impedes. Hence, the system gets destabilized.

The influence of Weber's number on the growth of perturbations is shown in figure 4.7. Weber number is an important non-dimensional number for flow related to the capillary phenomenon. On increasing the Weber number, the perturbation's growth decreases which suggest the stabilizing character of the Weber number. As we know that the Weber number is the ratio of inertia force to the surface tension force and therefore, one can say that inertia force makes stabilizing impact on the interface while surface tension has destabilizing nature. Generally, inertia force produces by the density of the fluid and therefore, the density of Walter's B fluid induces stability to the system. The perturbations take more time to travel in a more dense fluid than the less dense fluid and instability delays. Hence, the interface involving denser Walter's B fluid is more stable.

4.6 CONCLUSIONS

The theoretical study of the stability of viscous fluid- Walter's B viscoelastic fluid interface is done when the fluid phases are transferring heat and mass through the interface. The fluids lie in the annular region enclosed by two rigid cylinders and the irrotational flow theory of viscous-viscoelastic fluid is employed to work out the mathematical equations. The algebraic equation of the growth rate parameter is computed and analyzed numerically. The effects of various non-dimensional variables are shown on the instability of the interface. The transport of heat is found to stabilize the interface by enlarging the stability range while the surface tension has destabilizing nature. The viscoelasticity of Walter's B fluid destabilizes the interface while the density of the viscoelastic fluid induces stability in the system. The viscosity of Walter's B fluid has stabilizing nature.

Table 4.1: Parameters values for numerical computation

Parameter	values
ρ	0.01
μ	0.001
Ca	0.07
We	0.7
α	0.01
λ_o	0.2

Table 4.2: Variation of perturbations maximum growth with heat transfer coefficient $\hat{\alpha}$

heat transfer coefficient $\hat{\alpha}$	Maximum growth $(N_i)_{\max}$ when $\lambda_0 = 0.0$	Maximum growth $(N_i)_{\max}$ when $\lambda_0 = 0.2$
0.001	0.1952	0.2081
0.002	0.1941	0.2069
0.003	0.1929	0.2056
0.004	0.1917	0.2044
0.005	0.1906	0.2031
0.006	0.1895	0.2019

0.007	0.1883	0.2007
0.008	0.1872	0.1994
0.009	0.1861	0.1982
0.010	0.1850	0.1970

Table 4.3: Variation of perturbations maximum growth with viscoelasticity λ_0

viscoelasticity λ_0	Maximum growth $(N_i)_{\max}$ when $\hat{\alpha} = 0.0$	Maximum growth $(N_i)_{\max}$ when $\hat{\alpha} = 0.10$
0.01	0.1970	0.1112
0.02	0.1976	0.1115
0.03	0.1981	0.1118
0.04	0.1987	0.1121
0.05	0.1993	0.1124
0.06	0.2000	0.1127
0.07	0.2006	0.1130
0.08	0.2012	0.1133
0.09	0.2018	0.1137
0.10	0.2025	0.1140

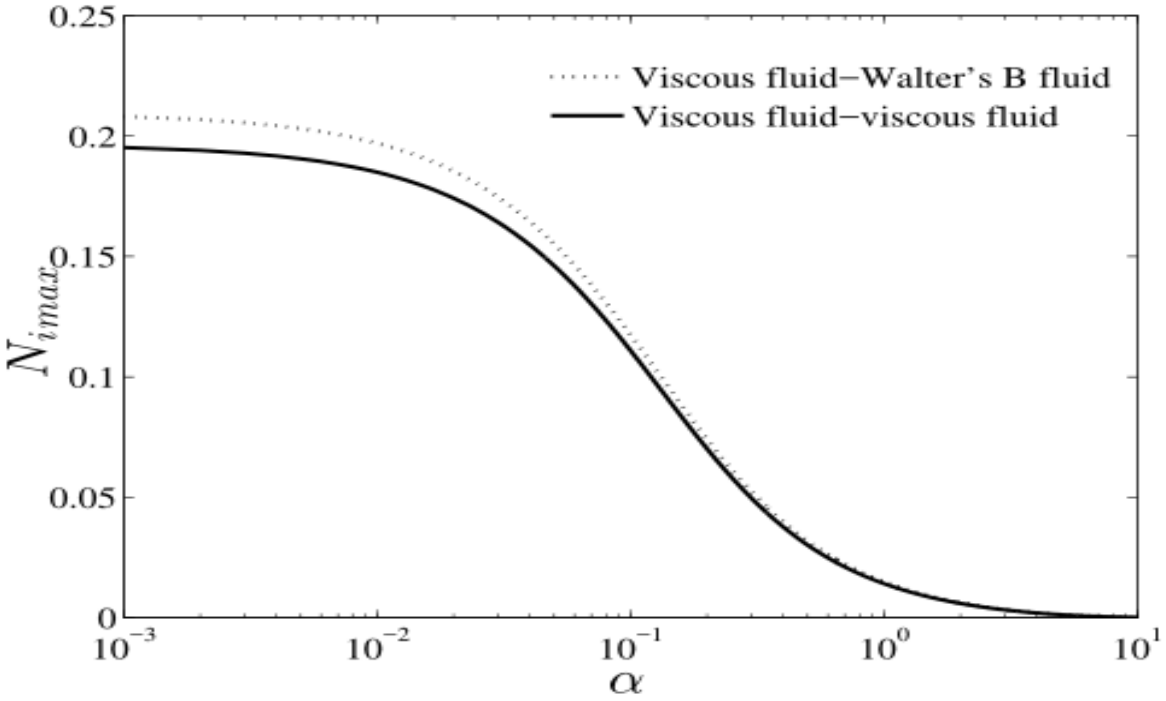

Figure 4.2: Comparison of perturbation's maximum growth for

$\lambda_o = 0.0$ and $\lambda_0 = 0.2$. ($\phi = 0.5, Ca = 0.007, We = 0.7, \rho = 0.01, \mu = 0.001$)

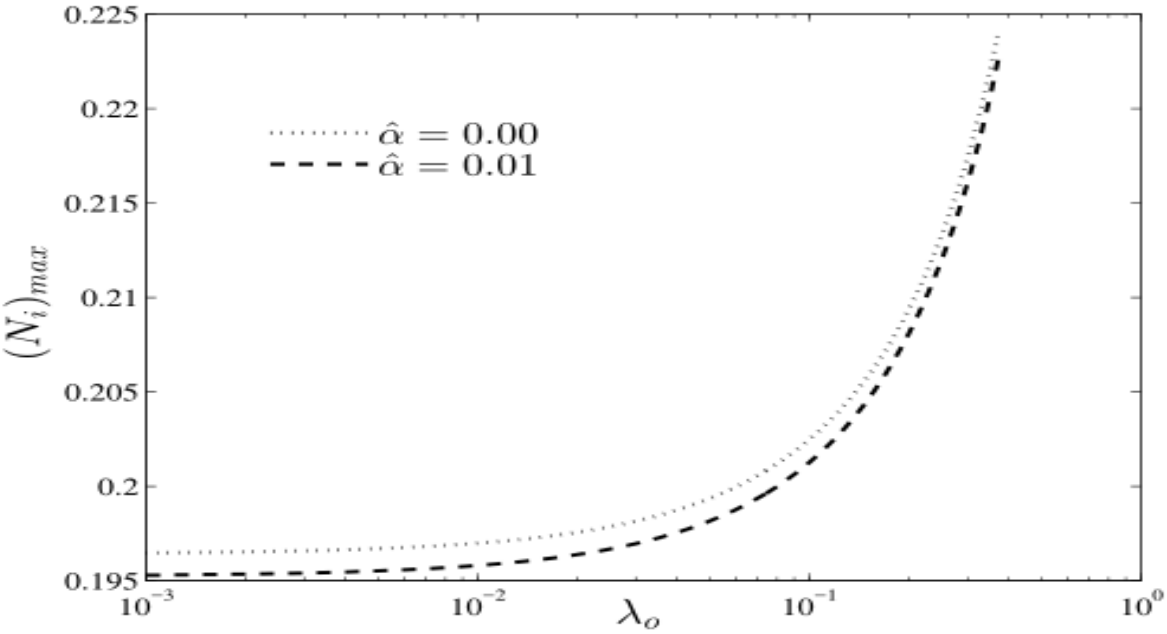

Figure 4.3: Effect of viscoelasticity for $\hat{\alpha} = 0.0$ and $\hat{\alpha} = 0.1$.

($\phi = 0.5, Ca = 0.007, We = 0.7, \rho = 0.01, \mu = 0.001$)

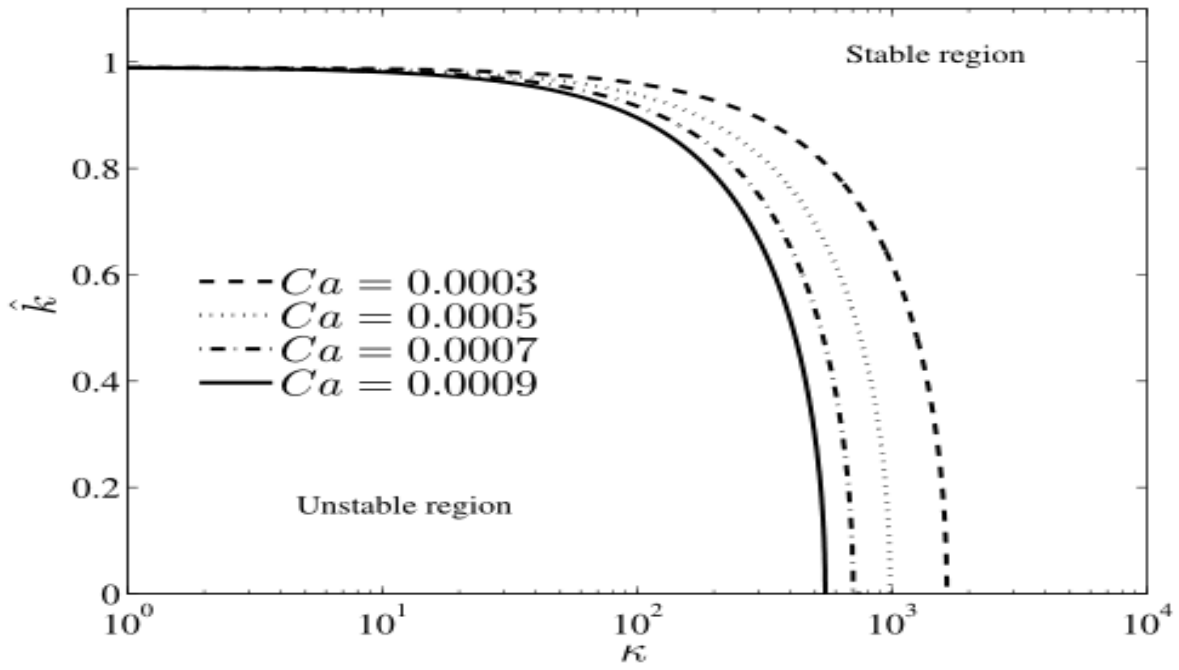

Figure 4.4: Effect of Capillary number $Ca.(\phi = 0.01, \hat{\alpha} = 0.01)$

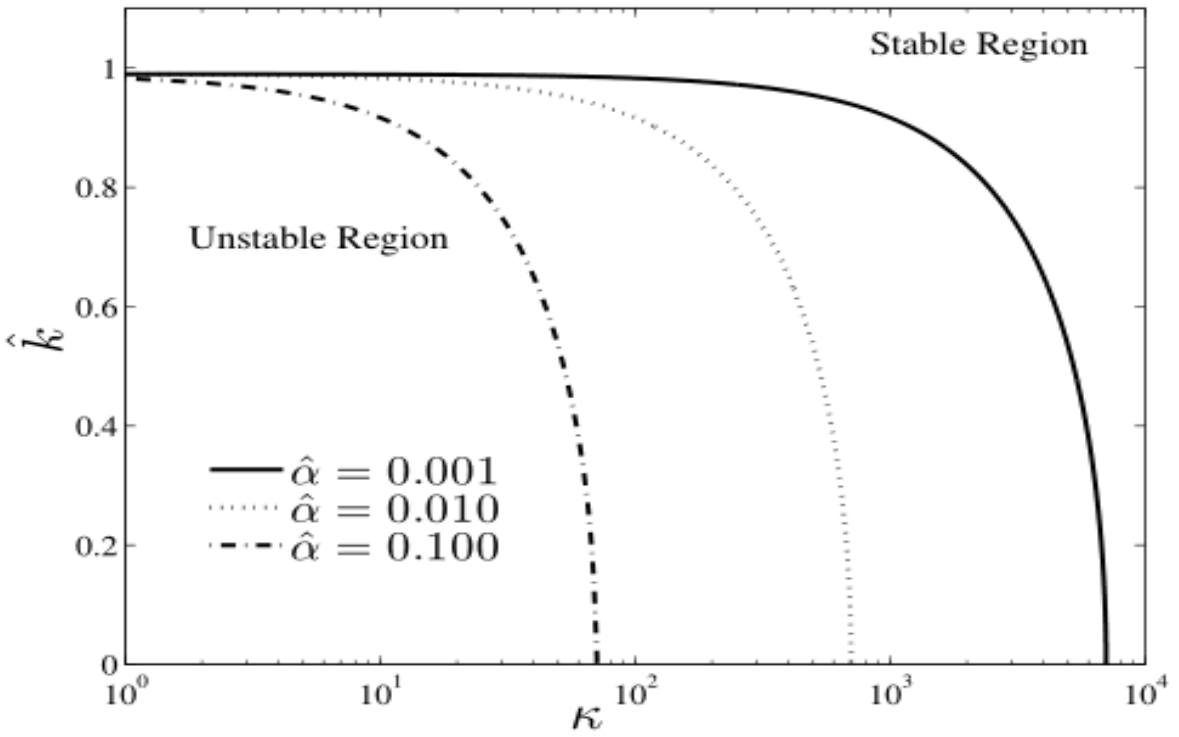

Figure 4.5: Effect of heat transfer $\hat{\alpha}.(\phi = 0.01, Ca = 0.0007)$

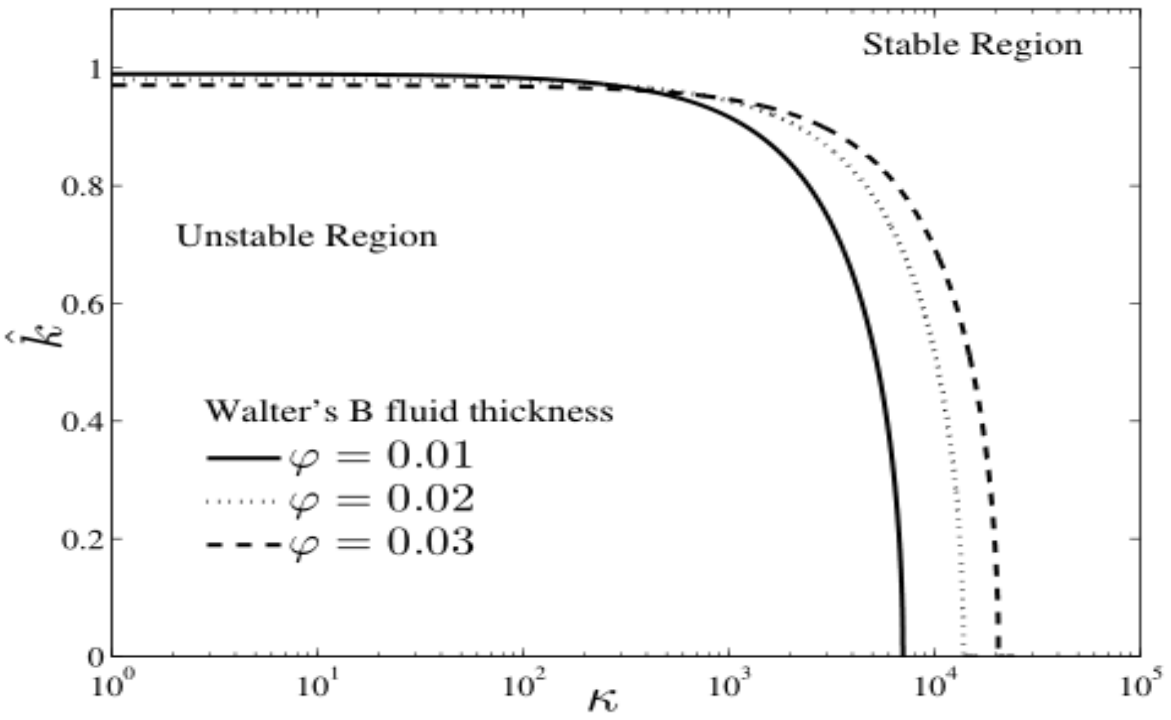

Figure 4.6: Effect of Walter's B fluid thickness. ($\hat{\alpha} = 0.001, Ca = 0.0007$)

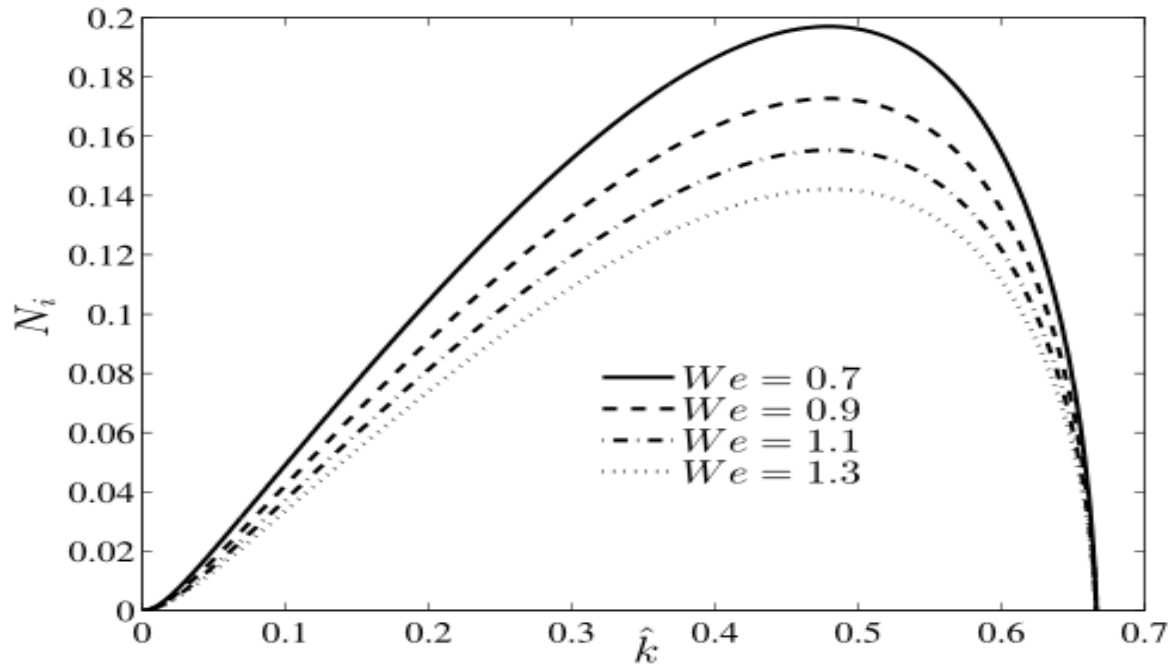

Figure 4.7: Effect of Weber number *We.*

($\phi = 0.5, Ca = 0.007, \rho = 0.01, \mu = 0.001, \lambda_o = 0.2$)

CHAPTER 5

CAPILLARY INSTABILITY OF CYLINDRICAL POWER-LAW VISCOELASTIC FLUID INTERFACE WITH MASS AND HEAT TRANSFER

The analytical study of heat and mass transport at the viscous fluid- viscoelastic fluid is carried out using the irrotational flow theory of viscous-viscoelastic fluids. The interface of viscous-viscoelastic fluid experiences capillary instability. The viscoelastic fluid is taken as power-law fluid and both asymmetric and axisymmetric disturbances are analyzed. The fluids are enclosed in an annular region bounded by two rigid concentric cylinders. The non-dimensional dispersion relation depends on the capillary number, Weber number, power-law index, heat transfer coefficient, viscosity ratio of fluids, etc. The transfer of heat and mass has a significant impact on the stability of the interface. It is also found that the viscosity of viscous fluid delays instability.

5.1 BACKGROUND

Capillary instability arises if a liquid cylinder collapses in an infinite fluid such as atmospheric air. The surface tension present at the free surface produces capillary forces and these capillary forces make the interface unstable. The various real-life phenomenons such as the breakup of the liquid jet, the formation of a water bubble, and in various metallurgical and chemical processes, this type of instability can be experienced.

The capillary instability of Newtonian-type fluids was first studied by Plateau [171] and later Rayleigh [174] followed his work using the irrotational theory of inviscid fluids. The linear analysis of fully viscous capillary instability was carried out by Tomotika [211]. The capillary instability of viscous fluids was computed by

Funada and Joseph [79] using irrotational flow theory. Moatimid et al. [152] considered the instability of rigid columns with the electric field while El-Dib et al. [62] investigated a similar analysis with a magnetic field.

Heat and mass transport plays a vital role in various industrial applications such as film-wise condensation and film boiling. The study of heat transport at the interface of two non-viscous fluids was carried out by [76, 131, and 164]. The viscosity along with heat transport at the interface of two fluids was analyzed by Kim et al. [115] using irrotational theory. The nonlinear study of heat transport on the interfacial instability in cylindrical flow was carried out by Awasthi et al. [15, 19, 24].

The manufacturing of plastic sheets, biological liquid movements, and lubricant performance are some industrial phenomenon where non-Newtonian fluids especially a power-law viscoelastic fluid is used. Therefore, the instability of a power-law viscoelastic fluid surrounded by a viscous fluid becomes very crucial. The viscoelastic jet breakup with various effects was examined by Awasthi et al. [36], Awasthi et al. [38], Fu et al. [75], and Shukla et al. [201]. It was concluded from the above studies that the Newtonian jet is more stable than the viscoelastic jet. Liu et al. [139] included the impact of surfactants in the analytical study of power-law fuel jets.

The heat transfer effect on the stability of a liquid jet was considered by Fu et al. [77]. Liu et al. [139] included the gas cross-flow in the stability of a liquid jet. The heat transport effect on the interface of power-law viscoelastic fluid and gas was studied by Wang et al. [226] and Awasthi et al. [36]. The results show that heat transfer destabilizes the interface in Kelvin-Helmholtz instability (Wang et al. [226]) while it has stabilizing character in capillary instability (Awasthi et al. [36]). In both the studies, the gas was taken as non-viscous fluid and therefore, these studies inspire us to examine the instability of interface with heat transport when the gas is viscous.

In this chapter, the instability of the viscous fluid-viscoelastic fluid is investigated when the interface transports heat along with the mass. The viscous-viscoelastic irrotational flow theory is employed to include the viscosity of both fluids. The interfacial stability of the inviscid fluid-power-law liquid interface in an annular region with heat and mass transport was examined by Awasthi et al. [36] but their analysis does not include viscosity of the inner fluid. We are considering the stability of the viscous gas-power-law liquid interface bounded by two concentric cylinders. The mathematical modeling is presented in section 5.2 and conditions at the boundary and interface are written. The normal mode theory and linear perturbed equations are also achieved in section 5.2 and section 5.3 contains a dispersion relationship. The obtained results are discussed in section 5.4. The key results are concluded in section 5.

5.2 MATHEMATICAL DESCRIPTION

The geometrical configuration displayed in figure 5.1 consists of a viscous gas surrounded by a power-law viscoelastic fluid enclosed by two cylinders of radii r_i, r_o $(r_i < r_o)$. The viscous gas has density ρ_i, viscosity μ_i, and temperature T_i whereas power-law fluid has density ρ_o, viscosity μ_o, and temperature T_o.

If $\vec{\boldsymbol{q}}_{\boldsymbol{o}} = (u_{r,o}, v_{r,o}, w_{r,o})$ is the outer phase velocity, the mathematical equations for the power-law fluid phase can be written as

$$\left.\begin{aligned} &\nabla \bullet \vec{\boldsymbol{q}}_{\boldsymbol{o}} = 0 \\ &\rho_o\left(\frac{\partial \vec{\boldsymbol{q}}_{\boldsymbol{o}}}{\partial t} + \left(\vec{\boldsymbol{q}}_{\boldsymbol{o}} \bullet \nabla\right)\vec{\boldsymbol{q}}_{\boldsymbol{o}}\right) = -\nabla p_o + \nabla \bullet \boldsymbol{\tau}_{\boldsymbol{o}} \end{aligned}\right\} \tag{5.1}$$

The stress ($\boldsymbol{\tau}_{\boldsymbol{o}}$)-strain $\tau_{\boldsymbol{o}} = \left((\nabla \vec{\boldsymbol{q}}_{\boldsymbol{o}}) + (\nabla \vec{\boldsymbol{q}}_{\boldsymbol{o}})^T\right)$ relationship is given by the expression

$$\boldsymbol{\tau}_{\boldsymbol{o}} = \mu_o(\gamma_o)\gamma_o \tag{5.2}$$

The power-law index is denoted by n and K is the consistency coefficient. The expression of viscosity for the power-law fluid is given as;

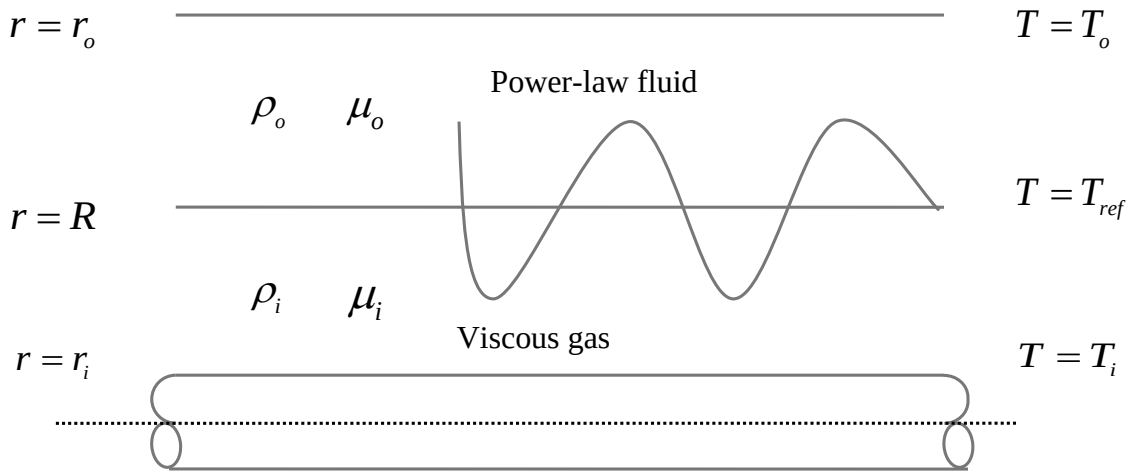

Figure 5.1: Flow diagram.

$$\mu_o = K\left(\frac{1}{2}\boldsymbol{\gamma_o}\cdot\boldsymbol{\gamma_o}\right)^{\frac{n-1}{2}} \tag{5.3}$$

If $\vec{\boldsymbol{q}}_{\boldsymbol{i}} = (u_{r,i}, v_{r,i}, w_{r,i})$ is the inner phase velocity, the equations can be written as

$$\left.\begin{aligned}&\nabla\bullet\vec{\boldsymbol{q}}_{\boldsymbol{i}} = 0\\&\rho_i\left(\frac{\partial\vec{\boldsymbol{q}}_{\boldsymbol{i}}}{\partial t} + \left(\vec{\boldsymbol{q}}_{\boldsymbol{i}}\cdot\nabla\right)\vec{\boldsymbol{q}}_{\boldsymbol{i}}\right) = -\nabla p_i + \mu_i\nabla^2\vec{\boldsymbol{q}}_{\boldsymbol{i}}\end{aligned}\right\}, \qquad \nabla^2 = \frac{\partial^2}{\partial r^2} + \frac{1}{r^2}\frac{\partial}{\partial\theta^2} + \frac{1}{r}\frac{\partial}{\partial r} + \frac{\partial^2}{\partial z^2} \tag{5.4}$$

At the interface, the mass is transported from one phase to the other phase. In mathematics form, we write

$$\rho_i\left(\frac{df}{dt} + \vec{\boldsymbol{q}}_{\boldsymbol{i}}\bullet\nabla f\right) = \rho_o\left(\frac{df}{dt} + \vec{\boldsymbol{q}}_{\boldsymbol{o}}\bullet\nabla f\right) \tag{5.5}$$

Here $f(r,\theta,z,t)$ is the interface equation.

We assume that the inner fluid phase has a temperature T_i and the outer fluid phase has a temperature T_o . Also, the fluids are in thermodynamics equilibrium in the basic situation and the saturation temperature is T_{ref} . Heat transport treatment is analyzed

hereby accepting the model of Awasthi et al. [36]. The total heat flux is equated to the latent heat and therefore,

$$L\rho_i\left(\frac{\partial f}{\partial t}+\vec{\boldsymbol{q}}_{\boldsymbol{i}}\bullet\nabla f\right)=H(r)=\frac{\kappa_o(T_{ref}-T_o)}{r[\ln r_o-\ln r]}-\frac{\kappa_i(T_i-T_{ref})}{r[\ln r-\ln r_i]} \tag{5.6}$$

where L and $H(r)$ represent latent heat and total heat flux, respectively. Here κ_i,κ_o denote the thermal conductivities.

The stress equilibrium at the interface is written as

$$\left(p_o-2\mu_o(\gamma_o)\hat{\boldsymbol{n}}\cdot\nabla\otimes\vec{\boldsymbol{q}}_{\boldsymbol{o}}\cdot\hat{\boldsymbol{n}}\right)-\left(p_i-2\mu_i\hat{\boldsymbol{n}}\cdot\nabla\otimes\vec{\boldsymbol{q}}_{\boldsymbol{i}}\cdot\hat{\boldsymbol{n}}\right)=\sigma\nabla\cdot\hat{\boldsymbol{n}} \tag{5.7}$$

Here $\hat{\boldsymbol{n}}$ is the outward unit normal.

5.2.1 Basic state

The equation $r=R$ refers to the initial location of the interface. The velocity in the inner fluid phase and outer fluid phase is given by $(0,0,0)$, $(0,0,0)$ and pressures are P_i,P_o, respectively. Therefore, equations (5.1) and (5.4) tell us that

$$P_i=P_o=\text{constant} \tag{5.8}$$

Initially, the mass transfer will not happen at the interface and total heat flux on both sides are equal. Hence,

$$\frac{\kappa_o(T_{ref}-T_o)}{R[\ln r_o-\ln R]}=\frac{\kappa_i(T_i-T_{ref})}{R[\ln R-\ln r_i]}=\frac{(T_i-T_o)}{[\ln(R/r_i)/\kappa_i+\ln(r_o/R)/\kappa_o]}=Q(\text{say}) \tag{5.9}$$

5.2.2 Perturbed state

The small-scale disturbance is employed to the initial state and the interface takes the form $r=R+\xi(\theta,z,t)$. The annular region flow is also distorted with the disturbed pressure and flow velocity i.e. $\left[u_{r,i},v_{r,i},w_{r,i},p_{r,i},u_{r,o},v_{r,o},w_{r,o},p_o\right]=\left[\tilde{u}_{r,i},\tilde{v}_{r,i},\tilde{w}_{r,i},\right.$ $\left.P_i+\tilde{p}_i,\tilde{u}_{r,o},\tilde{v}_{r,o},\tilde{w}_{r,o},P_o+\tilde{p}_o\right]$. The linear perturbed equations can be expressed as

$$\left.\begin{aligned} &\nabla \bullet \tilde{\boldsymbol{q}}_{\boldsymbol{o}}' = 0 \\ &\rho_o \frac{\partial \tilde{\boldsymbol{q}}_{\boldsymbol{o}}'}{\partial t} = -\nabla \tilde{p}_o + \nabla \bullet \tilde{\boldsymbol{\tau}}_{\boldsymbol{o}} \end{aligned}\right\} \tag{5.10}$$

$$\left.\begin{aligned} &\nabla \bullet \tilde{\boldsymbol{q}}_{\boldsymbol{i}}' = 0 \\ &\rho_i \frac{\partial \tilde{\boldsymbol{q}}_{\boldsymbol{i}}'}{\partial t} = -\nabla \tilde{p}_i + \mu_i \nabla^2 \tilde{\boldsymbol{q}}_{\boldsymbol{i}}' \end{aligned}\right\} \tag{5.11}$$

To simplify the stress vector for power-law fluid, the generalized Binomial expansion theorem with coefficient 'q' is employed (Awasthi et [36], Wang et al.[226])

$$\tilde{\boldsymbol{\tau}}_{\boldsymbol{o}} = K\left(2\tilde{\boldsymbol{\gamma}}_{\boldsymbol{o}}\right)^n \approx K\left((2q)^n + 2n(2q)^{n-1}\tilde{\boldsymbol{\gamma}}_{\boldsymbol{o}} + ...\right) \tag{5.12}$$

Here, $2\tilde{\boldsymbol{\gamma}}_{\boldsymbol{o}}$ is taken as we are taking the symmetric part of $\boldsymbol{\gamma}_{\boldsymbol{o}}$.

The mass transport in the perturbed state will be

$$\rho_i\left(\tilde{u}_i - \frac{\partial \xi}{\partial t}\right) = \rho_o\left(\tilde{u}_o - \frac{\partial \xi}{\partial t}\right) \tag{5.13}$$

The heat transport in linear form is given as

$$L\rho_i\left(\tilde{u}_i - \frac{\partial \xi}{\partial t}\right) = H(R+\xi) \tag{5.14}$$

In linear case $H(R+\xi) = H(R) + \xi H'(R)$ and $H(R) = 0$. Hence $H(R+\xi) = \xi H'(R)$.

Now, the equation (14) takes form as

$$\rho_i\left(\tilde{u}_i - \frac{\partial \xi}{\partial t}\right) = \alpha\xi \tag{5.15}$$

where $\alpha = \dfrac{H'(R)}{L}$

Also, there will be no flow normal to the boundaries $r = r_i$ and $r = r_o$ i.e.

$$\left.\begin{aligned} &\tilde{u}_{r,i} = 0 \qquad \text{at} \quad r = r_i \\ &\tilde{u}_{r,o} = 0 \qquad \text{at} \quad r = r_o \end{aligned}\right\} \tag{5.16}$$

5.3 DISPERSION RELATION

The disturbance modes are expressed in the form as $\hat{F}(r,\theta,z,t) = \hat{f}(r)E$ where $E = \exp(im\theta - i\omega t + ikz)$. The interface distortion $\xi(\theta,z,t)$ will take form as $\xi = \hat{\xi}E + c.c.$.

The perturbed fluid motion is considered to be irrotational and so $\tilde{\boldsymbol{q}}_{\boldsymbol{i}}' = (\tilde{u}_{r,i}, \tilde{v}_{r,i}, \tilde{w}_{r,i}) = \nabla\Phi_i$ and $\tilde{\boldsymbol{q}}_{\boldsymbol{o}}' = (\tilde{u}_{r,o}, \tilde{v}_{r,o}, \tilde{w}_{r,o}) = \nabla\Phi_o$. The expressions for potential functions are computed as;

$$\Phi_i = \frac{1}{k}\left(\frac{\alpha}{\rho_i} - i\omega\right)A_i(kr)\hat{\xi}E + c.c. \tag{5.17}$$

$$\Phi_o = \frac{1}{k}\left(\frac{\alpha}{\rho_o} - i\omega\right)A_o(kr)\hat{\xi}E + c.c. \tag{5.18}$$

$$A_i(kr) = \frac{I_m'(kr_i)K_m(kr) - I_m(kr)K_m'(kr_i)}{K_m'(kR)I_m'(kr_i) - K_m'(kr_i)I_m'(kR)},\quad A_o(kr) = \frac{I_m'(kr_o)K_m(kr) - I_m(kr)K_m'(kr_o)}{K_m'(kR)I_m'(kr_o) - K_m'(kr_o)I_m'(kR)}$$

Taking the help of equation (5.12), the linear form of equation (5.7) in perturbed form can be written as

$$\tilde{p}_o - \tilde{p}_i - 2nK(2q)^{n-1}\frac{\partial^2\Phi_o}{\partial r^2} + 2\mu_i\frac{\partial^2\Phi_i}{\partial r^2} = \sigma\left(\frac{\partial^2\xi}{\partial z^2} + \frac{1}{R^2}\frac{\partial^2\xi}{\partial\theta^2} + \frac{\xi}{R^2}\right) \tag{5.19}$$

We calculate pressure using Bernoulli's equation and we get

$$\rho_o\left(\frac{\partial\Phi_o}{\partial t}\right) + 2nK(2q)^{n-1}\frac{\partial^2\Phi_o}{\partial r^2} - \rho_i\left(\frac{\partial\Phi_i}{\partial t}\right) - 2\mu_i\frac{\partial^2\Phi_i}{\partial r^2} = -\sigma\left(\frac{\partial^2\xi}{\partial z^2} + \frac{1}{R^2}\frac{\partial^2\xi}{\partial\theta^2} + \frac{\xi}{R^2}\right) \tag{5.20}$$

As, the functions Φ_i, Φ_o and ξ are known and therefore, we get

$$\beta_1\omega^2 + i\beta_2\omega - \beta_3 = 0 \tag{5.21}$$

$$\beta_1 = \rho_i A_i(kR) - \rho_o A_o(kR)$$

$$\beta_2 = \alpha\left(A_i(kR) - A_o(kR)\right) + 2k^2\left(\mu_i B_i(kR) - nK(2q)^{n-1}B_o(kR)\right)$$

$$\beta_3 = \frac{\sigma k}{R^2}\left(k^2R^2 + m^2 - 1\right) + 2k^2\alpha\left(\frac{\mu_i}{\rho_i}B_i(kR) - \frac{nK(2q)^{n-1}}{\rho_o}B_o(kR)\right)$$

$$B_j(kR) = \left(1 + \frac{m^2}{k^2R^2}\right)A_j(kR) - \frac{1}{kR}, \quad (j = i, o)$$

As $\omega = \omega_R + i\omega_I$ we can get from (5.21) as;

$$\left.\begin{aligned} 2\beta_1\omega_R\omega_I + \beta_2\omega_R = 0 \Rightarrow \omega_R = 0 \\ \beta_1(\omega_R^2 - \omega_I^2) - \beta_2\omega_I + \beta_3 = 0 \end{aligned}\right\} \tag{5.22}$$

The value ω_R obtained from the first part will be used in the second part and we get

$$\beta_1\omega_I^2 + \beta_2\omega_I + \beta_3 = 0 \tag{5.23}$$

We can get the expression of Kim et al. [115] taking $n = 1$. A similar problem with inviscid gas was studied by Awasthi et al. [36], however, they have not used irrotational theory.

It should be noted that if $\beta_1 > 0, \beta_2 > 0, \beta_3 > 0$, the roots of equation (5.23) will have negative real part and interface will be stable. If we make use of modified Bessel functions properties, β_1 and β_2 will always be positive and therefore the stability norm will be $\beta_3 > 0$. The neutral stable state is expressed as

$$\frac{\sigma k}{R^2}\left(k^2R^2 + m^2 - 1\right) + 2k^2\alpha\left(\frac{\mu_i}{\rho_i}B_i(kR) - \frac{nK(2q)^{n-1}}{\rho_o}B_o(kR)\right) = 0 \tag{5.24}$$

Taking reference length $R_H = b - a$ and reference velocity V, equation (5.23) in dimensionless form can be written as

$$N^2\left[\rho A_i(\tilde{kR})-A_o(\tilde{kR})\right]+N\left[\Lambda\left(A_i(\tilde{kR})-A_o(\tilde{kR})\right)+2\tilde{k}^2\frac{Ca_l}{We_l}\left(\mu_l B_i(\tilde{kR})-nB_o(\tilde{kR})\right)\right]$$
$$+\left[\frac{\tilde{k}}{We_l}\left(\tilde{k}^2+\frac{m^2-1}{\tilde{R}^2}\right)+2\Lambda\tilde{k}^2\frac{Ca_l}{We_l}\left(\frac{\mu_l}{\rho}B_i(\tilde{kR})-nB_o(\tilde{kR})\right)\right]=0 \qquad (5.25)$$

Here $N=\frac{\omega H}{V}$ $\rho=\frac{\rho_i}{\rho_o}$, the generalized viscosity ratio $\mu_l=\frac{\mu_i}{K(2q)^{n-1}}$, the generalized capillary number $Ca_l=\frac{KV}{(2q)^{-n+1}\sigma}$, the generalized Weber number $We_l=\frac{\rho_o V^2 R_H}{\sigma}$ and $\Lambda=\frac{\alpha H}{\rho_o V}$.

The neutral stable state in the non-dimensional form will be

$$\tilde{k}^2+2\Lambda\tilde{k}Ca_l\left(\frac{\mu_l}{\rho}B_i(\tilde{kR})-nB_o(\tilde{kR})\right)+\frac{m^2-1}{\tilde{R}^2}=0 \qquad (5.26)$$

When disturbance waves have a small wavelength i.e. $k\to\infty$, the above equation reduces to

$$\tilde{k}^2+2\Lambda\tilde{k}Ca_l\left(\frac{\mu_l}{\rho}+n\right)=0 \qquad (5.27)$$

As Λ,ρ,μ_l and n are positive, $\tilde{k}_c$ is always negative.

For large wavelength disturbance waves $(k\to 0)$, equation (5.26) becomes

$$\left(m^2+\tilde{k}^2\tilde{R}^2-1\right)+2\Lambda\tilde{R}^2Ca_l\left(\frac{\mu_l}{\rho}\left(\frac{2\tilde{R}}{\tilde{R}^2-r_i^2}-\frac{1}{\tilde{R}}\right)-\left(\frac{2\tilde{R}}{r_o^2-\tilde{R}^2}-\frac{1}{\tilde{R}}\right)\right)=0 \qquad (5.28)$$

As $\Lambda Ca_l\left(\frac{\mu_l}{\rho}\left(\frac{2\tilde{R}}{\tilde{R}^2-r_i^2}-\frac{1}{\tilde{R}}\right)-\left(\frac{2\tilde{R}}{r_o^2-\tilde{R}^2}-\frac{1}{\tilde{R}}\right)\right)>\frac{1}{2}$, no critical wave number was found in this case.

It should be noted that one cannot achieve real k from equation (5.26) for $m \geq 1$ and therefore for numerical discussions, we will plot the axisymmetric disturbances.

5.4 RESULTS AND DISCUSSIONS

The transport of mass and heat is a coupled phenomenon because when a hot and soluble viscous fluid mixes with another viscous fluid, the concentration changes along with the heat. This is the reason to study the coupled effect here. The essential dimensionless parameters which direct the perturbation's growth are the heat transfer Λ, the capillary number Ca, the Weber number We, and the power-law index n.

The criteria obtained for the stability of the considered system have been analyzed numerically. The results are numerically computed for the equations (5.25) and (5.26). Equation (5.25) is an algebraic equation in degree 2 and for the particular values of other physical variables, the equation provides 2 roots. The maximum of these two roots has been displayed here. On the other hand, equation (5.26) is an implicit function and the well-known Newton-Raphson procedure is used hare to compute the wave-number $\tilde{k}$. The non-dimensional parameters are given in Table 5.1.

Figure 5.2 shows the maximum growth curves of perturbation for two different combinations of inner fluid; namely inviscid inner fluid and viscous inner fluid, therefore, this figure will help us to investigate the response of inner fluid's viscosity on the interface. Awasthi et al. [36] studied the interface of inviscid gas and power-law viscoelastic fluid including heat transport. It can be easily seen from this figure that the growth of perturbations is higher in the case of inviscid inner fluid than the viscous one indicating that viscosity of the inner fluid induces stability to the interface. The viscosity produces the viscous forces that are absent in the inviscid

fluid. These viscous forces oppose the growth of perturbations and instability delays. It should also be noted that the maximum growth of perturbations decays with the increase in the heat transport at the interface. At the higher rate of heat transport, the growth vanishes and this value will give us the threshold wave-number numerically. The expression of threshold wave-number is already obtained in equation (5.26). The nature of curves shows that the transport of heat at the interface delays the instability and this trend is the same for both the inviscid inner fluid and viscous inner fluid.

The degree of non-Newtonian behavior of a fluid can be measured in terms of the power-law index n. Based on the power-law index, a fluid can be categorized into three types; shear-thickening fluid $(n>1)$, Newtonian fluid $(n=1)$, and shear-thinning fluid $(n<1)$. The maximum growth curves for a range of the power-law index are shown in figure 5.3. On increasing the power-law index, the viscous stress tends to increase and these viscous stresses increase the viscous forces. An increase in viscous forces makes it difficult for perturbations to move fast and interface moves towards stability. The same observation is achieved from figure 3 and is consistent with Awasthi et al. [36]. One can also observe that the perturbation's growth is higher for shear-thinning fluid $(n=0.8)$ than the Newtonian fluid $(n=1)$ and shear-thickening fluid $(n=1.2,1.4)$. Hence, shear-thickening fluid may form large-scale droplets than the Newtonian fluid while shear-thinning may form small-scale droplets.

The behavior of capillary numbers Ca on the wave-number curves has been shown in figure 5.4. The region above the wave number curve is stable while the below region is unstable. The figure suggested that an increment in the capillary number expands the stable region revealing the stabilizing nature of capillary number. As per the definition, the capillary number directly depends on consistency coefficient

K and inversely varies with surface tension σ and coefficient q and therefore, the consistency coefficient has stabilizing nature while σ and q increases the perturbation's growth. The increase in surface tension increases capillary forces and these capillary forces increase the amplitude of perturbation so that droplets are formed more quickly. An increment inconsistency coefficient will increase the amount of viscous forces at the interface and consequently stability rises.

It can also be recognized from figure 4 that the region of stability increase with the increase of viscosity ratio μ_l and therefore, the viscosity ratio μ_l acts to prevent the instability. As viscosity ratio μ_l depends directly on the viscosity of the inner fluid indicating that the inner fluid's viscosity has stabilizing character. On increasing the viscosity, the flow impedes and interface stabilizes. On the other hand, the coefficient q has destabilizing nature as μ_l inversely proportional to q.

The region of stability with various values of heat transfer coefficient Λ is displayed in figure 5.5. The unstable region shrinks with increasing heat transfer rate illustrating the stabilizing nature of Λ. Kim et al. [115] and Awasthi et al. [36] also found the same character of heat transport on the interface in an annular region. The effect of the transport of heat along with mass at the interface can be ascribed to relative evaporation and condensation. The viscous fluid region is hot and close to the peaks while the power-law fluid region is close to the trough so condensation at the troughs will occur while the peaks will evaporate. The power-law fluid will expand closer to the hot viscous fluid and the rate of evaporation will increase. This increased rate of evaporation will prevent the increase of perturbation and the interface will acquire instability late. The maximum growth rate is shown in Table 5.2 for different

values of heat transfer coefficient. One can observe that the perturbations growth decays as heat transport increases.

The increase in power-law fluid thickness tends to increase the evaporation rate at the interface but the condensation decreases because the viscous fluid thickness decreases (needless to say that the annular region is fixed). This one-sided evaporation will increase the amplitude of perturbations and they will travel faster. Hence, an interface with a thin power-law fluid layer is more stable than the thick power-law fluid layer as observed from figure 5.6.

The influence of Weber number on the maximum growth of perturbations is plotted in figure 5.7. The perturbation's growth decreases with an increase in Weber number specifying the stabilizing behavior of Weber number. The inertia forces induce stability to the interface as Weber number directly depends on inertia force; meanwhile, surface tension has destabilizing character. The growth rate curves with fluid density ratio are displayed in figure 5.8. The perturbation's growth decays with the rise of fluid's density ratio and therefore, density ratio plays stabilizing role at the interface. Since the density ratio increases with the increase in the viscous fluid's density, the density of viscous fluid tend to reduce the flow of perturbation while the power-law fluid's density acts to stabilize the interface. By increasing the density of the viscous fluid, the inertia force acts as a neutral force against disturbances and slows down the flow of disturbances. As the density of the power-law fluid increases, more momentum is transferred from the viscoelastic fluid to the viscous fluid, and this momentum increases the aerodynamics effects consequently increasing the amplitude of disturbances and destabilizing the interface.

5.5 CONCLUSIONS

The capillary instability at the viscous fluid-viscoelastic fluid interface is studied analytically. The power-law viscoelastic is considered and the interface is transporting heat along with mass from one fluid phase to another. The irrotational flow theory of viscous-viscoelastic fluid is employed to work out the mathematical equations. The algebraic equation of the growth rate parameter is computed and analyzed numerically. The effects of various non-dimensional variables are shown on the instability of the interface. The transport of heat is found to stabilize the interface by enlarging the stability range. The viscosity of the viscous fluid is preventing the perturbation's growth. The power-law index and consistency coefficient have stabilizing character while the density of power-law has an inverse effect. Surface tension supports the perturbation's growth. It is also found that the shear-thickening fluid interface is more stable than the shear-thinning fluid interface.

Table 5.1: Parameters values for numerical computation

Parameter	values
μ_l	0.01
ρ	0.001
Ca	0.07
We	0.7
n	0.8
Λ	0.01

Table 5.2: Variation of perturbations maximum growth with heat transfer coefficient Λ

heat transfer coefficient Λ	Maximum growth $(N_i)_{\max}$ when $n = 0.8$
0.001	0.2648
0.002	0.2638
0.003	0.2628
0.004	0.2617
0.005	0.2607
0.006	0.2597
0.007	0.2587
0.008	0.2577
0.009	0.2566
0.010	0.2556

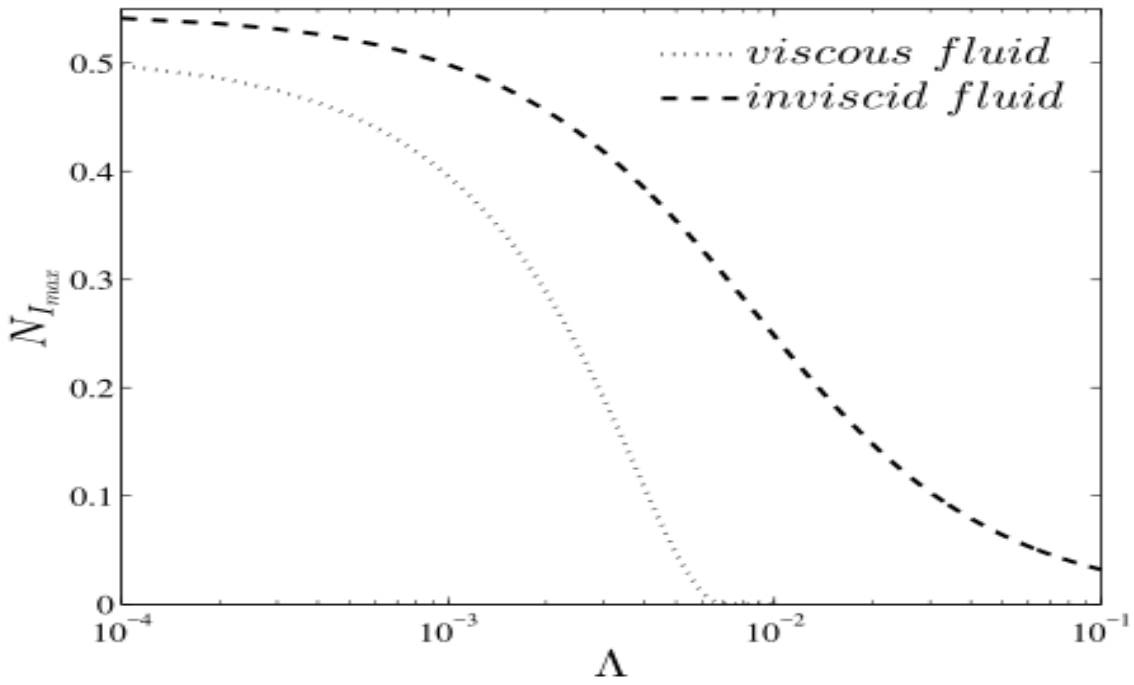

Figure 5.2: Effect of inner fluid's viscosity ($Ca = 0.07, We = 0.7, n = 0.8, \rho = 0.001$).

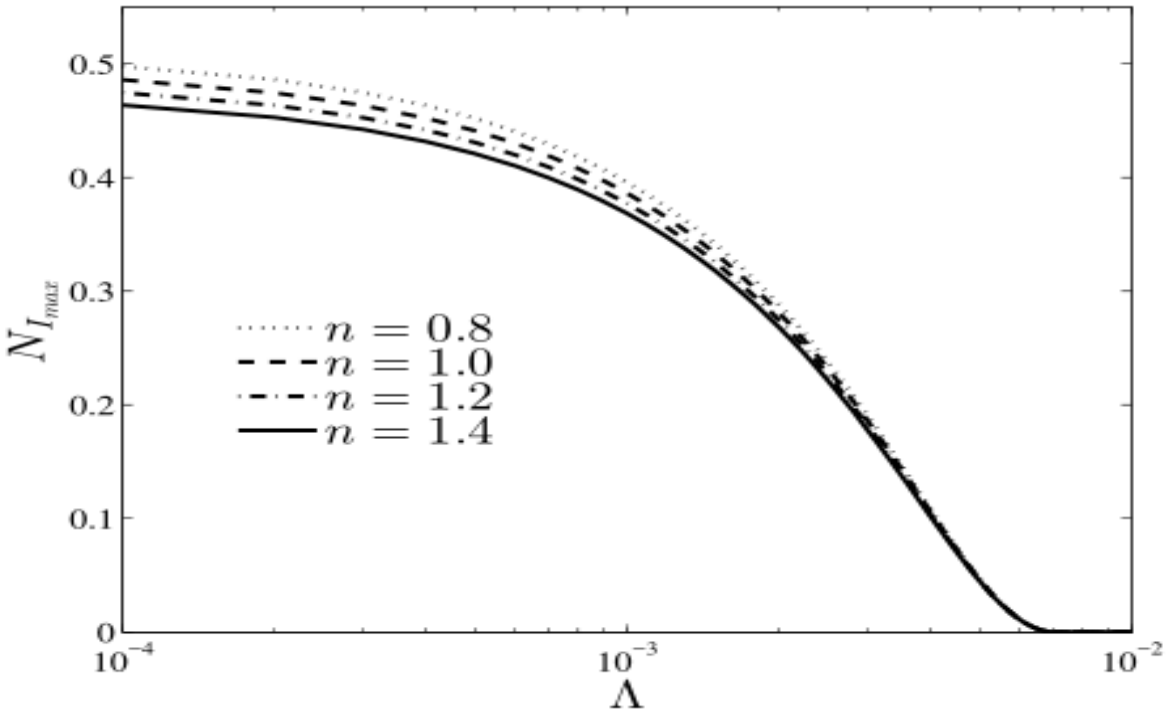

Figure 5.3: Effect of power-law index ($Ca = 0.07, We = 0.7, \mu_l = 0.01, \rho = 0.001$).

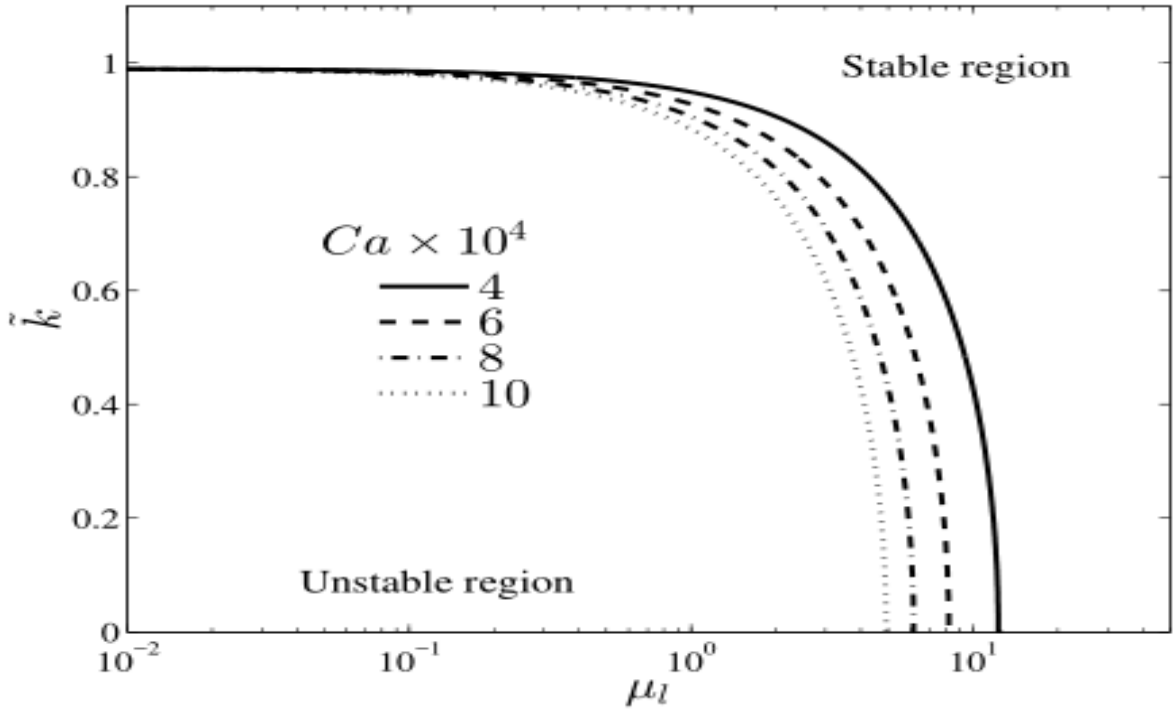

Figure 5.4: Effect of capillary number ($\Lambda = 0.01, n = 0.8, \rho = 0.01$).

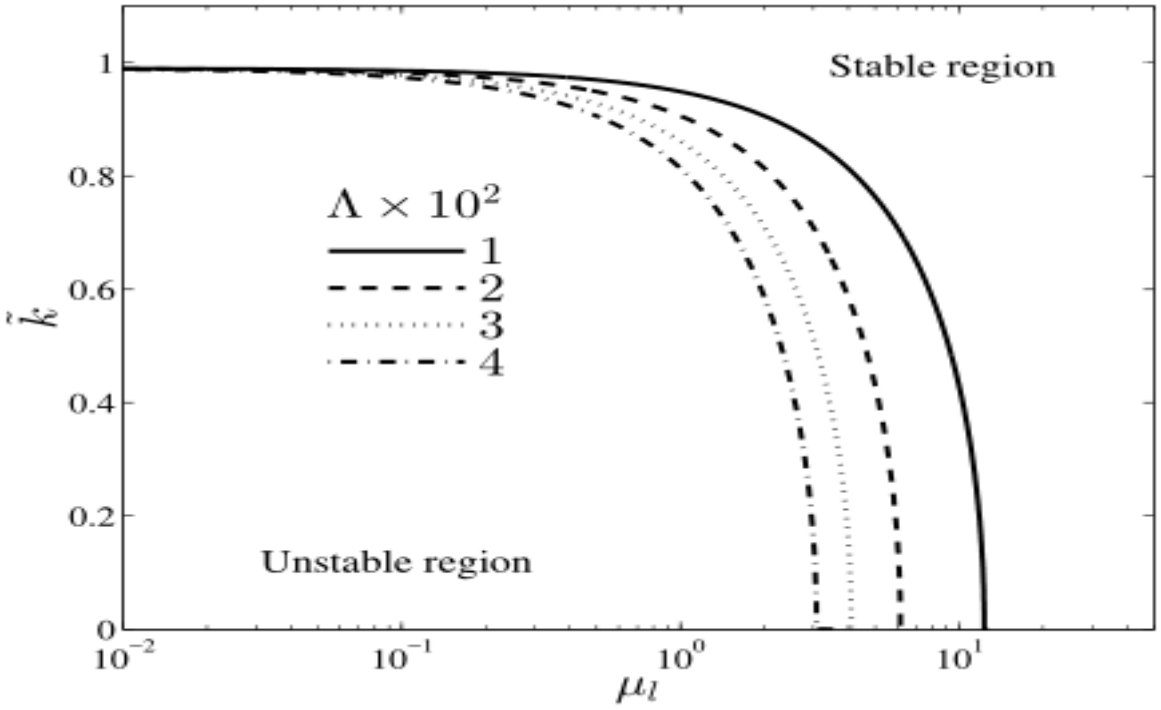

Figure 5.5: Effect of heat transport ($Ca = 0.0004, n = 0.8, \rho = 0.01$).

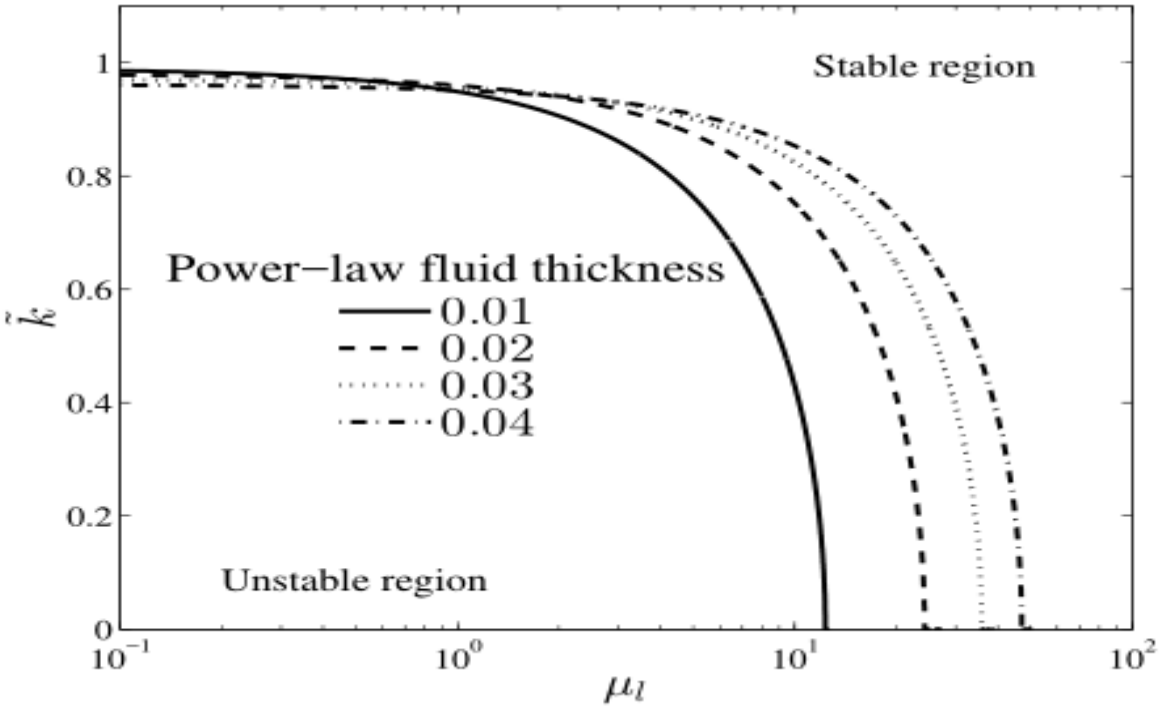

Figure 5.6: Effect of power-fluid thickness ($Ca = 0.0004, n = 0.8, \Lambda = 0.01, \rho = 0.01$).

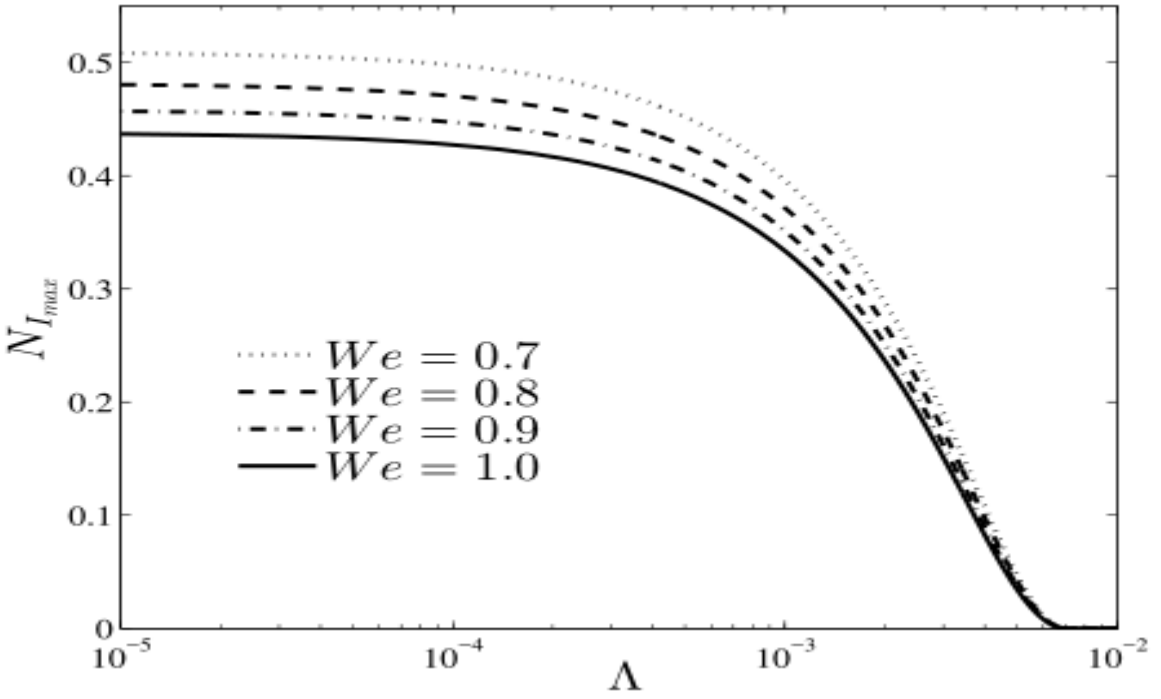

Figure 5.7: Effect of Weber number ($Ca = 0.07, \mu_l = 0.01, n = 0.8, \rho = 0.001$).

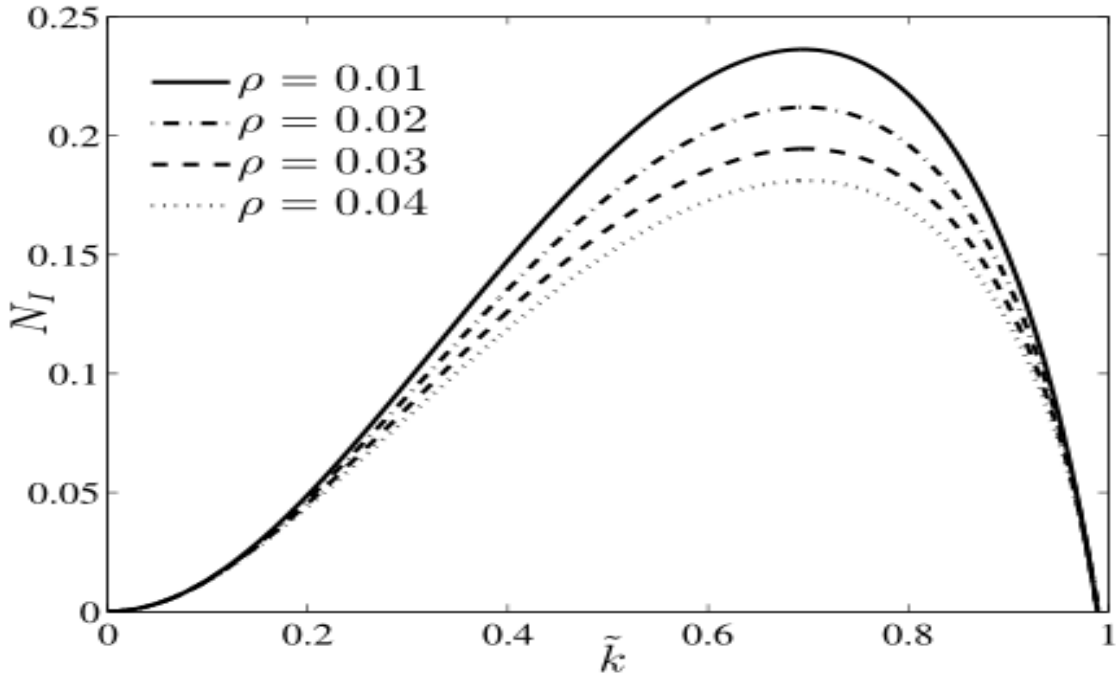

Figure 5.8: Effect of density ratio of fluids ($Ca = 0.0007, \mu_l = 0.01, n = 0.8, \Lambda = 0.01$).

CHAPTER 6

INSTABILITY OF NANOFLUID LAYER IN A CIRCULAR CYLINDRICAL CAVITY

The instability of an interface formed at the boundary of a circular cylindrical cavity is examined through an irrotational theory of viscous fluids. The cavity is assumed to be an infinite circular cylinder and the flow is considered to be two-dimensional. The cavity is filled with the Newtonian viscous fluid while the fluid outside the cavity is taken as Newtonian nanofluid. The normal mode procedure is employed and the growth rate parameter is calculated. The quadratic relationship in growth rate is achieved and for larger modes, it reduces to the case of the planar interface. The variety of nanofluids' physical parameters is studied on the instability of the interface. The density of nanofluid makes the interface more unstable while nanofluid's viscosity has stabilizing nature. The nanofluid with larger radius nanoparticles form a more unstable interface than the smaller sized nanoparticles.

6.1 BACKGROUND

The interface formed by two fluids will be unstable due to gravitational acceleration if denser fluid lies above the lighter one. This type of instability is known as Rayleigh-Taylor instability (RTI) and can be observed in fusion reactors and inertial confinement fusion. In the Earth's gravity, water placed over oil is an example of RTI. RTI can occur when fluids are at rest or are accelerating (Rayleigh [174], Taylor [208]). The process of RTI occurrence was explained by Sharp [198]. Zhou [241-242] reviewed the RTI and Richtmyer–Meshkov instability with the mixing layer concept. Boffeta and Mazzino [45] and Kull [118] also provide a comprehensive and systematic study on RTI.

Apart from natural phenomena, RTI also contributes significantly to industrial developments such as die-casting processes in which liquid metal is injected through an air-filled cavity. The cylindrical jet breakup of a fluid with a combined effect of capillary force and the electro-magnetic field was explained by Moatimid et al. [153]. Carpentier et al. [48] included the effect of transverse acoustic waves in a low-velocity jet. The HYLIFE-II inertial fusion reactor is the best example where the RTI exists at the interface of an infinite cylinder surrounded by another fluid. Chen et al. [52] studied the stability of a circular interface of two non-viscous fluids. They have considered the flow as two-dimensional. The study RTI with a hybrid granular model was done by Vinningland et al. [220]. Ueno et al. [216] presented the collapsing and condensing process of a bubble injected into a pool.

The irrotational theory of viscous fluids was presented by Joseph and Liao [105] and they were suggesting that for an irrotational motion of fluids, the viscosity may not be zero. Joseph et al. [107] applied this theory to study the RTI at the interface of two viscous fluids. This study was extended for viscous/viscoelastic fluids by Joseph et al. [106]. Various authors in the literature ([11, 18, 23, 201]) have also employed the irrotational theory of viscous (viscoelastic fluids) to investigate the instability of an interface.

The instability at the interface of an infinite circular cylinder can be described by a two-dimensional flow. Awasthi and Agarwal [21] examined the interfacial instability at an infinite circular cylinder. The nonlinear evolution of single-mode RTI in two-dimensional cylindrical flow was analytically studied by Zhao et al. [240]. The instability of the rotating cylindrical fluid column with a magnetic field was analyzed by El-Dib et al. [62]. The rotating cylindrical porous column with various external effects such as electric field, Marangoni convection, etc. was investigated by

Moatimid et al. [156-157]. The RTI in a spherical configuration was studied by Awasthi and Agarwal [22].

In recent years, the study of nanofluids has obtained special consideration due to their applications in several parts of science, engineering, and technology, such as material development, petroleum, chemical, and nuclear manufacturing, geological storage of carbon dioxide, and bioengineering. The interfacial instability of a Newtonian/non-Newtonian nanofluid has been considered very much attention by researchers in the past few years. The analytical, as well as numerical linear study of the stability of viscoelastic nanofluid with electromagnetic effects, was made by Hassan [93]. Moatimid and Hassan [149] studied the convective linear stability of Walter's type nanofluid. The stability of the interface formed by two nanofluid layers was examined by Moatimid and Hassan [150]. Moatimid et al. [152] included the swirling effect on the stability of nanofluid layers. Awasthi et al. [36] studied the RTI of a power-law nanofluid in a planar configuration. Han [91] examined the Kelvin-Helmholtz instability in a nanofluid layer with heat and mass transfer.

All the studies on the interfacial instability of nanofluid layers to date have been done either in plane geometry or in a cylindrical configuration. To the best of my knowledge, no study is found in the literature dealing with interfacial instability in a cavity. This is an attempt to investigate the instability of the circular interface formed at the boundary of the circular cavity. The Newtonian nanofluid lies outside the cavity while the inside region is filled with the Newtonian viscous fluid. We use VPF theory which is based on the irrotational motion of fluids but viscosity is not zero. The nanofluid viscosity depends upon the shape of the nanoparticles, fractal aggregates, base fluid viscosity, and volume fractions of nanoparticles. The dispersion relationship is achieved in the growth rate of perturbations and it is shown that this

relation reduces to the same relation of Joseph et al. [107] for larger modes. The modeled governing equations are presented in section 6.2 and section 6.3 contains the dispersion relationship. The results are discussed in section 6.4 and conclusions are presented in section 6.5.

6.2 MATHEMATICAL MODEL

We consider an infinite circular cylindrical cavity of radius R filled with a fluid of density ρ_i and viscosity μ_i (figure 6.1) surrounded by a Newtonian incompressible nanofluid of density ρ_o and viscosity μ_o. The viscous fluid lies in the region $r < R$ while the region $r > R$ contains the nanofluid; the circular boundary $r = R$ represents the interface of viscous fluid-nanofluid. The nanofluid is considered heavier than the viscous fluid and therefore the interface of viscous fluid-nanofluid will be unstable due to gravitational acceleration and the interface will experience Rayleigh-Taylor instability.

If $\vec{q}_o$ and $\vec{q}_i$ are velocities of fluids outside and inside cavity, the governing partial differential equations can be written as

$$\left.\begin{aligned} &\nabla \bullet \vec{q}_o = 0 \\ &\rho_o\left(\frac{\partial \vec{q}_o}{\partial t} + (\vec{q}_o \bullet \nabla)\vec{q}_o\right) = -\nabla p_o + \mu_o \nabla^2 \vec{q}_o \end{aligned}\right\} \tag{6.1}$$

$$\left.\begin{aligned} &\nabla \bullet \vec{q}_i = 0 \\ &\rho_i\left(\frac{\partial \vec{q}_i}{\partial t} + (\vec{q}_i \bullet \nabla)\vec{q}_i\right) = -\nabla p_i + \mu_i \nabla^2 \vec{q}_i \end{aligned}\right\}, \quad \nabla^2 = \frac{\partial^2}{\partial r^2} + \frac{1}{r^2}\frac{\partial}{\partial \theta^2} + \frac{1}{r}\frac{\partial}{\partial r} \tag{6.2}$$

The density ρ_o and viscosity μ_o can be expressed as follows (Awasthi et al. [38])

$$\rho_o = \phi\rho_p + (1-\phi)\rho_f \tag{6.3}$$

Here, ρ_f is the density of the base fluid, ρ_p is the density of metal particles and the nanoparticle volume fraction is denoted by ϕ.

$$\mu_o = \mu_{ef}\left(1-\frac{\phi_{ag}}{\phi_m}\right)^{-[\delta]\phi_m} \tag{6.4}$$

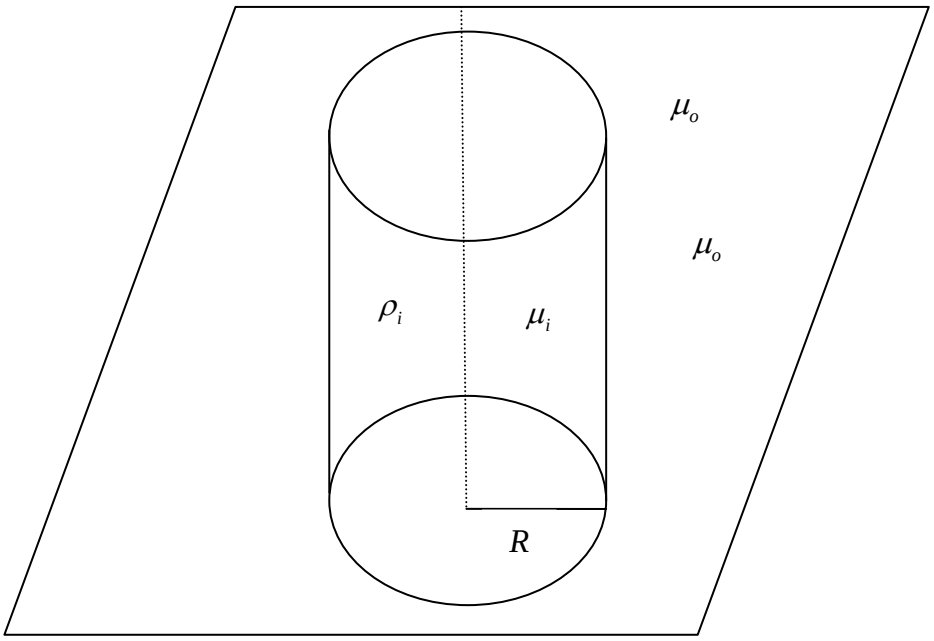

Figure 6.1: Flow diagram

Here, μ_{ef} is the density of the pure fluid, ϕ_m is the maximum volume fractions for spheroids nanoparticles and the nanoparticles shape parameter is denoted by δ. The nanoparticles aggregate volume fraction ϕ_{ag} can be written in terms of nanoparticles equivalent volume fractions ϕ_{mod} and fractal index d as (Awasthi et al. [38]);

$$\phi_{ag} = \phi_{\text{mod}}\left(\frac{r_a}{r}\right)^{3-d} \tag{6.5}$$

Here, nanoparticle's equivalent volume fractions ϕ_{mod} in terms of volume fraction ϕ, interfacial layer thickness γ, lengths of nanoparticles semi-minor and semi-major axes b and a, respectively, can be expressed

$$\phi_{\text{mod}} = \phi\left(1+\frac{\gamma}{a}\right)\left(1+\frac{\gamma}{b}\right)^2 \tag{6.6}$$

The circular interface is perturbed by imposing a small disturbance and the interface reduces to the form $r = R + \xi(\theta,t)$, where, $\xi(\theta,t) = \varsigma e^{\omega t}\cos n\theta$.

6.3 DISPERSION RELATIONSHIP

Initially, fluids are at rest i.e. $\vec{q}_o = \vec{q}_i = 0$. The flow velocity in a perturbed state can be written as $\vec{q}_o = 0 + \vec{q}_o'$; $\vec{q}_i = 0 + \vec{q}_i'$. In this theoretical analysis, the perturbed flow is taken as irrotational i.e. $\vec{q}_o' = \nabla\Phi_o(r,\theta,t)$; $\vec{q}_i' = \nabla\Phi_i(r,\theta,t)$ and these potential functions are harmonic i.e. $\nabla^2\Phi_o = 0$; $\nabla^2\Phi_i = 0$.

The well-known normal mode expansion for perturbed quantities is employed and therefore, the expressions for potential functions can be written as

$$\Phi_o(r,\theta,t) = H_o(r)e^{\omega t}\cos n\theta \tag{6.7}$$

$$\Phi_i(r,\theta,t) = H_i(r)e^{\omega t}\cos n\theta \tag{6.8}$$

Using the harmonic conditions, the differential equations for $H_o(r)$ and $H_i(r)$ can be obtained as

$$r^2\frac{d^2H_o}{dr^2} + r\frac{dH_o}{dr} - n^2H_o = 0 \;\Rightarrow\; H_o(r) = A_o r^{-n} + B_o r^n \tag{6.9}$$

$$r^2\frac{d^2H_i}{dr^2} + r\frac{dH_i}{dr} - n^2H_i = 0 \;\Rightarrow\; H_i(r) = A_i r^{n} + B_i r^{-n} \tag{6.10}$$

The coefficient B_o will be zero as the solution must be finite when $r \to \infty$ and similarly B_i is also zero.

Hence, the potential functions for outside and inside perturbed flow can be expressed as

$$\Phi_o(r,\theta,t) = A_o e^{\omega t} r^{-n} \cos n\theta, \qquad r > R \tag{6.11}$$

$$\Phi_i(r,\theta,t) = A_i e^{\omega t} r^{n} \cos n\theta, \qquad r < R \tag{6.12}$$

As kinematic boundary condition says that if a fluid particle is at the interface, it will remain at the interface throughout the analysis, and therefore, the normal velocity of the interfacial boundary is zero i.e. at $r = R + \xi(\theta,t)$

$$\frac{\partial \xi}{\partial t} + \frac{1}{r^2}\frac{\partial \Phi_o}{\partial \theta}\frac{\partial \xi}{\partial \theta} - \frac{\partial \Phi_o}{\partial r} = 0 \tag{6.13}$$

$$\frac{\partial \xi}{\partial t} + \frac{1}{r^2}\frac{\partial \Phi_i}{\partial \theta}\frac{\partial \xi}{\partial \theta} - \frac{\partial \Phi_i}{\partial r} = 0 \tag{6.14}$$

If we use equation (6.13) for equation (6.11) and equation (6.14) for equation (6.12), the expressions for potential functions can be obtained as

$$\Phi_o(r,\theta,t) = -\varsigma\omega\frac{R}{n}e^{\omega t}\left(\frac{R}{r}\right)^n \cos n\theta, \qquad r > R \tag{6.15}$$

$$\Phi_o(r,\theta,t) = \varsigma\omega\frac{R}{n}e^{\omega t}\left(\frac{r}{R}\right)^n \cos n\theta, \qquad r < R \tag{6.16}$$

The difference of irrotational viscous stresses is neutralized by the surface tension force. Mathematically

$$\left(P_o - 2\mu_o\frac{\partial^2 \Phi_o}{\partial r^2}\right) - \left(P_i - 2\mu_i\frac{\partial^2 \Phi_i}{\partial r^2}\right) = \frac{\sigma}{R_p} \tag{6.17}$$

Here, σ is the surface tension and R_p denotes the principal radius. Taking the linear perturbations, the value of R_p can be computed as

$$\frac{1}{R_p} = \left(n^2 - 1\right)\frac{\xi}{R^2} \tag{6.18}$$

The pressures will be computed using Bernoulli's equation and equation (6.17) will be expressed as

$$\rho_o\left[\frac{\partial\Phi_o}{\partial t}+g\xi\right]+2\mu_{ef}\left(1-\frac{\phi_{ag}}{\phi_m}\right)^{-[\delta]\phi_m}\frac{\partial^2\Phi_o}{\partial r^2}-\rho_i\left[\frac{\partial\Phi_i}{\partial t}+g\xi\right]-2\mu_i\frac{\partial^2\Phi_i}{\partial r^2}=\sigma\left(n^2-1\right)\frac{\xi}{R^2} \tag{6.19}$$

The expressions (6.15) and (6.16) will be used in equation (6.19) and the dispersion relationship is achieved as

$$\omega^2+C\omega+D=0 \tag{6.20}$$

$$C=\frac{2n}{R^2\left(\rho_n+\rho_u\right)}\left(\mu_{ef}\left(1-\frac{\phi_{ag}}{\phi_m}\right)^{-[\delta]\phi_m}(n+1)+\mu_u(n-1)\right)$$

$$D=\frac{1}{\left(\rho_u+\rho_n\right)}\left[\frac{\left(\rho_u-\rho_n\right)gn}{R}+\frac{\sigma n\left(n^2-1\right)}{R^3}\right]$$

Here, ω is a complex variable i.e. $\omega=\omega_r+i\omega_i$ and if we compute the imaginary component of equation (6.20), we get either $\omega_i=0$ or $\omega_r=-C/2$. As C is always positive and we are examining the instability of the interface, we cannot choose $\omega_r=-C/2$. Using the expression $\omega_i=0$ in the real component of equation (6.20), we get

$$\omega_r^2+C\omega_r+D=0 \tag{6.21}$$

$$\text{Then } \omega_r=\frac{-C\pm\sqrt{C^2-4D}}{2}$$

As C is always positive, ω_r will be positive (i.e. unstable situation) if $C<\sqrt{C^2-4D}$ i.e. $D<0$. Hence, the stability criterion is expressed as

$$\left(n^2-1\right)>g\frac{R}{\sigma}\left(\rho_n-\rho_u\right) \tag{6.22}$$

It should be noted from equation (18) that the viscosity of the inside/outside fluids does not influence the stability margins which is expressed as

$$\left(n^2-1\right)-g\frac{R}{\sigma}\left(\rho_n-\rho_u\right)=0 \tag{6.23}$$

6.4 CONVERGENT AND DIVERGENT CONFIGURATIONS

The RTI occurs in convergence geometry for inertial confinement fusion and supernova explosions. For the case of convergent circular configuration, the gravitational acceleration can be written as $\boldsymbol{g}=-g\hat{\boldsymbol{e}}_{\boldsymbol{r}}$ and therefore, equation (6.23) takes form as

$$\left(n^2-1\right)+g\frac{R}{\sigma}\left(\rho_n-\rho_u\right)=0 \tag{6.24}$$

Here, instability at the interface arises if $R<\dfrac{\sigma}{g\left(\rho_o-\rho_i\right)}$. The radius of the circular interface is always positive and therefore the convergent circular interface is always stable if the inside fluid density is greater than the outside fluid density (i.e. $\rho_i>\rho_o$).

If the circular configuration is divergent i.e. $\boldsymbol{g}=g\hat{\boldsymbol{e}}_{\boldsymbol{r}}$, the stability criterion takes form as

$$\left(n^2-1\right)-g\frac{R}{\sigma}\left(\rho_o-\rho_i\right)=0 \tag{6.25}$$

It should be noted here that $R>-\dfrac{\sigma}{g\left(\rho_o-\rho_i\right)}$. Hence instability occurs only if $\rho_o<\rho_i$.

6.5 COMPARISON WITH A PLANAR CONFIGURATION

Here, one can assume that the modes n can be shown in terms of the radius of the circular cavity R as $n=kR$, where k denotes wave number.

So, if the radius of the cavity is very large, the perturbation modes will also be large i.e. as $R \to \infty, n \to \infty$.

Taking the approximation $n = kR$ in the equation (6.20) and making $R \to \infty$, we get

$$\omega_r^2 + \left[\frac{2k^2}{(\rho_o + \rho_i)} \left(\mu_{ef} \left(1 - \frac{\phi_{ag}}{\phi_m} \right)^{-[\delta]\phi_m} + \mu_u \right) \right] \omega_r + \frac{1}{(\rho_i + \rho_o)} \left[(\rho_i - \rho_o) gk + \sigma k^3 \right] = 0 \tag{6.26}$$

If the outside fluid is Newtonian viscous fluid i.e. $\phi_{ag} = 0$, equation (6.26) reduces to the equation (6.24) of Joseph et al. [107]. Hence, one can conclude that at the very large modes, the circular geometry behavior is similar to the planar one.

6.6 DIMENSIONLESS ANALYSIS

The non-dimensional form of equation (6.21) can be written as

$$N^2 + \frac{2n}{(1+\rho)\,\mathrm{Re}_n} \left(\left(1 - \frac{\phi_{ag}}{\phi_m} \right)^{-[\delta]\phi_m} (n+1) + \mu(n-1) \right) N + \frac{1}{(1+\rho)} \left[(\rho - 1)\,\hat{g}n + \frac{n\left(n^2 - 1\right)}{We_n} \right] = 0 \tag{6.27}$$

Here, $N = \omega_r \tau$, $\rho = \frac{\rho_i}{\rho_o}$, $\mu = \frac{\mu_i}{\mu_{ef}}$, $\mathrm{Re_n} = \frac{\rho_n V R}{\mu_{ef}}$, $We_n = \frac{\rho_n V^2 R}{\sigma}$, $\hat{\mathrm{g}} = \frac{gR}{V^2}$, $\tau = \frac{R}{V}$,

V is the characteristic velocity and R represents the characteristic length.

6.7 NUMERICAL RESULTS AND DISCUSSIONS

The numerical computation has been made here for the interface formed by water and $ZnO-$Ethylene Glycol nanofluid. The nanofluid is considered outside the cavity while water lies inside. Hence, viscosity and density of inside fluid are taken as $0.000891\ Kg/m\text{-}s$ (at $25^0 C$) and $1027\ Kg/mt^3$. The density and viscosity of $ZnO-$Ethylene Glycol nanofluid with 3% volume fraction are $1128.5\ Kg/mt^3$ and

$0.01620\ Kg/m\text{-}s$ (at 25^0C). The surface tension at the interface is taken as $0.0473\ N/mt$.

In this analysis, the shape of the nanoparticles is taken as a sphere. Experimentally, it was shown that the value of shape parameter δ for sphere-shaped nanoparticles is 2.5 and ϕ_m lies between the range 0.68-0.75. In this paper ϕ_m is considered as 0.74. The fractal index for sphere-shaped nanoparticles is taken as 1.8 and $\gamma = 2\times10^{-9}$. The values of a, b and r are taken as $a = b = r = 15\times10^{-9}$.

The irrotational theory of viscous fluids includes viscous effects in terms of normal viscous stresses while the IPF theory ignores viscous effects completely. To examine the influence of viscous effects on the interface of water-ZnO – Ethylene Glycol nanofluid, figure 6.2 has been displayed. It can be easily seen that the perturbations are growing faster in the IPF analysis than in the VPF theory. Viscosity is the ability of the fluid to resist the flow layers and therefore, the inclusion of viscosity makes it difficult for the perturbations to travel. Hence, VPF theory predicts a more stable interface than the IPF analysis.

The ratio of inertia force to the viscous force is known as the Reynolds number. The effect of Reynolds number on the water-ZnO – Ethylene Glycol nanofluid is shown in figure 6.3. It should be noted from figure 3 that the Reynolds number has destabilizing nature. If Reynolds number increases, either inertia force increases or viscous force decreases. As the viscosity of the fluids increases, the disturbed flow retarded, and instability delays. Hence, viscous forces have stabilizing character. Inertia force depends on the density of the fluid and as density increases; gravitational acceleration boosts the perturbation's growth and the interface moves towards instability. From the definition of Reynolds number in this problem,

$\mathrm{Re}_n \propto \rho_n$ and $\frac{1}{\mu_{ef}}$ and therefore, the density of nanofluids has destabilizing nature while the viscosity of Ethylene Glycol base fluid makes the interface more stable.

It should be noted from figure 6.4 that the volume fraction of nanoparticles induces stability at the interface because as the volume fraction ϕ of nanoparticles increases, the growth of perturbations decreases. When the volume fraction of nanoparticles increases in a fixed volume of base fluid, the produced nanofluid will be denser and the motion of perturbation waves in a denser medium will be slow. Hence, the nanofluid volume fraction makes the interface more stable.

The effect of the density ratio of viscous fluid to the nanofluid is examined in figure 6.5. It is observed from this figure that on increasing the density ratio, the growth of the perturbation decreases, and therefore, it can be concluded that the density of fluids has a stabilizing impact on the stability of the interface. Hence, the density of the viscous fluid induces stability while the density of nanofluid makes the interface more unstable. The gravitational acceleration plays a significant role in the analysis of the density of fluids. On increasing inside fluid density, gravitational acceleration works as retardation, and therefore, the growth of perturbations slows. On the other hand, if the density of nanofluid (outside fluid) increases, the gravitational acceleration moves the perturbation faster instability arises.

In the present analysis, sphere-shaped nanoparticles are considered and hence semi-major and semi-minor axes will be equal to the radius of nanoparticles i.e. $(a = b = r)$. The impact of nanoparticle radius on the interfacial instability is shown in figure 6.6. In this figure, we have plotted the maximum growth of perturbations with the fluids viscosity ratio. It can be seen that as the fluids viscosity ratio increases, the

perturbations maximum growth also increases indicating that the fluids viscosity ratio μ has destabilizing character. Since μ increases with the viscosity of the inside fluid and therefore the inside fluid viscosity tends to destabilize the interface. An increase in the inside fluid viscosity adds more energy to the amplitude of perturbations and the system gets destabilized. However, the outside fluid viscosity makes the interface stable.

It can also be noted from figure 6.6 that an increase in the radius of sphere-shaped nanoparticles grows the amplitude of perturbations. In other words, one can say that the nanofluid with larger nanoparticles form a more unstable interface than the nanofluid with smaller nanoparticles. As per the experimental observations, the volume of the interfacial layer depends directly on the surface area of the dispersed system, and therefore, for large nanoparticles, the global surface area decreases which finally decreases the volume of the interfacial layer. The decrement in the interfacial layer volume decreases viscosity and therefore, larger-sized nanoparticles have a lower viscosity than the smaller-sized particles. Hence, smaller-sized nanoparticles form a more stable interface.

Figure 6.7 examines the influence of nanoparticles fractal index on the instability of the system. The perturbations maximum growth decreases with the increase in nanoparticles fractal index suggesting that nanoparticles fractal index has stabilizing character. The influence of the fractal index can be explained from equation (6.5). For the fixed values of nanoparticles radius and nanoparticles volume fraction, the aggregate nanoparticles volume fraction ϕ_{ag} decreases with the increase in the fractal index. If the aggregate nanoparticles volume fraction ϕ_{ag} decreases, the viscosity of the nanofluid increases, and therefore, a nanofluid with a high fractal

index has a lower viscosity. As nanofluid viscosity stabilizes the interface and therefore, fractal index induces stability.

The effect of surface tension is shown in figure 6.8. Here, we have plotted the dispersion relation in the dimensional form. As surface tension increases, the force at the free surface increases because the interface length is fixed. This force at the free surface opposes the growth of perturbations and subsequently, the amplitude of perturbations diminishes. Hence, surface tension has stabilizing character as observed from figure 6.8.

6.8 CONCLUSIONS

The Rayleigh-Taylor instability in a circular cavity occurring at the interface of viscous fluid and nanofluid is investigated. The viscous fluid is inside the cavity while nanofluid is outside the cavity and both the fluids form a circular interface. The dispersion relationship is quadratic in growth rate and it reduces to the case of plane interface for larger modes of perturbations. The interfacial stability increases with an increase in the viscosity of the nanofluids while the density of nanofluids has destabilizing character. The nanoparticles volume fraction induces stability in the system. The viscosity of the inside fluid supports the growth of the perturbation while the density of the inside fluid has stabilizing nature. The radius of nanoparticles is delaying the stability while nanofluids fractal index has a stabilizing role. The VPF theory predicts a more stable interface than the IPF theory.

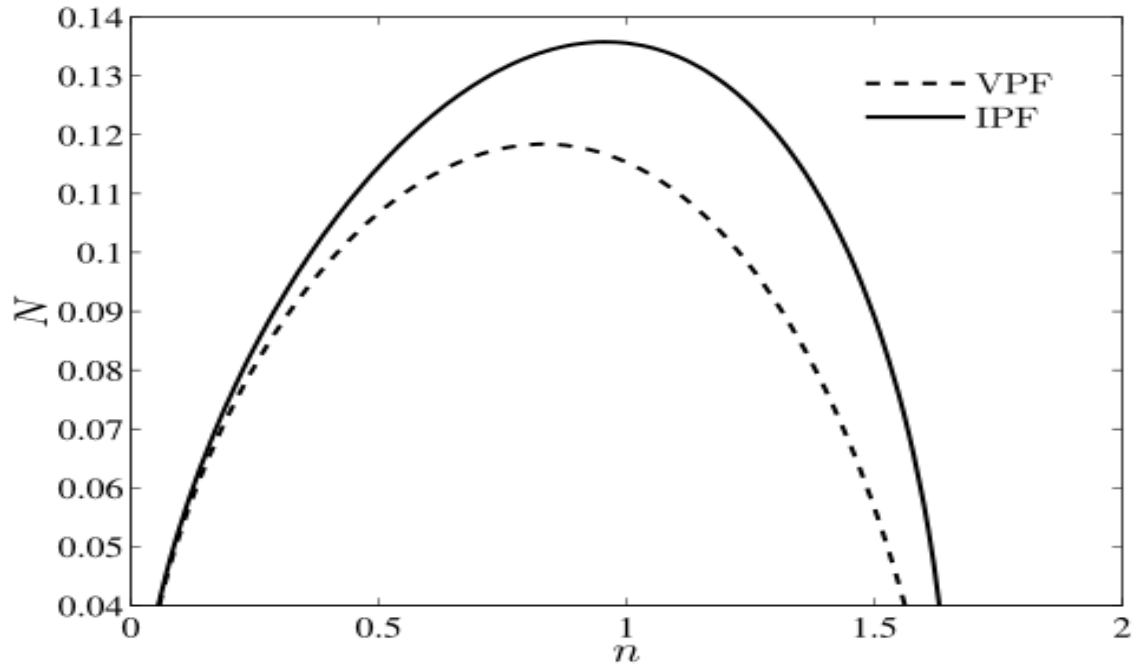

Figure 6.2: Comparison of IPF and VPF theories.

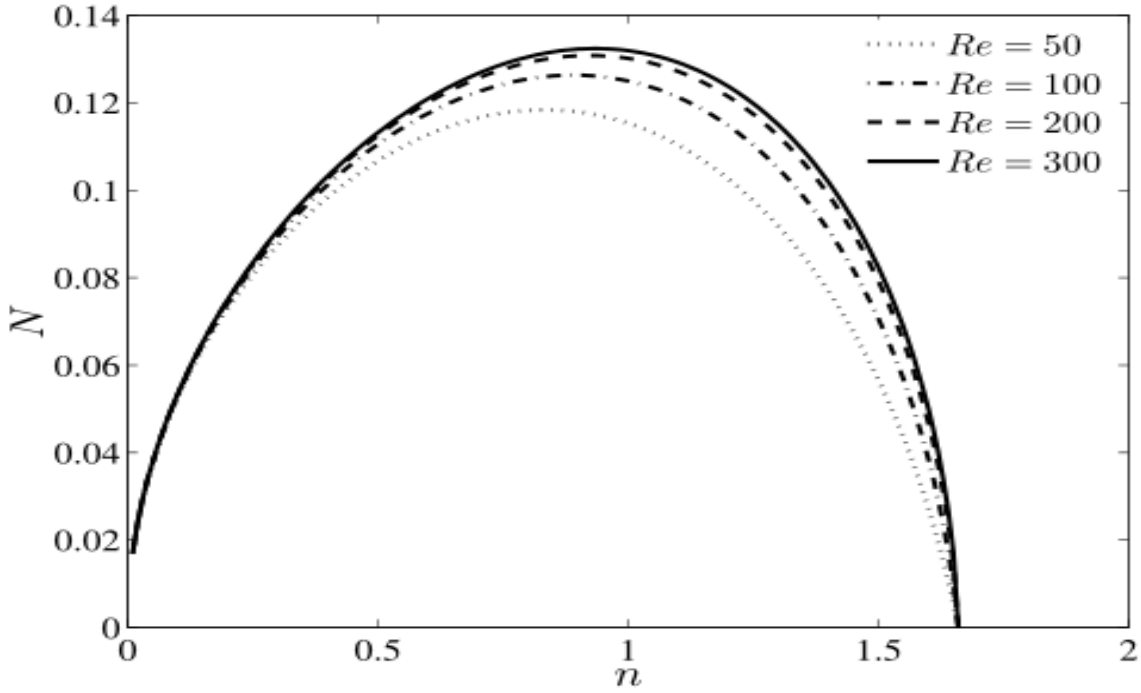

Figure 6.3: Effect of Reynolds number.

$(\rho = 0.91, \mu = 0.055, We_n = 50, \phi = 0.05, r = 15\times10^{-9}, d = 1.8, \delta = 2.5)$

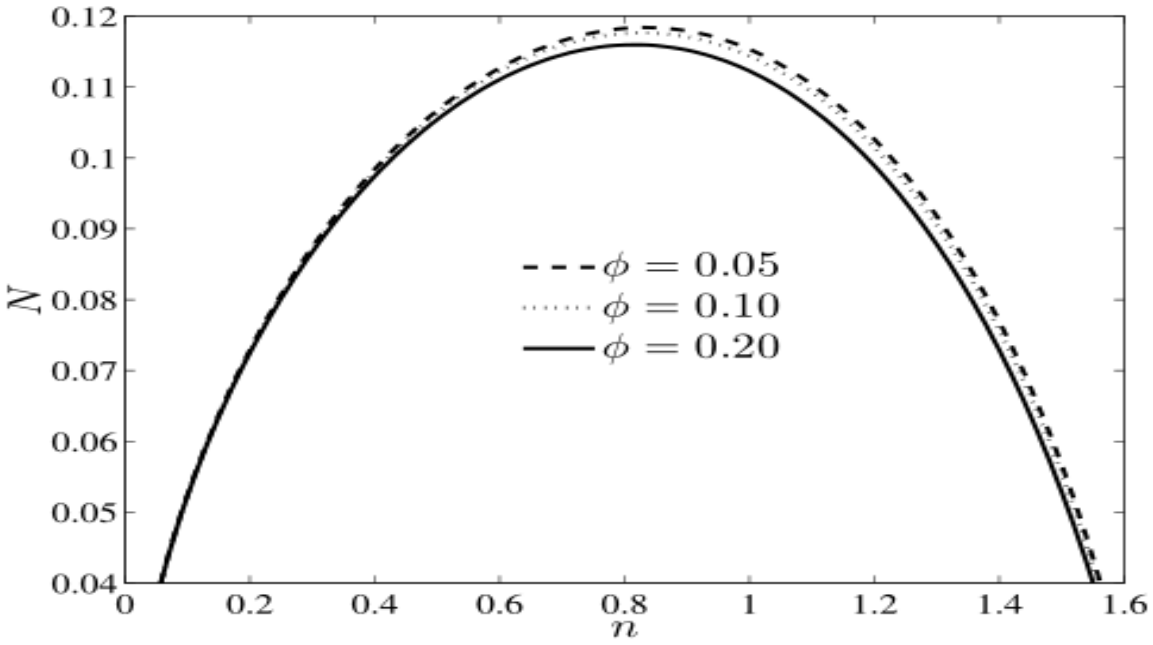

Figure 6.4: Effect of nanofluid volume fraction.

($\rho = 0.91, \mu = 0.055, We_n = 50, \mathrm{Re}_n = 50, r = 15\times10^{-9}, d = 1.8, \delta = 2.5$)

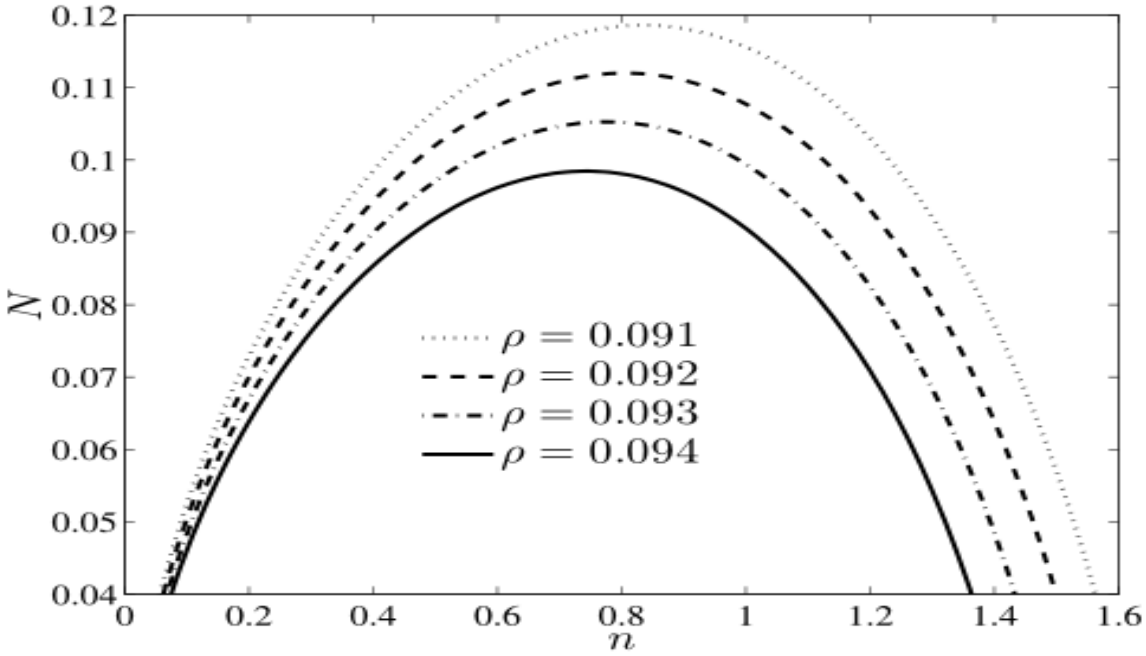

Figure 6.5: Effect of density ratio of fluids.

($\phi = 0.05, \mu = 0.055, We_n = 50, \mathrm{Re}_n = 50, r = 15\times10^{-9}, d = 1.8, \delta = 2.5$)

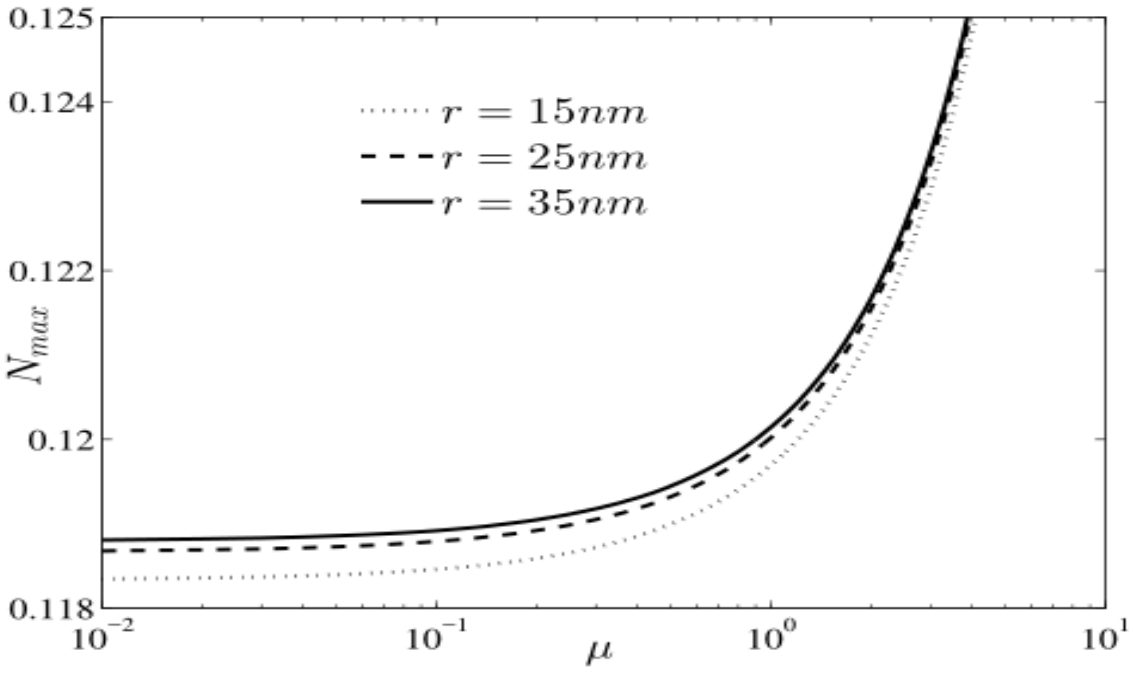

Figure 6.6: Effect of the radius of nanoparticles.

$(\phi = 0.05, We_n = 50, \mathrm{Re}_n = 50, d = 1.8, \delta = 2.5)$

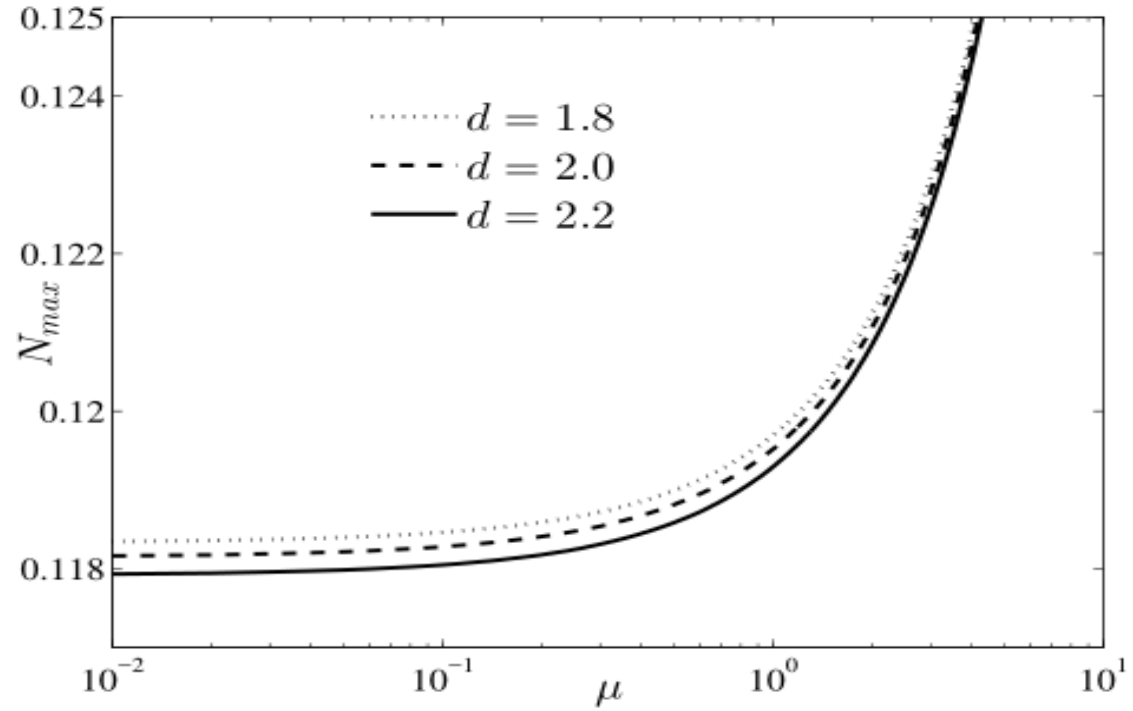

Figure 6.7: Effect of nanoparticles fractal index.

$(\phi = 0.05, We_n = 50, \mathrm{Re}_n = 50, \phi = 0.05, \delta = 2.5)$

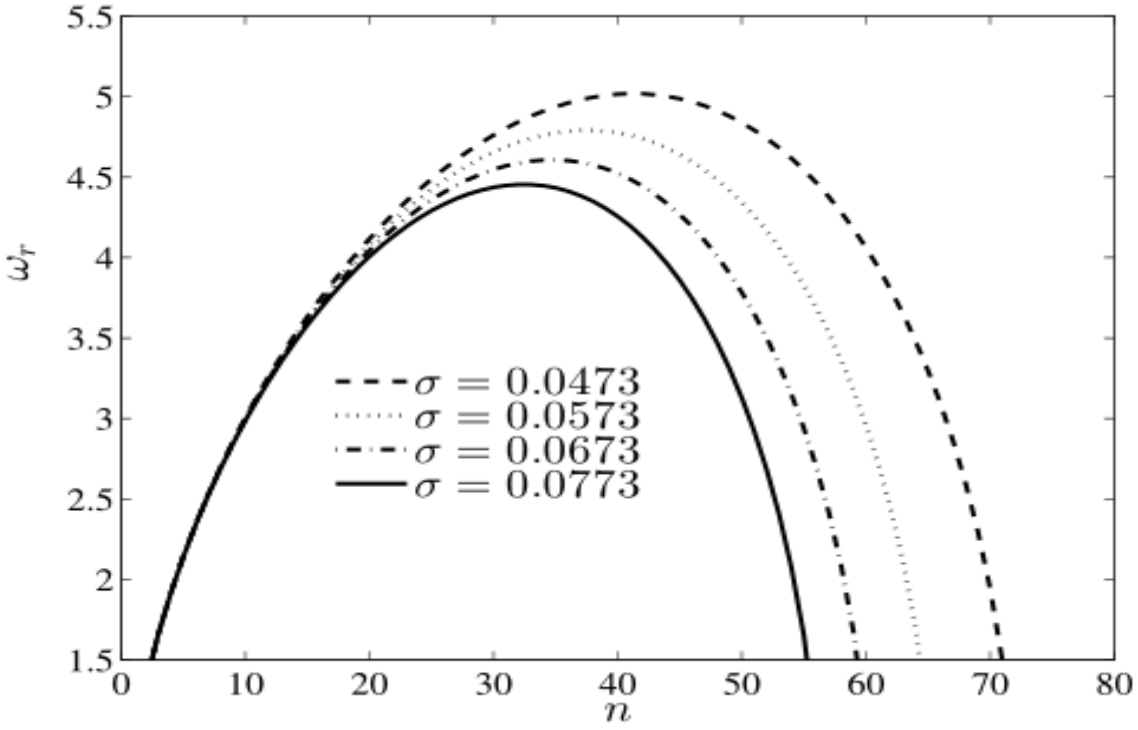

Figure 6.8: Effect of surface tension.

CHAPTER 7
CAPILLARY INSTABILITY AT THE INTERFACE OF TWO COMPRESSIBLE VISCOUS FLUIDS

This chapter reports the results of linear instability analysis of capillary stability at the viscous compressible fluid's interface. The compressible viscous fluid in the cylindrical coordinate system is surrounded by another viscous compressible fluid. The investigation was done by utilizing the potential flow theory (VPF theory) for the fluid satisfying the compressible flow model. A second-order implicit expression for the growth rate parameter is achieved and examined numerically. It is found that inside fluid viscosity slows the growth of disturbance but an increase in outside fluid viscosity makes the interface unstable. The interface goes towards instability when the surface tension increases at the interface.

7.1. BACKGROUND

If a liquid cylindrical column crashes into another liquid, the interface of fluids destabilizes and the instability is called capillary instability. Various natural phenomena such as bubble formation, the disintegration of the liquid jet, film boiling, and film-wise condensation where capillary instability can be observed. This instability is also called Plateau-Rayleigh instability as this is first discovered by Joseph Plateau and Lord Rayleigh. Plateau [171] observed the capillary instability experimentally at the interface of two fluids and Rayleigh [174] modeled this phenomenon in non-viscous fluids through irrotational theory. The interface of two viscous fluids was analyzed by Tomotika [211] using the normal mode procedure.

It is now universally accepted that the viscous flow motions can be evaluated by irrotational flow theory. Joseph and Liao [105] came up with the idea that viscous

flow motion can also be irrotational and the stress equation at the interface includes viscosity. Funada and Joseph [79] utilized this theory to solve the capillary stability problem at the two viscous fluids. The achieved outcomes were agreed with experimental observations. Funada and Joseph [80] continued their study of capillary stability for the viscoelastic fluid of Oldroyd B type and established that the fluid elasticity enhances the growth of the perturbation. Asthana et al. [10] utilized the above theory to analyze the Rayleigh-Taylor instability (RTI) in a cylindrical coordinate system. Moatimid et al. [152] considered the instability of rigid columns with the electric field while El-Dib et al. [62] investigated a similar analysis with a magnetic field.

The fluid's compressibility has a significant impact on designing the industrial process system and maintaining the infrastructure efficiency of the calibration lab. The compressible fluid's flow through channels and pipelines is generally affected by changing the flow parameters such as density, pressure, velocity, etc. Mitchner and Landshoff [148] analyzed RTI in compressible fluids for constant density and sound velocity. The stability of electrically conducting compressible fluid with magnetic field and Hall currents were examined by Ariel [7]. The joint effect of viscosity and magnetic field on the RTI of compressible fluids was analyzed by Bhatia [43]. Ogbonna and Bhatia [165] included frictional and Hall current effects in the study of Bhatia [43]. The compressible fluid layer of variable density was examined by Khan and Bhatia [111]. Yu and Livescu [237] analyzed the RTI at non-viscous compressible fluids in a cylindrical coordinate system. A new approach was proposed by Piriz et al. [170] to solve Rayleigh-Taylor instability for non-ideal fluids. The acceleration impact on the Rayleigh-Taylor instability was considered by Ghasemized et al. [86].

After reviewing the literature very carefully, the only study of viscous compressible fluids through irrotational theory was done by Funada et al. [83]. Even in their study, the inside fluid was taken as incompressible. They have studied the disintegration of an incompressible liquid jet in viscous compressible air.

In this chapter, an endeavor is made to examine the capillary instability of the viscous compressible fluids. The arrangement is taken in such a way that one cylindrical compressible fluid is surrounded by another compressible fluid. The viscous potential flow theory (VPF) is utilized for investigation and viscous fluids having different dynamic viscosities are assumed. The normal mode procedure is utilized to understand the instability of the considered arrangement. The instability-stability criteria are talked over and marginal stability curves are plotted.

7.2 MATHEMATICAL MODELING

As shown in figure 7.1, a cylindrical viscous compressible fluid column of density ρ_i, radius R, and viscosity μ_i is surrounded by a compressible viscous fluid with density ρ_o and viscosity μ_o. The interface experiences tension σ and there is no temperature difference in the fluid phases. The region $0 \le r \le R$ is filled with inside fluid while outside fluid lies in the region $R \le r < \infty$ and the fluids meet at $r = R$. The symmetric perturbations are included in this analysis.

The governing equations in terms of potential functions for the fluid phases can be written as

$$\left.\begin{aligned} \frac{\partial \rho_i}{\partial t} + \left(\nabla \Phi_i \cdot \nabla\right)\rho_i + \rho^{(1)}\nabla^2 \Phi_i = 0 \\ T_i^{ij} = 2\mu_i \frac{\partial^2 \Phi_i}{\partial x^i \partial x^j} - \frac{2\mu_i}{3}\left(\nabla^2 \Phi_i\right)\delta_{ij} \\ \frac{\partial \Phi_i}{\partial t} + \frac{1}{2}\left|\nabla \Phi_i\right|^2 + \frac{\gamma_i}{\gamma_i - 1}\frac{p_i}{\rho_i} - \frac{4\mu_i}{3\rho_i}\nabla^2 \Phi_i = B_i(t) \\ p_i = A\rho_i^{\gamma_i},\ \frac{dp_i}{d\rho_i} = \gamma_i A\rho_i^{\gamma_i - 1} = \gamma_i \frac{p_i}{\rho_i} = c_i^2 \end{aligned}\right\} \tag{7.1}$$

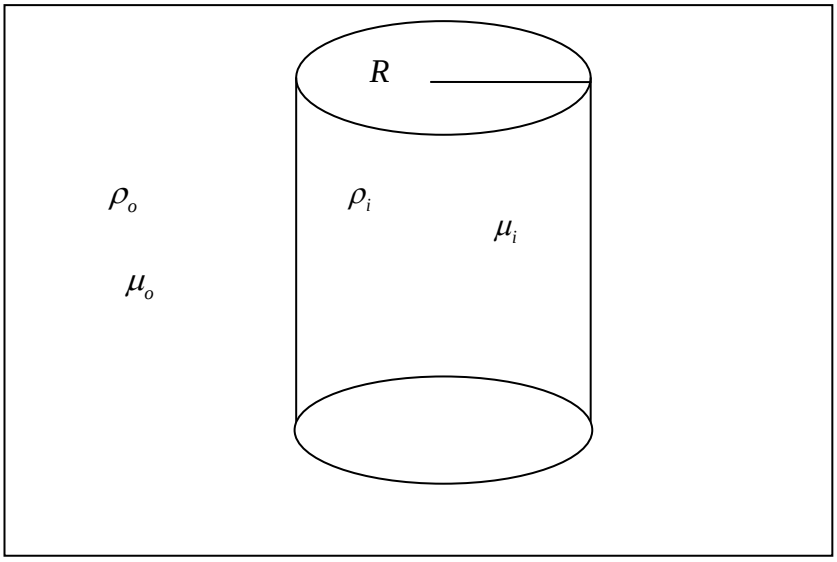

Figure 7.1: Schematic diagram.

$$\left.\begin{aligned} \frac{\partial \rho_o}{\partial t} + \left(\nabla \Phi_o \cdot \nabla\right)\rho_o + \rho_o \nabla^2 \Phi_o = 0 \\ T_o^{ij} = 2\mu_o \frac{\partial^2 \Phi_o}{\partial x^i \partial x^j} - \frac{2\mu_o}{3}\left(\nabla^2 \Phi_o\right)\delta_{ij} \\ \frac{\partial \Phi_o}{\partial t} + \frac{1}{2}\left|\nabla \Phi_o\right|^2 + \frac{\gamma_o}{\gamma_o - 1}\frac{p_o}{\rho_o} - \frac{4\mu_o}{3\rho_o}\nabla^2 \Phi_o = B_o(t) \\ p_o = A\rho_o^{\gamma_o},\ \frac{dp_o}{d\rho_o} = \gamma_o A\rho_o^{\gamma_o - 1} = \gamma_o \frac{p_o}{\rho_o} = c_o^2 \end{aligned}\right\} \tag{7.2}$$

The potential function Φ_i must be finite at $r = 0$ while Φ_o will be finite when $r \to \infty$.

It should be noted that the normal velocity of the interface must be zero and therefore,

$$\frac{df}{dt} = \frac{\partial f}{\partial t} + \left(\nabla \Phi_l \cdot \nabla\right) f \qquad (l = 1, 2) \tag{7.3}$$

The stress equation at the interface is written as

$$p_o - p_i + \left(n^i T_i^{ij} n^j\right) - \left(n^i T_o^{ij} n^j\right) = \sigma \nabla \cdot \boldsymbol{n} \tag{7.4}$$

7.3. Dispersion Relation

a. Basic State

In the undisturbed situation $(r = R)$, the inside fluid has uniform flow $\Phi_i = (0, 0, 0)$ in the frame (r, θ, z) and with the constant density ρ_i^c and pressure p_i^c, and a basic state of outside fluid has uniform flow $\nabla \Phi_o = (0, 0, 0)$ in the coordinates (r, θ, z) and with the constant density ρ_o^c and pressure p_o^c. The isentropic relation and Bernoulli's for the two compressible fluids in the basic state become:

$$\left.\begin{aligned} p_i^c = A\rho_i^{c\gamma_i},\ \frac{dp_i^c}{d\rho_i^c} = \gamma_i A \rho_i^{c\gamma_i - 1} = \gamma_i \frac{p_i^c}{\rho_i^c} = c_i^2 \\ \frac{\gamma_i}{\gamma_i - 1}\frac{p_i^c}{\rho_i^c} = \frac{c_i^2}{\gamma_i - 1} = B_i(t) \end{aligned}\right\} \tag{7.5}$$

$$\left.\begin{aligned} p_o^c = A\rho_o^{c\gamma_o},\ \frac{dp_o^c}{d\rho_o^c} = \gamma_o A \rho_o^{c\gamma_o - 1} = \gamma_o \frac{p_o^c}{\rho_o^c} = c_o^2 \\ \frac{\gamma_o}{\gamma_o - 1}\frac{p_o^c}{\rho_o^c} = \frac{c_o^2}{\gamma_o - 1} = B_o(t) \end{aligned}\right\} \tag{7.6}$$

b. Perturbed state

If we impose small disturbances on basic flows, then the interface equation becomes

$$f = r - R - \xi(z, t) = 0 \tag{7.7}$$

The variables in the perturbed state become

$$\left.\begin{aligned} \Phi_i &= \tilde{\Phi}_i, \;\; p_i = p_i^c + \tilde{p}_i, \;\; \rho_i = \rho_i^c + \tilde{\rho}_i \\ \Phi_o &= \tilde{\Phi}_o, \;\; p_o = p_o^c + \tilde{p}_o, \;\; \rho_o = \rho_o^c + \tilde{\rho}_o \end{aligned}\right\} \tag{7.8}$$

The isentropic relation gives:

$$\left.\begin{aligned} p_i^c = A\rho_i^{c\gamma_i}, \text{ hence } \;\; p_i^c = A\rho_i^{c\gamma_i}, \;\; \tilde{p}_i \approx A\rho_i^{c\gamma_i}\gamma_i \frac{\tilde{\rho}_i}{\rho_i^c} = c_i^2\tilde{\rho}_i \\ \frac{\gamma_i}{\gamma_i - 1}\frac{p_i}{\rho_i} = \frac{c_i^2}{\gamma_i - 1} + c_i^2\frac{\tilde{\rho}_i}{\rho_i^c} = \frac{c_i^2}{\gamma_i - 1} + \frac{\tilde{p}_i}{\rho_i^c} \end{aligned}\right\} \tag{7.9}$$

$$\left.\begin{aligned} p_o^c = A\rho_o^{c\gamma_o}, \text{ hence } \;\; p_o^c = A\rho_o^{c\gamma_o}, \;\; \tilde{p}_o \approx A\rho_o^{c\gamma_o}\gamma_o \frac{\tilde{\rho}_o}{\rho_o^c} = c_o^2\tilde{\rho}_o \\ \frac{\gamma_o}{\gamma_o - 1}\frac{p_o}{\rho_o} = \frac{c_o^2}{\gamma_o - 1} + c_o^2\frac{\tilde{\rho}_o}{\rho_o^c} = \frac{c_o^2}{\gamma_o - 1} + \frac{\tilde{p}_o}{\rho_o^c} \end{aligned}\right\} \tag{7.10}$$

At the interface, the conditions for potential functions are given as

$$\frac{\partial\xi}{\partial t} = \frac{\partial\tilde{\Phi}_i}{\partial r}, \qquad\qquad \frac{\partial\xi}{\partial t} = \frac{\partial\tilde{\Phi}_o}{\partial r} \tag{7.11}$$

Hence the equations for linear analysis of disturbances for inside and outside fluids are;

$$\left.\begin{aligned} \frac{\partial\tilde{\rho}_i}{\partial t} + \rho_i^c\nabla^2\tilde{\Phi}_i = 0 \\ \frac{\partial\tilde{\Phi}_i}{\partial t} + c_i^2\frac{\tilde{\rho}_i}{\rho_i^c} - \frac{4\mu_i}{3\rho_i^c}\nabla^2\tilde{\Phi}_i = 0 \end{aligned}\right\} \tag{7.12}$$

So
$$\left(\frac{\partial\tilde{\Phi}_i}{\partial t}\right)^2 = \left[c_i^2 + \frac{4\mu_i}{3\rho_i^c}\frac{\partial}{\partial t}\right]\nabla^2\tilde{\Phi}_i \tag{7.13}$$

and
$$\left.\begin{aligned} \frac{\partial\tilde{\rho}_o}{\partial t} + \rho_o^c\nabla^2\tilde{\Phi}_o = 0 \\ \frac{\partial\tilde{\Phi}_o}{\partial t} + c_o^2\frac{\tilde{\rho}_o}{\rho_o^c} - \frac{4\mu_o}{3\rho_o^c}\nabla^2\tilde{\Phi}_o = 0 \end{aligned}\right\} \tag{7.14}$$

So
$$\left(\frac{\partial\tilde{\Phi}_o}{\partial t}\right)^2 = \left[c_o^2 + \frac{4\mu_o}{3\rho_o^c}\frac{\partial}{\partial t}\right]\nabla^2\tilde{\Phi}_o \tag{7.15}$$

The disturbance modes are expressed in the form of $\widehat{F}(r,\theta,z,t) = H(r)E$ where $E = \exp(-i\omega t + ikz)$. The interface distortion $\xi(z,t)$ will take the form as $\xi = \hat{\xi}E + c.c.$.

The expressions for potential functions are computed as

$$\tilde{\Phi}_i = -\frac{i\omega}{\kappa_i} H \frac{I_0(\kappa_i r)}{I_1(\kappa_i r)} E + c.c. \tag{7.16}$$

$$\tilde{\Phi}_o = \frac{i\omega}{\kappa_o} H \frac{K_0(\kappa_o r)}{K_1(\kappa_o r)} E + c.c. \tag{7.17}$$

where $\kappa_i^2 = k^2 - \frac{\omega^2}{\left[c_i^2 - i\frac{4\mu_i}{3\rho_i}\omega\right]}$, $\kappa_o^2 = k^2 - \frac{\omega^2}{\left[c_o^2 - i\frac{4\mu_o}{3\rho_o}\omega\right]}$ and

$I_0(kR), I_1(kR), K_0(kR)$ $K_1(kR)$ have their usual meanings

Eliminating pressure using Bernoulli's function, equation (7.7) becomes

$$-\rho_o^c \frac{\partial\tilde{\Phi}_o}{\partial t} + 2\mu_o\left(\nabla^2\tilde{\Phi}_o - \frac{\partial^2\tilde{\Phi}_o}{\partial r^2}\right) + \rho_i^c \frac{\partial\tilde{\Phi}_i}{\partial t} - 2\mu_i\left(\nabla^2\tilde{\Phi}_i - \frac{\partial^2\tilde{\Phi}_i}{\partial r^2}\right) = \sigma\left(\frac{\partial^2\xi}{\partial z^2} + \frac{\xi}{R^2}\right) \tag{7.18}$$

By substituting the values ξ, $\tilde{\Phi}_i, \tilde{\Phi}_o$ in equation (6.18), one can get

$$\begin{aligned}&\left[\rho_o^c\omega^2 - 2i\mu_o\omega(\kappa_o^2 - k^2)\right]\frac{K_0(\kappa_o R)}{\kappa_o K_1(\kappa_o R)} - \left[\rho_i^c\omega^2 - 2i\mu_i\omega(\kappa_i^2 - k^2)\right]\frac{I_0(\kappa_i R)}{\kappa_i I_1(\kappa_i R)} \\ &+2i\mu_o\omega\kappa_o\left(\frac{K_0(\kappa_o R)}{K_1(\kappa_o R)} + \frac{1}{\kappa_o R}\right) + 2i\mu_i\omega\kappa_i\left(\frac{I_0(\kappa_i R)}{I_1(\kappa_i R)} - \frac{1}{\kappa_i R}\right) + \sigma\left(k^2 - \frac{1}{R^2}\right) = 0\end{aligned} \tag{7.19}$$

Taking reference length R and reference velocity c_o, equation (7.19) in dimensionless form can be written as

$$\left[N^2-\frac{2i}{\mathrm{Re}}N(\tilde{\kappa}_o^2-\tilde{k}^2)\right]\frac{K_0(\tilde{\kappa}_o)}{\tilde{\kappa}_o K_1(\tilde{\kappa}_o)}-\left[\rho\omega^2-\frac{2i}{\mathrm{Re}}\mu N(\tilde{\kappa}_i^2-\tilde{k}^2)\right]\frac{I_0(\tilde{\kappa}_i)}{\tilde{\kappa}_i I_1(\tilde{\kappa}_i)}$$
$$+\frac{2i}{\mathrm{Re}}N\tilde{\kappa}_o\left(\frac{K_0(\tilde{\kappa}_o)}{K_1(\tilde{\kappa}_o)}+\frac{1}{\tilde{\kappa}_o}\right)+\frac{2i}{\mathrm{Re}}\frac{\mu}{\rho}N\tilde{\kappa}_i\left(\frac{I_0(\tilde{\kappa}_i)}{I_1(\tilde{\kappa}_i)}-\frac{1}{\tilde{\kappa}_i}\right)+\frac{1}{We}\left(\tilde{k}^2-1\right)=0 \tag{7.20}$$

$$\tilde{\kappa}_i^2=\tilde{k}^2-\frac{N^2}{\left[c^2-i\frac{4\mu}{3\rho\,\mathrm{Re}}N\right]},\quad \tilde{\kappa}_o^2=\tilde{k}^2-\frac{N^2}{\left[1-i\frac{4}{3\mathrm{Re}}N\right]} \tag{7.21}$$

Here $N=\frac{\omega R}{c_o},\tilde{\kappa}_i=\kappa_i R,\tilde{\kappa}_o=\kappa_o R,\tilde{k}=kR,c=\frac{c_i}{c_o}$, density ratio $\rho=\frac{\rho_i^c}{\rho_o^c}$, viscosity ratio $\mu=\frac{\mu_i}{\mu_o}$, Reynolds number $\mathrm{Re}=\frac{\rho_o^c c_o R}{\mu_o}$ and Weber number $We=\frac{\rho_o^c c_o^2 R}{\sigma}$.

7.4. RESULTS AND DISCUSSIONS

This section is dedicated to examining the influence of flow parameters on the disturbance growth of the interface. The various figures are plotted for various values of physical quantities like Reynolds number, density ratio, viscosity ratio, etc. For the numeric computation, values of the flow parameters are given below-

$$\rho=0.0012,\ \mu=10.018,\ \mathrm{Re}=100,\ We=50,\ c=1.31$$

Figure 7.2 shows the behavior of the Weber number for the cylindrical interface of two compressible fluids. The proliferation of the non-dimensional Weber number We leads off down the growth line curves showing stabilizing behavior of the Weber number We. The values of maximum growth are tabulated in Table 7.1. This non-dimensional number is the ratio of inertial forces to the surface forces, and it has a compatible impact on inertial forces; also, in capillary confutation, gravity is affectless at the interface; therefore, an increase in inertial forces prevents the perturbation growth. Moreover, surface tension has an opposite impact on the stability

of the compressible interface. The surface forces provide more energy to the perturbations and their amplitude grows, consequently, the interface gets destabilized.

The densities of the compressible fluids are assumed to be different in the outer and inner cylindrical regions. Figure 7.3 represents the ratio of inner fluid-to-outer fluid density and varies from 0.001 to 0.004, whereas other flow parameters are fixed. Table 7.2 is also showing the variation of growth with density ratio. The above graphics show that the dispersal of density ratio helps to increase disturbance growth curves, implying destabilizing character of density ratio on the compressible fluids interface in the cylindrical region. Actually, more value of the outer compressible fluid density hinders the flow of the interface, and the resulting interface stabilizes. However, inner fluid density is destabilizing the interface.

The growth curves for various values of non-dimensional Reynolds numbers are portrayed in figure 7.4. The above representation indicates the decreasing growth lines with a relevant increase in Reynolds number. The values of growth rate are presented in Table 7.3. Reynolds number (Re) is the ratio of inertial-to-viscous forces. Viscous force is the antithesis of the Reynolds number implying destabilizing character of viscous force. Since density hinders the travel of fluid layers, disturbance growth takes more time to grow. Thus, inertial force helps the interface to be stable.

Figure 7.5 displays the growth rate curve for the distinct value of the inner fluid viscosity-to-outer fluid viscosity. An increment in the viscosity ratio leads to a decrease in the disturbance growth curves of the compressible cylindrical interface showing stabilizing character of the viscosity ratio (μ). The values have been shown in Table 7.4. The viscosity ratio is directly related to the viscosity of the inner compressible fluid and inversely to the outer fluid viscosity. Therefore, the non-

dimensional viscosity ratio decreases with an increase in outer compressible fluid viscosity. Hence, one can say that inner compressible fluid viscosity stabilizes while outer compressible fluid viscosity destabilizes the interface. An interruption occurs on perturbation flow during a small increment in inner compressible fluid viscosity, so interfacial growth is slowed. Thus viscosity fevered stability.

Concretely, the VPF theory is used in the present investigation; therefore, comparative analysis between potential flow theory and inviscid flow theory can lead us to understand the results better. Figure 7.6 shows the compression between the disturbances growth rate of inviscid compressible fluid and the disturbances growth rate of viscous compressible liquid. The above graphics show that disturbance growth found utilizing IPF theory gets more hike than the disturbance growth found utilizing VPF theory. Therefore, the viscous potential theory offers more interface stability than the inviscid flow theory. Hence viscosity induces stability.

The comparison between the compressible fluid interface and incompressible fluid interface has been made in the figure. 7.7. It can be seen in the above figure that for minimal wave number, the compressible fluid interface stabilized while for other values of the compressible fluid interface destabilized. For the current problem, we can say that point 0.3 is the critical value of the wave number. For the lower value of 0.3, the compressible interface stabilized, while for the more significant value of 0.3, the compressible fluid interface gets destabilized.

7.5. CONCLUSIONS

In this chapter, the Rayleigh instability is examined for two different densities of viscous compressible fluids interface. The dispersion relationship is quadratic in terms of the growth rate achieved and plotted with the help of MATLAB software for

various flow parameters. The interfacial stability increases with an increase in the non-dimensional viscosity ratio parameter of the compressible fluids and while the density ratio of compressible fluids interface has destabilizing character. Also, one can say that outer fluid density stabilized the interface. VPF theory predicts a more stable interface than the IPF theory. The inertial forces influence the interface to be stable. A comparison has been done between the incompressible interface and compressible interface and the compressible fluid is found more stable.

Table 7.1: Variation of perturbations maximum growth with Weber number We

Weber number We	Maximum grow rate $(N_i)_{\max}$	Maximum wave number $k_{\max}$
50	0.1159	0.496
60	0.1056	0.503
70	0.0986	0.505
80	0.0915	0.515
90	0.0851	0.526

Table 7.2: Variation of perturbations maximum growth with density ratio ρ

density ratio ρ	Maximum grow rate $(N_i)_{\max}$	Maximum wave number $k_{\max}$
0.001	0.1087	0.522
0.002	0.1104	0.517
0.003	0.1125	0.506
0.004	0.1154	0.503
0.005	0.1159	0.496

Table 7.3: Variation of perturbations maximum growth with Reynolds number Re

Reynolds number Re	Maximum grow rate $(N_i)_{\max}$	Maximum wave number $k_{\max}$
100	0.1159	0.496
200	0.1145	0.503
300	0.1127	0.503
400	0.1105	0.505
500	0.1094	0.512

Table 7.4: Variation of perturbations maximum growth with viscosity ratio μ

viscosity ratio μ	Maximum grow rate $(N_i)_{\max}$	Maximum wave number $k_{\max}$
0.018	0.1159	0.496
0.030	0.1154	0.503
0.040	0.1134	0.527
0.050	0.1105	0.537
0.060	0.1084	0.551

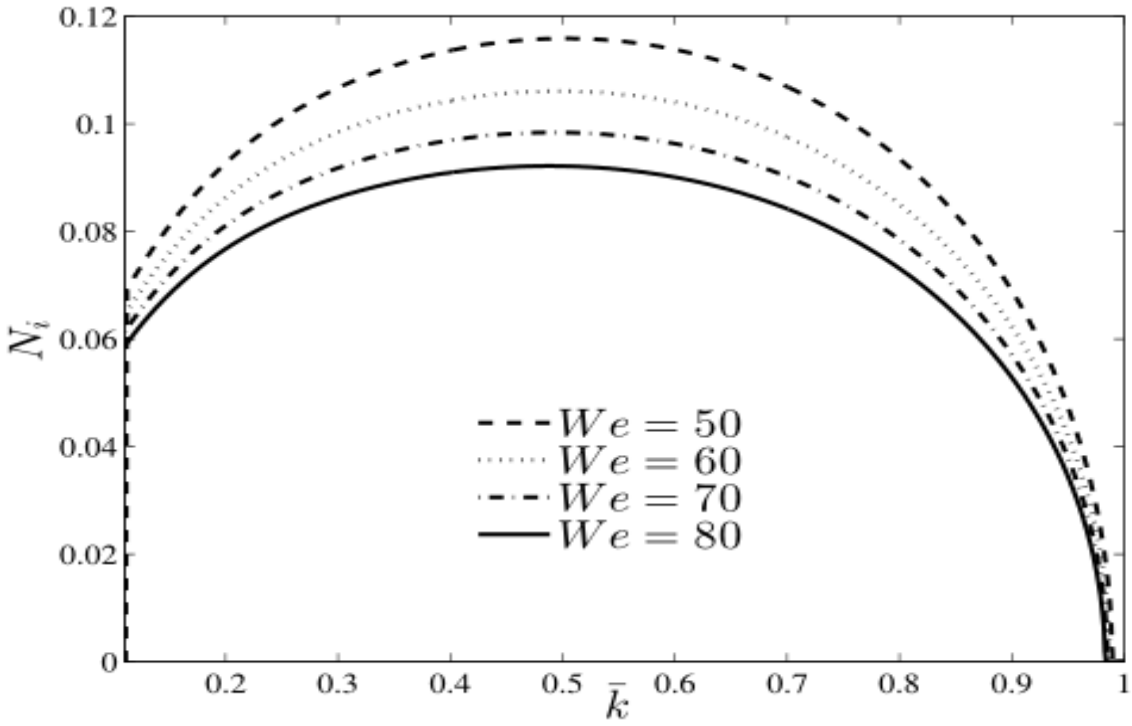

Figure 7.2: Effect of Weber Number.

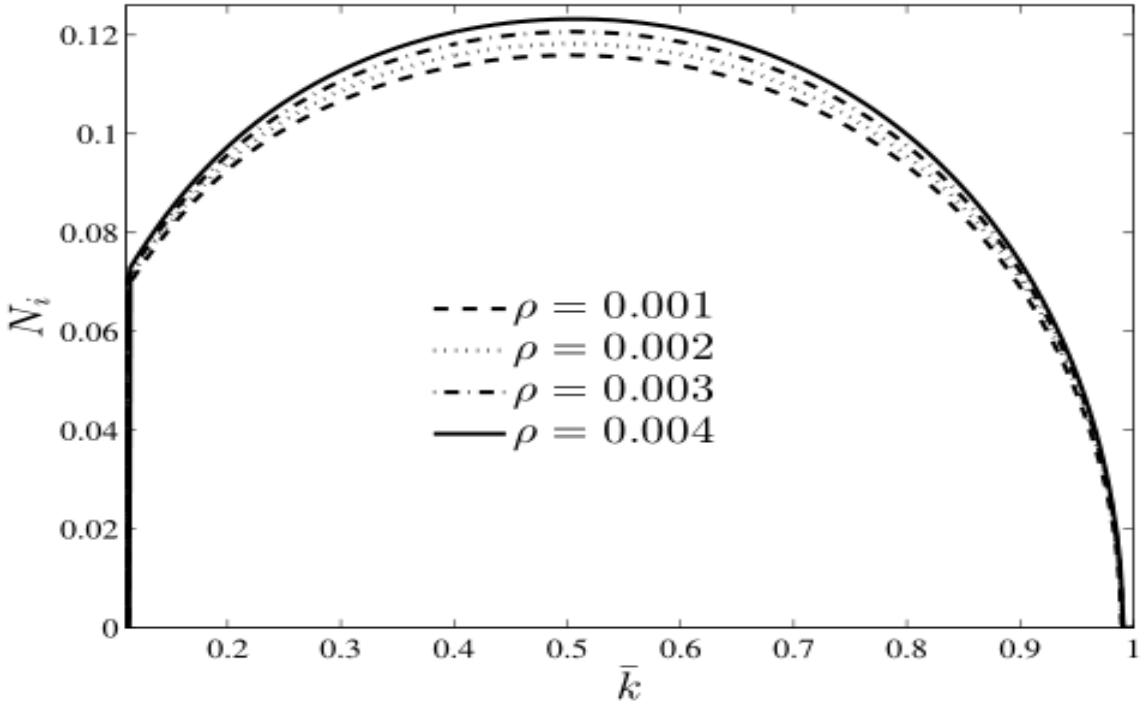

Figure 7.3: Effect of fluid's density ratio.

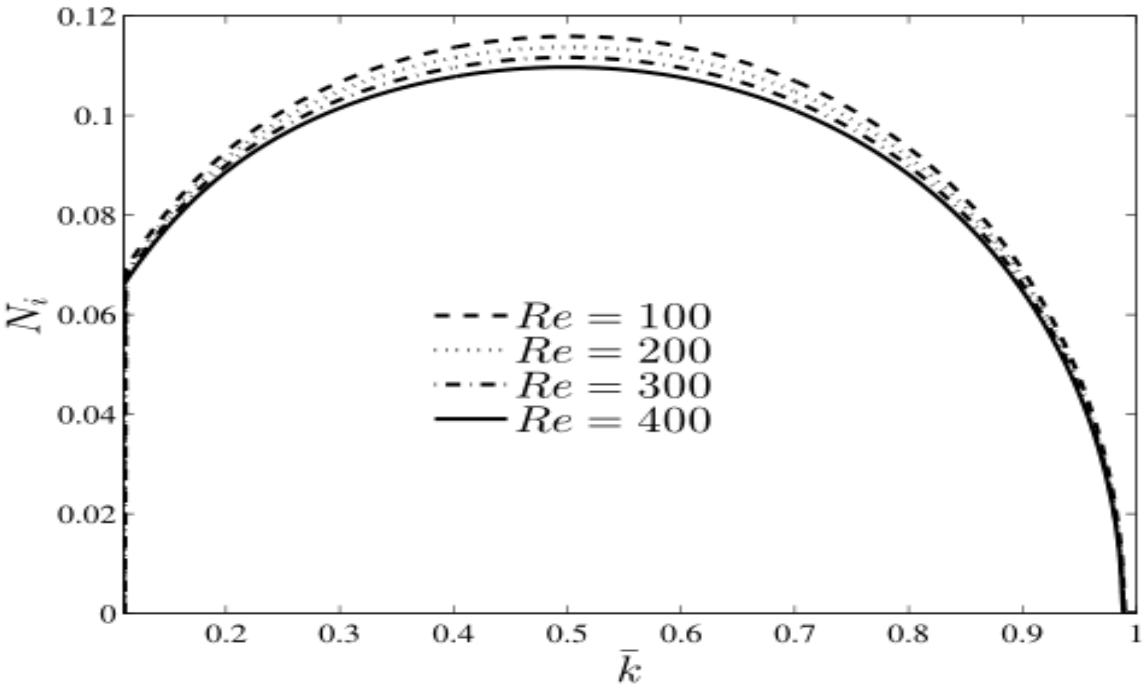

Figure 7.4: Effect of Reynolds number.

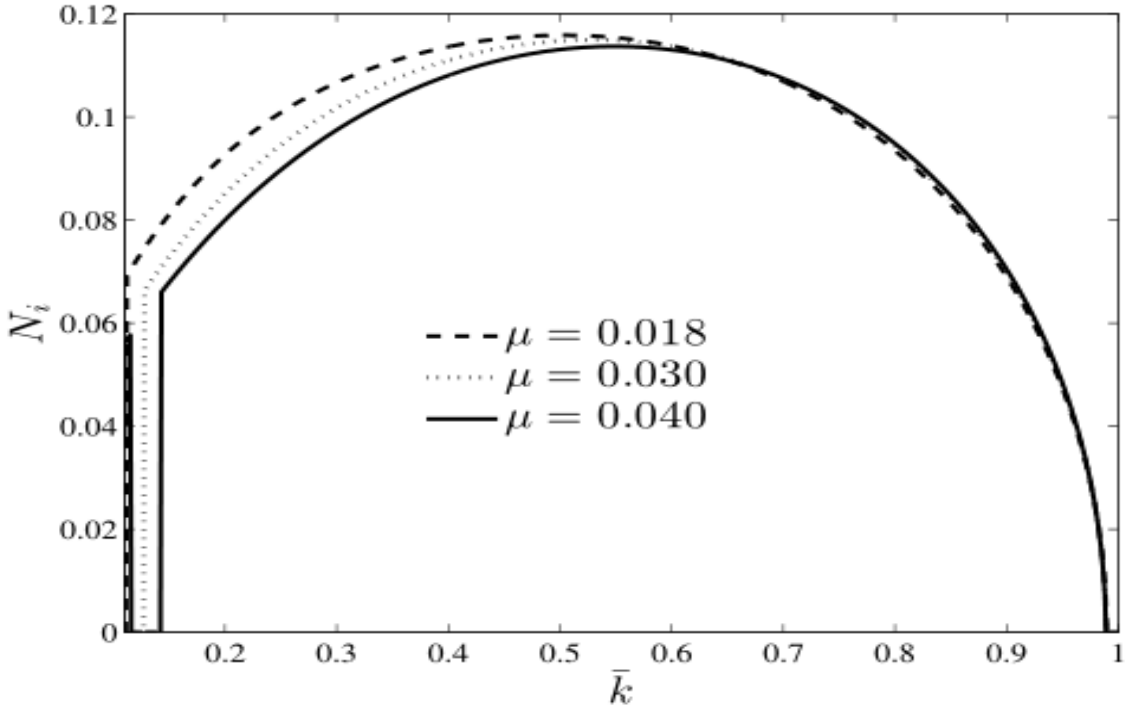

Figure 7.5: Effect of fluid's viscosity ratio.

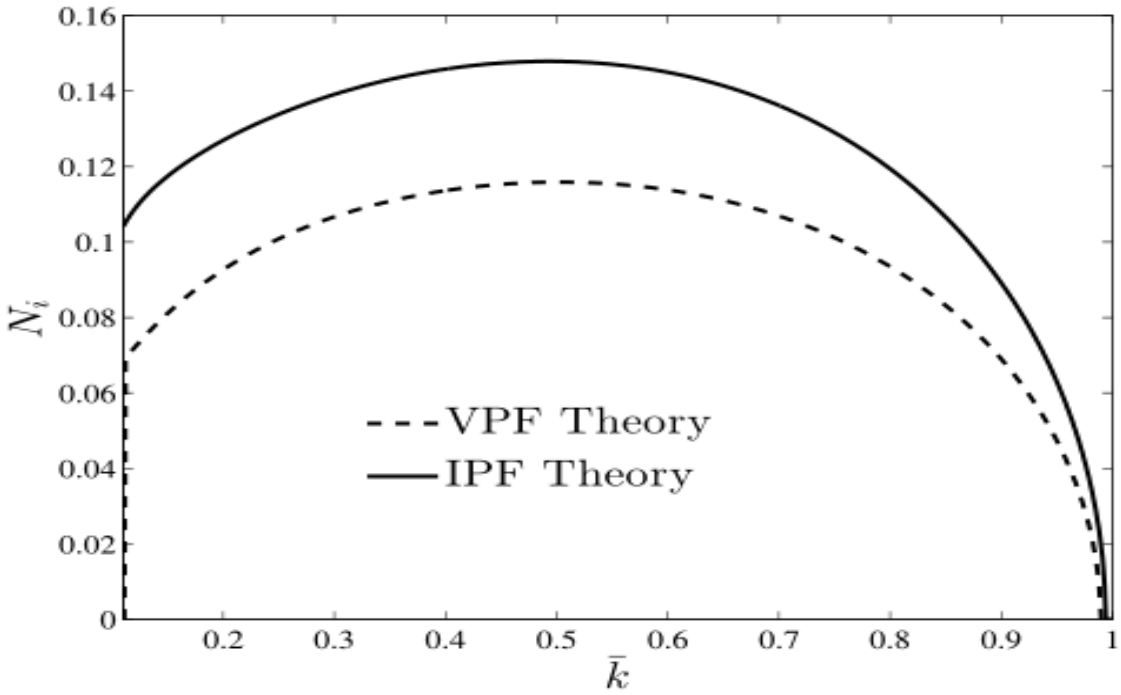

Figure 7.6: Comparison of IPF and VPF theories.

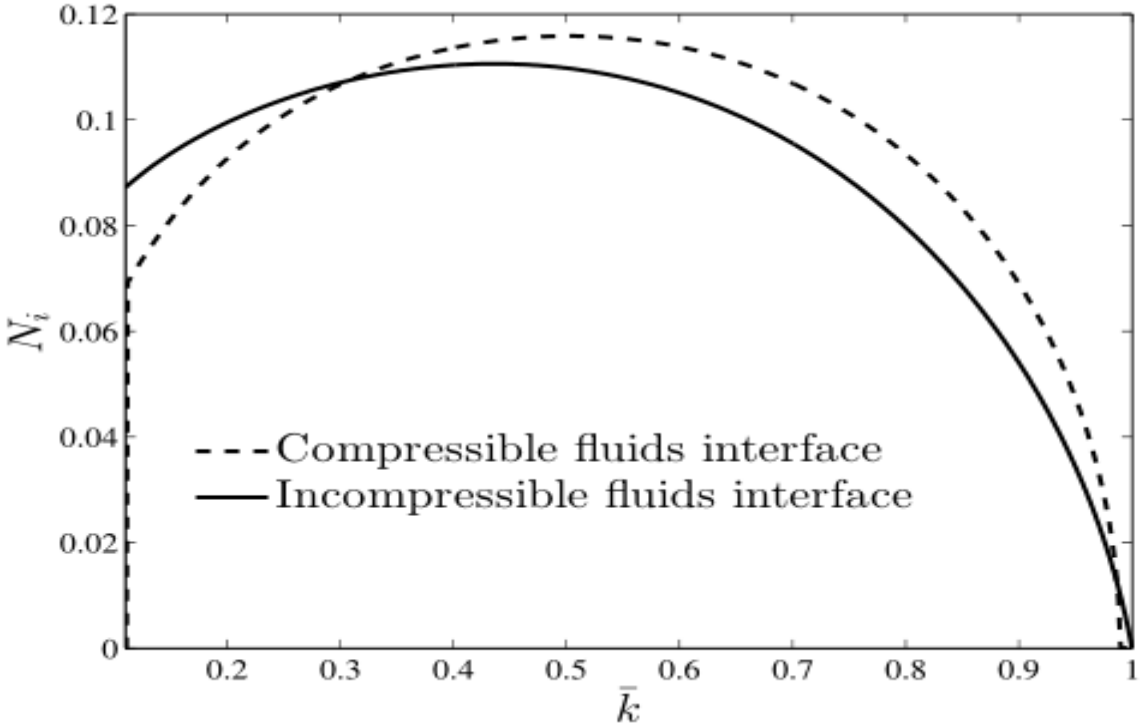

Figure 7.7: Comparison of compressible and incompressible fluid interfaces.

CHAPTER 8
CONCLUSIONS AND FUTURE SCOPE

Sir G.G. Stokes developed the theory of the potential flow of a viscous fluid. Based on the presumption that viscosity is non-vanishing but velocity is determined by the gradient of the potential function, the viscous potential flow (VPF) hypothesis was developed. The VPF hypothesis does not take the impact of shearing stresses into account when describing how viscosity arises from normal stress equilibrium. It has been noted that adding irrotational viscous forces alters the stability findings from the IPF hypothesis.

The mass transfer phenomenon coexists with the heat transfer scenario in a two-phase flow. As an example, consider a situation where the liquid lies between two plates of film stacked one on top of the other. As an example, consider a situation where the liquid lies between two plates of film stacked one on top of the other. Moreover, the vapor will condense due to the lower temperature of the upper plate. Consequently, a mass transfer will occur at both plates as a result of the altered temperature gradients.

Many real-world situations, such film-wise condensation and gas bubble breakdown, involve the capillary instability of two viscous fluids in the presence of heat and mass transfer. When there is mass and heat transfer across the interface, the stability criteria for the viscous potential flow analysis of capillary instability has been addressed. The stability of the system is observed to be stabilized by the heat and mass transfer, and this impact is amplified by the presence of irrotational tangential stresses. The Chapter wise is presented as follows;

The stability of the Rivlin-Ericksen fluid-viscous fluid interface when the interface is transferring mass and heat is theoretically studied in **chapter 2**. The inquiry is

based on the potential flow theory of viscoelastic/viscous fluids, and the stability of the interface is computed using the normal mode theory. The two-degree equation is established and examined in terms of the growth rate of the perturbation. The findings show that when heat transfer increases, the stability of the arrangement improves, but surface tension causes the opposite effect. Whether or not heat is transferred, the viscoelasticity of the R-E fluid exhibits stabilizing characteristics. The system becomes stable due to the R-E fluid's density and viscosity. The findings show that increasing the transmission of heat does not modify the nature of viscoelasticity while improving the stability of the arrangement.

In **chapter 3**, the linear temporal instability of the Walter's B viscoelastic fluid–viscous fluid interaction is investigated. Since there is no gravity in the study but there is surface tension, instability is treated as capillary instability. The mathematical problems are resolved using the potential flow theory of viscous fluids. In order to study the impact of physical characteristics like viscoelasticity, viscosity, etc., we achieve a second-order polynomial in the growth rate parameter and plot its imaginary portion. It is found that while the density of the outside fluid has a destabilizing character, the viscosities of the interior and outside fluids enhance stability at the interface. Surface tension causes instability.

Chapter 4 theoretically studies he stability of the viscous fluid Walter's B viscoelastic fluid interface is when the fluid phases are moving mass and heat across the interface. The fluids are located in an annular region that is bounded by two rigid cylinders, and the mathematical equations are solved using the irrotational flow theory of viscous viscoelastic fluid. The growth rate parameter's algebraic equation is computed and numerically examined. While surface tension has a destabilizing character, it is discovered that the transport of heat stabilizes the interface by

expanding the stability range. When compared to the density of the viscoelastic fluid, Walter's B fluid's viscoelasticity destabilizes the interface. The Walter's B fluid's viscosity provides a stabilizing effect.

The capillary instability at the viscous fluid- power-law viscoelastic fluid interface is studied analytically in **chapter 5**. The interface is transporting heat along with mass from one fluid phase to another. The irrotational flow theory of viscous-viscoelastic fluid is employed to work out the mathematical equations. The algebraic equation of the growth rate parameter is computed and analyzed numerically. The transport of heat is found to stabilize the interface by enlarging the stability range. The viscosity of the viscous fluid is preventing the perturbation's growth. The power-law index and consistency coefficient have stabilizing character while the density of power-law has an inverse effect. It is also found that the shear-thickening fluid interface is more stable than the shear-thinning fluid interface.

At the viscous fluid-nanofluid interface, the Rayleigh-Taylor instability in a circular cavity is studied in **chapter 6**. While the nanofluid is outside the cavity, the viscous fluid is inside, forming a circular interface.. In the case of larger modes of disturbance, the dispersion relationship reduces to the situation of a planar contact and has a quadratic growth rate. While the density of nanofluid has a destabilizing effect, the interfacial stability increases as the viscosity of the nanofluid increases. The volume percentage of nanoparticles causes stability in the system. While the density of the interior fluid has a stabilizing effect, its viscosity promotes the growth of the perturbation. While the fractal index of nanofluid plays a stabilizing role, the radius of nanoparticles delays stabilization. In comparison to the IPF theory, the VPF theory predicts a more stable interface

Chapter 7 examines the linear instability analysis of capillary stability at the viscous compressible fluid's interface. The compressible viscous fluid in the cylindrical coordinate system is surrounded by another viscous compressible fluid. The investigation was done by utilizing the potential flow theory (VPF theory) for the fluid satisfying the compressible flow model. A second-order implicit expression for the growth rate parameter is achieved and examined numerically. It is found that inside fluid viscosity slows the growth of disturbance but an increase in outside fluid viscosity makes the interface unstable. The interface goes towards instability when the surface tension increases at the interface.

The above studies are restricted to the linear theory of stability analysis. The nonlinear analysis of interfacial stability problems is very important because the governing equations describing these flows are nonlinear in nature. Thus nonlinearity modifies the stability results obtained in frame work of linear theory. There is a scope to study the nonlinear analysis of the problems considered in present thesis.

The effect of electric and magnetic field also modifies the stability results at an interface. The electric produces a polarization force if fluids are dielectric and conducting force for the conducting fluids. The magnetic field generates the Lorentz force. These forces affect the interface and stability may increase or decrease. The electric field and magnetic field effects can also be considered on the problems presented here.

The VPF theory includes only normal viscous stress and shearing stresses are taken as zero at the interface. The theory which includes both shearing and normal viscous stresses is called VCVPF theory. The VCVPF theory can also be applied to the problems considered in this thesis.

REFERENCES

1. **Ahmad, S., Khan, M. N., and Nadeem, S.** (2020). Mathematical analysis of heat and mass transfer in a Maxwell fluid with double stratification. Physica Scripta, 96(2), 025202.
2. **Ahmad, S., Khan, M. N., Rehman, A., Felemban, B. F., Alqurashi, M. S., Alharbi, F. M., and Galal, A. M.,** (2021). Analysis of Heat and Mass Transfer Features of Hybrid Casson Nanofluid Flow with the Magnetic Dipole Past a Stretched Cylinder. Applied Sciences, 11(23), 11203.
3. **Ahmad, S., Nadeem, S., and Khan, M. N.** (2021). Mixed convection hybridized micropolar nanofluid with triple stratification and CattaneoChristov heat flux model. Physica scripta, 96(7), 075205.
4. **Ahmad, S., Nadeem, S., and Khan, M. N**. (2022). Enhanced transport properties and its theoretical analysis in two-phase hybrid nanofluid. Applied Nanoscience, 12(3), 309-316.
5. **Ahmad, S., Nadeem, S., and Khan, M. N.** (2022). Heat enhancement analysis of the hybridized micro polar nanofluid with Cattaneo Christov and stratification effects. Proceedings of the Institution of Mechanical Engineers, Part C: Journal of Mechanical Engineering Science, 236(2), 943-955.
6. **Allah, M. O.,** (2011). Viscous potential flow analysis of interfacial stability with mass transfer through porous media. Applied mathematics and computation, 217(20), 7920-7931.
7. **Ariel, P. D.,**(1971). Rayleigh-Taylor instability of compressible fluids in the presence of a vertical magnetic field. Applied Scientific Research, 24(1), 294-304.

8. **Ashgriz, N., and Mashayek, F.,**(1995). Temporal analysis of capillary jet breakup. Journal of Fluid Mechanics,291,163-190.

9. **Asthana, R., and Agrawal, G. S.,** (2007). Viscous potential flow analysis of Kelvin-Helmholtz instability with mass transfer and vaporization. Physica A 382, 389–404.

10. **Asthana, R., Awasthi, M. K. And Agrawal, G.S.,** (2012). Viscous potential flow analysis of Rayleigh-Taylor instability of cylindrical interface. Applied Mechanics and Materials, 110-116, 769-775.

11. **Asthana, R., Awasthi, M. K., and Agrawal, G.S.** (2011). Kelvin-Helmholtz instability of two viscous fluids in porous media. Int J Appl Math Mech 8(14):1–10.

12. **Awasthi, M. K.and Agrawal G. S.,** (2011). Viscous potential flow analysis of Kelvin-Helmholtz instability of cylindrical interface. Int. J. App. Math. Comp., 3, 131-138.

13. **Awasthi, M. K.and Asthana, R.,** (2013). Viscous potential flow analysis of capillary instability with heat and mass transfer through porous media. International communications in heat and mass transfer, 40, 7-11.

14. **Awasthi, M. K.,** (2013). Study on hydro-magnetic capillary instability with mass transfer through porous media. Int. J of Dynamics and Control, 1(2), 164-171.

15. **Awasthi, M. K.,** (2014). Nonlinear analysis of capillary instability with mass transfer through porous media. The European Physical Journal Plus, 129(5), 1-11.

16. **Awasthi, M. K.,** (2014). Study on electro hydrodynamic capillary instability of viscoelastic fluids with radial electric field. Int. Journal of Applied Mechanics, 6(04), 1450037.

17. **Awasthi, M. K.,** (2014). Three-dimensional magnetohydrodynamic Kelvin-Helmholtz instability of cylindrical flow with permeable boundaries. Physics of Plasmas, 21(3), 032124.
18. **Awasthi, M. K.,** (2019). Rayleigh Taylor Instability of swirling annular layer with mass transfer. Journal of Fluids Engineering, 141(7).
19. **Awasthi, M. K.,** (2020). Capillary instability of viscoelastic liquid film with heat and mass transfer. Journal of Heat Transfer, 142(2), 022108.
20. **Awasthi, M. K.,** (2021). Kelvin-Helmholtz instability of viscoelastic liquid-viscous gas interface with heat and mass transfer. Int. Journal of Thermal Sciences, 161, 106710.
21. **Awasthi, M. K., and Agarwal, S.** (2020). Instability of a radially moving cylindrical surface: A viscous potential flow approach. Journal of Fluids Engineering, 142(9), 094501.
22. **Awasthi, M. K., and Agarwal, S.,** (2020). Rayleigh-Taylor instability in a spherical configuration: A viscous potential flow approach. Chinese Journal of Physics, 686-873.
23. **Awasthi, M. K., and Agrawal G. S.,** (2011). Viscous potential flow analysis of Rayleigh-Taylor instability with heat and mass transfer. Int J Appl Math Mech 7(12), 73–84.
24. **Awasthi, M. K., and Agrawal G. S.,** (2012). Nonlinear analysis of capillary instability with heat and mass transfer. Commun Non Sci NumerSimulate 17, 2463–2475.
25. **Awasthi, M. K.,and Agrawal G. S.,** (2012). Viscous contributions to the pressure for potential flow analysis of magnetohydrodynamic Kelvin-Helmholtz instability. Int J Appl Mech 4, 1–16.

26. Awasthi, M. K., and Agrawal, G. S., (2011). Viscous contributions to the pressure for the electro-viscous potential flow analysis of capillary instability. Int. Journal of Theoretical and Applied Multiscale Mechanics 2, 131–145.

27. Awasthi, M. K., and Agrawal, G. S., (2012). Viscous contributions to the pressure for the potential flow analysis of magnetohydrodynamic Kelvin-Helmholtz instability. Int. J. App. Mech. 4(1), 1250001, 1-16.

28. Awasthi, M. K., Asthana R, and Agrawal G. S., (2012). Viscous corrections for the viscous potential flow analysis of magnetohydrodynamic Kelvin-Helmholtz instability with and mass transfer. Eur Phys J 48, 174-183.

29. Awasthi, M. K., Asthana R., and Agrawal G. S., (2012). Viscous potential flow analysis of nonlinear Rayleigh-Taylor instability with heat and mass transfer. Microgravity Sci Technol 24, 351–363

30. Awasthi, M. K., Asthana, R.and Agrawal, G. S., (2014). Viscoelastic potential flow analysis of stability of a cylindrical jet. Scientia Iranica, 21(3), 578-586.

31. Awasthi, M. K., Asthana, R., and Agrawal, G. S., (2014). Viscous correction for the viscous potential flow analysis of Kelvin-Helmholtz instability of cylindrical flow with heat and mass transfer. International Journal of Heat and Mass Transfer, 78, 251-259.

32. Awasthi, M. K., Asthana, R., and Agrawal, G. S., (2012). Pressure corrections for the potential flow analysis of Kelvin-Helmholtz instability with heat and mass transfer. International journal of heat and mass transfer, 55(9-10), 2345-2352.

33. Awasthi, M. K., Asthana, R., and Agrawal, G. S., (2012). Pressure corrections for the potential flow analysis of Kelvin-Helmholtz instability. Applied Mechanics and Materials 110–116, 4628–4635.

34. **Awasthi, M. K., Asthana, R., and Agrawal, G. S.,** (2013). Viscous correction for the viscous potential flow analysis of capillary instability with heat and mass transfer. Journal of Engineering Mathematics 80, 75-89.

35. **Awasthi, M. K., Asthana, R., and Uddin, Z.,** (2021). Evaporative Capillary Instability of Swirling Fluid Layer with Mass Transfer. In Differential Equations in Engineering (37-54). CRC Press.

36. **Awasthi, M. K., Shukla, A. K., and Yadav, D.,** (2021). Rayleigh instability of power-law viscoelastic liquid with heat and mass transfer. International Communications in Heat and Mass Transfer, 129, 105657.

37. **Awasthi, M. K., Tiwari, D. K.,and Asthana, R.,** (2012). Pressure corrections for the viscoelastic potential flow analysis of electrohydrodynamic capillary instability. International Journal of Applied Mechanics, 4(04), 1250047.

38. **Awasthi, M. K., Uddin, Z.and Asthana, R.,** (2021). Temporal instability of a power-law viscoelastic nanofluid layer. The European Physical Journal Special Topics, 230(5), 1427-1434.

39. **Ba, O., Cete, A. R., Mengi, S., Tuncer, I. H.,and Kaynak, U.,** (2017). A novel alternating cell directions implicit method for the solution of incompressible Navier Stokes equations on unstructured grids. Journal of Applied Fluid Mechanics, 10(6), 1561-1570.

40. **Babu, B. H., Srinivasa Rao, P., Reddy, M. G., and Varma, S. V. K.,** (2021). Modeling of Cattaneo-Christov heat and mass flux on non-Newtonian hydromagnetic fluid with variable thermal and solutal properties. Proceedings of the Institution of Mechanical Engineers, Part E: Journal of Process Mechanical Engineering, 09544089211046081.

41. **Barik, R. N., Dash, G. C.and Rath, P. K.,** (2018). Steady laminar MHD flow of viscoelastic fluid through a porous pipe embedded in a porous medium. Alexandria Engineering Journal, 57(2), 973-982.

42. **Bau, H. H.**, (1982) Kelvin-Helmholtz instability for parallel flow in porous media: A linear theory Phys. Fluids 25, 1719-1722.

43. **Bhatia, P. K.**, (1974). Rayleigh-Taylor instability of a viscous compressible plasma of variable density. Astrophysics and Space Science, 26(2), 319-325.

44. **Blumen, W.,** (1971). Jet flow instability of an inviscid compressible fluid. Journal of Fluid Mechanics, 46(4), 737-747.

45. **Boffetta, G., and Mazzino, A.** (2017). Incompressible Rayleigh-Taylor turbulence. Annu. Rev. Fluid Mech. 49, 119143 (2017).

46. **Brenn, G., Liu, Z., and Durst, F.,** (2000). Linear analysis of the temporal instability of axisymmetrical non-Newtonian liquid jets. International journal of multiphase flow, 26(10), 1621-1644.

47. **Brown, W. B.,** (1967). Stability of compressible boundary layers. AIAA Journal, 5(10), 1753-1759.

48. **Carpentier, J. B., Baillot, F., Blaisot, J. B., and Dumouchel, C.,** (2009). Behavior of cylindrical liquid jets evolving in a transverse acoustic field. Physics of Fluids, 21(2), 023601.

49. **Chakraborty, S., and Panigrahi, P. K.,** (2020). Stability of nanofluid: A review. Applied Thermal Engineering, 174, 115259.

50. **Chandrasekhar, S.**, (1981). Hydrodynamic and Hydromagnetic Stability. Dover publications, New York.

51. **Chattopadhyay, G., Usha, R., and Sahu, K. C.,** (2017). Core-annular miscible two-fluid flow in a slippery pipe: A stability analysis. Phy. Fluid, 29, 097106.

52. **Chen, X. M., Schrock, V. E.and Peterson, P. F.,** (1997). Rayleigh-Taylor instability of cylindrical jets with radial motion. Nuclear engineering and design, 177(1-3), 121-129.

53. **Deiber, J. A., and Schowalter, W. R.,** (1981). Modeling the flow of viscoelastic fluids through porous media. AIChE Journal, 27(6), 912-920.

54. **Dhananjay, Y., Agrawal, G. S.and Bhargava, R.,** (2011). Rayleigh-Bénard convection in nanofluid. International Journal of Applied Mathematics and Mechanics, 7(2), 61-76.

55. **Ding, Y., and Kawahara, M.,** (1998). Linear stability of incompressible fluid flow in a cavity using finite element method. International journal for numerical methods in fluids, 27(1-4), 139-157.

56. **Drazin, P. G.,** (1962). On stability of parallel flow of an incompressible fluid of variable density and viscosity. In Mathematical Proceedings of the Cambridge Philosophical Society, 58(4), 646-661.

57. **Drazin, P. G., and Reid W.H.,** (1981). Hydrodynamic Stability. Cambridge University Press, Cambridge.

58. **Dunn, D. W.and Lin, C. C.,** (1955). On the stability of the laminar boundary layer in a compressible fluid. Journal Aeronautical Sciences, 22(7), 455-477.

59. **Eckhoff, K. S., and Storesletten, L.,** (1980). On the stability of rotating compressible and inviscid fluids. Journal of Fluid Mechanics, 99(2), 433-448.

60. **Elcoot, A. E. K.,** (2007). Electroviscous potential flow in nonlinear analysis of capillary instability. European Journal of Mechanics B/Fluids 26, 431-443.

61. **Eldabe N.T.,** (1989). Effect of tangential electric field on Rayleigh-Taylor instability. J. Phy. Soc. Japan., 58, 115-120.

62. El-Dib, Y. O., Moatimid, G. M., Mady, A. A.and Zekry, M. H., (2022). Nonlinear hydromagnetic instability of oscillatory rotating rigid-fluid columns. Indian Journal of Physics, 96(3), 839-854.

63. Elhefanwy, A. R. F., Moatimid, G. M. and Elcoot, A. E. K., (2003). The effect of an axial electric field on the nonlinear stability between two uniform stream flows of finitely conducting cylinders. Canadian Journal of Physics 81, 805–821.

64. Elhefnawy A. R. F., (1994). Stability properties of a cylindrical flow in magnetic fluids: effect of mass and heat transfer and periodic radial field. Int J Eng Sci 32, 805–815.

65. Elhefnawy A. R. F., (1997). The nonlinear stability of mass and heat transfer in magnetic fluids. ZAMM 77, 19–31

66. Elhefnawy, A. R. F., and Radwan, A. E., (1992). The effect of magnetic fields on the stability of cylindrical flow with mass and heat transfer. Physica A: Statistical Mechanics and its Applications, 190(3-4), 330-345.

67. El-Sayed, M. F., (1998). Effect of normal electric fields on Kelvin-Helmholtz instability for porous media with Darcian and Forchheimer flows. Physica A: Statistical Mechanics and its Applications, 255(1-2), 1-14.

68. El-Sayed, M. F., (1999). EHD kelvin-Helmholtz instability in viscous porous medium permeated with suspended particles. Czechoslovak journal of physics, 49(4), 473-482.

69. El-Sayed, M. F., (2001). Electrohydrodynamic instability of two superposed Walters B viscoelastic fluids in relative motion through porous medium. Archive of Applied Mechanics, 71(11), 717-732.

70. El-Sayed, M. F., (2006). Electrohydrodynamic instability of dielectric fluid layer between two semi-infinite identical conducting fluids in porous medium. Physica A: Statistical Mechanics and its Applications, 367, 25-41.

71. El-Sayed, M. F., Eldabe, N. T., Haroun, M. H., and Mostafa, D. M., (2014). Nonlinear stability of viscoelastic fluids streaming through porous media under the influence of vertical electric fields producing surface charges. Int J Adv Appl Math Mech, 2(2), 110-125.

72. Fejer, J. A., (1964). Hydromagnetic stability at a fluid velocity discontinuity between compressible fluids. The Physics of Fluids, 7(4), 499-503.

73. Feldman, S., (1957). On the hydrodynamic stability of two viscous incompressible fluids in parallel uniform shearing motion. Journal of Fluid Mechanics, 2(4), 343-370.

74. Friedlander, S., and Vishik, M. M., (1991). Instability criteria for the flow of an inviscid incompressible fluid. Physical review letters, 66(17), 2204.

75. Fu, Q. F., Deng, X. D., and Yang, L. J., (2019). Kelvin-Helmholtz instability of confined Oldroyd-B liquid film with heat and mass transfer. Journal of Non-Newtonian Fluid Mechanics, 267, 28-34.

76. Fu, Q. F., Deng, X. D., Jia, B. Q., and Yang, L. J., (2018). Temporal instability of a confined liquid film with heat and mass transfer. AIAA Journal, 56(7), 2615-2622.

77. Fu, Q. F., Jia, B. Q., and Yang, L. J., (2017). Stability of a confined swirling annular liquid layer with heat and mass transfer. Int. J. Heat and Mass Transfer, 104, 644-649.

78. Funada, T., and Joseph, D. D., (2001). Viscous potential flow analysis of Kelvin-Helmholtz instability in a channel. Journal of Fluid Mechanics 445, 263–283.

79. Funada, T., and Joseph, D. D., (2002). Viscous potential flow analysis of capillary instability. International Journal of Multiphase Flow 28(9), 1459–1478.

80. Funada, T., and Joseph, D. D., (2003). Viscoelastic potential flow analysis of capillary instability. Journal of Non-Newtonian Fluid Mechanics 111, 87–105.

81. Funada, T., Joseph, D. D., and Yamashita, S., (2004). Stability of a liquid jet into incompressible gases and liquids. International journal of multiphase flow, 30(11), 1279-1310.

82. Funada, T., Saitoh, M., Wang, J., and Joseph, D. D., (2005). Stability of a liquid jet into incompressible gases and liquids: Part 2. Effects of the irrotational viscous pressure. International journal of multiphase flow, 31(10-11), 1134-1154.

83. Funada,T., Joseph, D. D., Saitoh, M., and Yamashita, S., (2006). Liquid jet in a high Mach number air stream. International journal of multiphase flow,32(1),20-50.

84. Furlani, E. P., and Hanchak, M. S., (2011). Nonlinear analysis of the deformation and breakup of viscous microjets using the method of lines. International journal for numerical methods in fluids,65(5),563-577.

85. Ghadimi, A., Saidur, R., and Metselaar, H. S. C., (2011). A review of nanofluid stability properties and characterization in stationary conditions. International journal of heat and mass transfer, 54(17-18), 4051-4068.

86. Ghasemizad, A., Zarringhalam, H., and Gholamzadeh, L., (2009). The investigation of Rayleigh-Taylor instability growth rate in inertial confinement fusion. Journal of Plasma Fusion Research, 8, 1234-1238.

87. Gill, G. K., Chhabra, R. K., and Trehan, S. K., (1995). Bubble formation in superposed magnetic fluids in the presence of heat and mass transfer. Zeitschrift für Naturforschung A, 50(9), 805-812.

88. Goldin, M., Yerushalmi, J., Pfeffer, R., and Shinnar, R., (1969). Breakup of a laminar capillary jet of a viscoelastic fluid. Journal of Fluid Mechanics, 38(4), 689-711.

89. Govindarajan, R.and Sahu, K. C., (2014). Instabilities in viscosity-stratified flow. Annu. Rev. Fluid Mech, 46(1), 331-353.

90. Gupta, U., and Sharma, G., (2007). On Rivlin-Erickson elastico-viscous fluid heated and soluted from below in the presence of compressibility, rotation and Hall currents. Journal of Applied Mathematics and Computing, 25(1), 51-66.

91. Han, Y., (2022). Kelvin-Helmholtz instability of a confined nano-liquid sheet with the effects of heat and mass transfer and marangoni convection. Atomization and Sprays, 32(1).

92. Han, Y., Hong, W., and Faidley, L., (2011). Coupled magnetic field and viscoelasticity of ferrogel. International Journal of Applied Mechanics 3(2), 259–278.

93. Hassan, M. A., (2020). Linear Instability of Electro- magnetic Viscoelastic Nanofluid: Analytical and Numerical Study. Differential Equations and Dynamical Systems, 1-29.

94. Hide, R., (1969). On hydromagnetic waves in a stratified rotating incompressible fluid. Journal of Fluid Mechanics, 39(2), 283-287.

95. Ho, S. P., (1980). Linear Rayleigh-Taylor stability of viscous fluids with mass and heat transfer. Journal of Fluid Mechanics, 101(1), 111-127.

96. Hoshoudy, G. A., (2014). Compressibility effects on Rayleigh-Taylor instability in a vertical inhomogeneous rotating plasma. Results in Physics, 4, 121-126.

97. Hoshoudy, G. A., (2016). Stability of finitely incompressible magnetized plasma layer through porous fluids. Physics of Plasmas, 23(12), 122901.

98. Howard, L. N., (1973). On the stability of compressible swirling flow. Studies in Applied Mathematics, 52(1), 39-43.

99. Hsieh, D. Y., (1972). Effects of heat and mass transfer on Rayleigh-Taylor instability, J. Basic Eng. Mar, 94(1), 156-160.

100. Hsieh, D. Y., (1972). Interfacial stability with mass and heat transfer. Physics of Fluids 21,745–748.

101. Jeffreys, H., (1930). The instability of a compressible fluid heated below. In Mathematical Proceedings of the Cambridge Philosophical Society, 26(2), 170-172.

102. Jia, B. Q., Yang, L. J., Xie, L., Fu, Q. F., and Cui, X., (2019). Linear stability of confined swirling annular liquid layers in the presence of gas velocity oscillations with heat and mass transfer. International Journal of Heat and Mass Transfer, 138, 117-125.

103. Joseph, D. D.and Wang, J., (2004). The dissipation approximation and viscous potential flow. Journal of Fluid Mechanics, 505, 365-377.

104. Joseph, D. D., (2006). Potential flow of viscous fluids: Historical notes. International Journal of Multiphase Flow, 32(3), 285-310.

105. Joseph, D. D., and Liao, T. Y., (1994). Potential flows of viscous and viscoelastic fluids. Journal of Fluid Mechanics, 265, 1-23.

106. Joseph, D. D., Beavers, G. S., and Funada, T., (2002). Rayleigh-Taylor instability of viscoelastic drops at high Weber numbers. Journal of Fluid Mechanics, 453, 109-132.

107. Joseph, D. D., Belanger, J.and Beavers, G. S., (1999). Breakup of a liquid drop suddenly exposed to a high-speed airstream. International Journal of Multiphase Flow, 25(6-7), 1263-1303.

108. Joseph, D. D., Funada, T., and Wang, J., (2007). Potential Flows of Viscous and Viscoelastic Fluids. Cambridge University Press, Cambridge.

109. Joshi, A. S., Radhakrishna, M. C., and Rudraiah, N., (2011). Kelvin-Helmholtz instability in viscoelastic fluids in presence of electro-magnetic fields. Physics of Fluids, 23(9), 094107.

110. Kango, S. K., and Singh, V., (2012). Thermal Instability of Rivlin-Ericksen elastico-viscous rotating fluid in porous medium in hydromagnetics. Applications and Applied Mathematics: An International Journal (AAM), 7(1), 17.

111. Khan, A., and Bhatia, P. K., (2003). Stability of a finitely conducting compressible fluid through porous medium. Ganita Sandesh, 17(1), 35-42.

112. Khan, M. N., Nadeem, S., Ahmad, S.,and Saleem, A., (2021). Mathematical analysis of heat and mass transfer in a Maxwell fluid. Proceedings of the Institution of Mechanical Engineers, Part C: Journal of Mechanical Engineering Science, 235(20), 4967-4976.

113. Khan, S. U., Ali, N., and Abbas, Z., (2015). Hydromagnetic flow and heat transfer over a porous oscillating stretching surface in a viscoelastic fluid with porous medium. PloS one, 10(12), e0144299.

114. Khodaparast K. A., Kawaji M.and Antar B. N., (1994). The Rayleigh–Taylor and Kelvin–Helmholtz stability of a viscous liquid–vapor interface with heat and mass transfer. Phys Fluids 7, 359–364.

115. Kim, H. J., Kwon, S. J., Padrino, J. C., and Funada, T., (2008). Viscous potential flow analysis of capillary instability with heat and mass transfer. Journal of Physics A: Mathematical and Theoretical, 41(33), 335205.

116. Kim, M. C., Lee, S. B., Kim, S., and Chung, B. J., (2003). Thermal instability of viscoelastic fluids in porous media. International journal of heat and mass transfer, 46(26), 5065-5072.

117. Klainerman, S., and Majda, A., (1982). Compressible and incompressible fluids. Communications in Pure Applied Mathematics, 35, 629-651.

118. Kull, H. J., (1991). Theory of the Rayleigh-Taylor instability. Physics reports, 206(5), 197-325.

119. Kumar, H., (2011). Heat transfer with radiation and temperature dependent heat source in MHD free convection flow confined between two vertical wavy walls. Int J Appl Math Mech, 7(2), 77-103.

120. Kumar, P.and Lal, R., (2007). On the Stability of Two Superposed Viscous-Viscoelastic (Walters B′) Fluids. The American Society of Mechanical Engineers, Journal of Fluids Engineering 129, 116-119.

121. Kumar, P.and Mohan, H., (2013). Instability of Streaming Viscoelastic Fluids in the Presence of 'Effective Interfacial Tension'Through Porous Medium. Transport in porous media, 96(1), 193-202.

122. Kumar, P., (1999). Stability of two superposed viscoelastic (Walters B') fluid-particle mixtures in porous medium. Zeitschrift für Naturforschung A, 54(5), 343-347.

123. Kumar, P., (2000). Rayleigh-Taylor instability of Rivlin-Ericksen elastico-viscous fluids in presence of suspended particles through porous medium. Indian journal of pure & applied mathematics, 31(5), 533-539.

124. Kumar, P., (2000). Stability of superposed viscous-viscoelastic (Rivlin-Ericksen) fluids in the presence of suspended particles through a porous medium. Zeitschrift für angewandteMathematik und Physik ZAMP, 51(6), 912-921.

125. Kumar, P., (2001). Effect of rotation on thermal instability in Walters elastico-viscous fluid. Proceedings-national academy of sciences India section A, (1), 33-42.

126. Kumar, P., (2012). Thermosolutal magneto-rotatory convection in couple-stress fluid through porous medium. Journal of Applied Fluid Mechanics, 5, 45-52.

127. Kumar, P., and Singh, G. J., (2010). On the stability of two stratified Walters B'viscoelastic superposed fluids. Studia Geotechnica et Mechanica, 32(4), 29-38.

128. Kumar, P., Mohan, H., and Singh, G. J., (2006). Stability of two superposed viscoelastic fluid-particle mixtures. ZAMM-Journal of Applied Mathematics and Mechanics/Zeitschrift für AngewandteMathematik und Mechanik: Applied Mathematics and Mechanics, 86(1), 72-77.

129. Lagerstrom, P. A., Cole, J. D., and Trilling, L., (1949). Problems in the theory of viscous compressible fluids. Unnamed report, Guggenheim Aeronautical Laboratory, Purdue University.

130. Le, T. T.and Koch, T., (2021). Interface stability of compressible fluids in porous media. Physics of Fluids, 33(8), 084102.

131. Lee, D. S., (2002). Nonlinear Rayleigh instability of cylindrical flow with mass and heat transfer. Journal of Physics A: Mathematical and General, 36(2), 573.

132. Lee, D. S., (2002). Nonlinear stability in magnetic fluids of cylindrical interface with mass and heat transfer. The European Physical Journal B-Condensed Matter and Complex Systems, 28(4), 495-503.

133. Lee, W. K., and Flumerfelt, R. W., (1981). Instability of stationary and uniformly moving cylindrical fluid bodies-I. Newtonian systems. International Journal of Multiphase Flow, 7(4), 363-383.

134. Lees, L., (1962). The stability of the laminar boundary layer in a compressible fluid. Jotnal of fluid mechanics 12(4), 555-590.

135. Lessen, M., Fox, J. A., and Zien, H. M., (1965). On the inviscid stability of the laminar mixing of two parallel streams of a compressible fluid. Journal of Fluid Mechanics, 23(2), 355-367.

136. Lewis, D. J., (1950). The instability of liquid surfaces when accelerated in a direction perpendicular to their planes. II. Proceedings of the Royal Society of London. Series A. Mathematical and Physical Sciences, 202(1068), 81-96.

137. Lifschitz, A., and Hameiri, E., (1991). Local stability conditions in fluid dynamics. Physics of Fluids A: Fluid Dynamics, 3(11), 2644-2651.

138. Lin, F. H., Liu, C., and Zhang, P., (2005). On hydrodynamics of viscoelastic fluids. Communications on Pure and Applied Mathematics, 58(11), 1437-1471.

139. Liu, Z. S., Swaddiwudhipong, S., Cui, F. S., Hong, W., Suo, Z., and Zhang, Y. W.,(2011). Analytical solutions of polymeric gel structures under buckling and wrinkle. International Journal of Applied Mechanics, 3(02), 235-257.

140. Mack, L. M., (1987). Review of linear compressible stability theory. In Stability of time dependent and spatially varying flows. Springer, New York, 164-187.

141. Marshall, R. J., and Metzner, A. B., (1967). Flow of viscoelastic fluids through porous media. Industrial & Engineering Chemistry Fundamentals, 6(3), 393-400.

142. Megahed, A. M., and Reddy, M. G., (2021). Numerical treatment for MHD viscoelastic fluid flow with variable fluid properties and viscous dissipation. Indian Journal of Physics, 95(4), 673-679.

143. Melcher, J. R.,and Taylor, G. I., (1969). Electrohydrodynamics: A review of the role of interfacial shear stresses. Annual Review of Fluid Mechanics 1, 111–146.

144. Merkin, D. R., (2012). Introduction to the Theory of Stability (Vol. 24). Springer Science & Business Media.

145. Metzner, A. B., and Park, M. G., (1964). Turbulent flow characteristics of viscoelastic fluids. Journal of Fluid Mechanics, 20(2), 291-303.

146. Middleman, S., (1965). Stability of a viscoelastic jet. Chemical Engineering Science, 20(12), 1037-1040.

147. Mishra, S. R., Dash, G. C., and Acharya, M., (2013). Mass and heat transfer effect on MHD flow of a visco-elastic fluid through porous medium with oscillatory suction and heat source. International Journal of Heat and Mass Transfer, 57(2), 433-438.

148. Mitchner, M., and Landshoff, R. K. M., (1964). Rayleigh-Taylor Instability for Compressible Fluids. The Physics of Fluids, 7(6), 862-866.

149. Moatimid, G. M.and Hassan, M. A., (2012). Viscous potential flow of electrohydrodynamic Kelvin-Helmholtz instability through two porous layers with suction/injection effect. International Journal of Engineering Science, 54, 15-26.

150. Moatimid, G. M.and Hassan, M. A., (2018). Linear instability of water-oil electrohydrodynamic nanofluid layers: Analytical and numerical study. Journal of Computational and Theoretical Nanoscience, 15(5), 1495-1510.

151. Moatimid, G. M.,(2002). On the stability of two rigidly rotating magnetic fluid columns in zero gravity in the presence of mass and heat transfer. Journal of colloid and interface science, 250(1), 108-120.

152. Moatimid, G. M., Amer, M. F., and Mohamed, M. A., (2021). EHD azimuthal instability of two rigid-rotating columns with Marangoni effect in porous media. Indian Journal of Physics, 1-17.

153. Moatimid, G. M., and Amer, M. F., (2021). EHD instability of two rigid rotating dielectric columns in porous media. Pramana, 95(1), 1-13.

154. Moatimid, G. M., and El-Dib, Y. O., (1996). Kelvin-Helmholtz instability of miscible ferrofluids. International Journal of Theoretical Physics, 35(2), 425-443.

155. Moatimid, G. M., and Hassan, M. A., (2017). Convection instability of non-Newtonian Walter's nanofluid along a vertical layer. Journal of the Egyptian Mathematical Society, 25(2), 220-229.

156. Moatimid, G. M., and Zekry, M. H., (2020). Nonlinear stability of electro-visco-elastic Walters' B type in porous media. Microsystem Technologies, 26(6), 2013-2027.

157. Moatimid, G. M., Hassan, M. A.and Mohamed, M. A., (2020). Temporal instability of a confined nano-liquid film with the Marangoni convection effect: viscous potential theory. Microsystem Technologies, 26(6), 2123-2136.

158. Moatimid, G. M., Mostapha, D. R., and Zekry, M. H., (2021). Nonlinear EHD stability of cylindrical walter's B fluids: effect of an axial time periodic electric field. Chinese Journal of Physics, 74, 106-128.

159. Mohamed, A. E. A., Elhefnawy A. R. F.and MahmoudY. D., (1993). Nonlinear electrohydrodynamic Rayleigh-Taylor instability with mass and heat transfer: Effect of a tangential field. Physica A, 195, 74-92.

160. Mohamed, A. M. A., and El-Shehawey E. F., (1983). Nonlinear electrohydrodynamic Rayleigh-Taylor instability Part 1: A perpendicular electric field in the absence of surface charge. J. Fluid. Mech., 129, 475-494.

161. Morris, P. J., (1983). Viscous stability of compressible axisymmetric jets. Aiaa Journal, 21(4), 481-482.

162. Nadeem, S., Ahmad, S., and Khan, M. N., (2021). Mixed convection flow of hybrid nanoparticle along a Riga surface with Thomson and Troian slip condition. Journal of Thermal Analysis and Calorimetry, 143(3), 2099-2109.

163. Nasiri, A., Shariaty-Niasar, M., Rashidi, A., Amrollahi, A., and Khodafarin, R., (2011). Effect of dispersion method on thermal conductivity and stability of nanofluid. Experimental thermal and fluid science, 35(4), 717-723.

164. Nayak, A. R.and Chakraborty, B. B., (1984). Kelvin- Helmholtz stability with mass and heat transfer. The Physics of fluids, 27(8), 1937-1941.

165. Ogbonna, N.and Bhatia, P. K., (1984). The Rayleigh Taylor instability of superposed partially-ionized plasmas. Astrophysics and space science, 103(2), 233-240.

166. Oosthuizen, P. H.,and Carscallen, W. E., (1997). Compressible fluid flow (Vol. 179). New York: McGraw-Hill.

167. Ozen, O.and Narayanan, R., (2004). The physics of evaporative instability in bilayer systems: Weak non-linear theory. Physics of Fluids,16(12),4653-4660.

168. Ozen, O., and Narayanan, R., (2004). The physics of evaporative and convective instabilities in bilayer systems: Linear theory. Physics of Fluids, 16(12), 4644-4652.

169. Park, H. M.and Lee, H. S., (1995). Nonlinear hydrodynamic stability of viscoelastic fluids heated from below. Journal of non-newtonian fluid mechanics, 60(1), 1-26.

170. Piriz, A. R., Cortazar, O. D., and Lopez Cela, J. J., Tahir, N. A. (2006). The Rayleigh-Taylor instability. American journal of physics, 74(12), 1095-1098.

171. Plateau, (1873), "Statique experimentale et theorique des liquids omis aux seules forces moleculaire," 2, 231.

172. Plesset, M. S., (1954). On the stability of fluid flows with spherical symmetry. Journal of Applied Physics, 25(1), 96-98.

173. Raghavan, R., and Marsden, S. S., (1973). A theoretical study of the instability in the parallel flow of immiscible liquids in a porous medium. The Quarterly Journal of Mechanics and Applied Mathematics, 26(2), 205-216.

174. Rayleigh, L., (1879). On the capillary phenomena of jets. Proceedings of Royal Society of London, 29(196-199), 71-97.

175. Rayleigh, L., (1890). Scientific paper, Cambridge, U.P., Cambridge, Vol. II, 200-207.

176. Rayleigh, L., (1892). XVI. On the instability of a cylinder of viscous liquid under capillary force. The London, Edinburgh, and Dublin Philosophical Magazine and Journal of Science, 34(207), 145-154.

177. Reddy, G. M., Gowda, R. J. P., Kumar, R. N., Prasannakumara, B. C., and Kumar, G. K. (2021). Analysis of modified Fourier law and melting heat transfer in a flow involving carbon nanotubes. Proceedings of the Institution of Mechanical Engineers, Part E: Journal of Process Mechanical Engineering, 235(5), 1259-1268.

178. **Reddy, G. M., Manjula, J. and Padma, P.,** (2017). Mass transfer flow of MHD radiative tangent hyperbolic fluid over a cylinder: a numerical study. International Journal of Applied and Computational Mathematics, 3(1), 447-472.

179. **Reddy, M. G., Sudharani, M. V. V. N. L., Praveena, M. M., and Kumar, K. G.,** (2022). Effect of thermal conductivity on Blasius-Rayleigh-Stokes flow and heat transfer over a moving plate by considering magnetic dipole moment. The European Physical Journal Plus, 137(1), 1-13.

180. **Rezazadeh, G., Pashapour, M., and Abdolkarimzadeh, F.,** (2011). Mechanical behavior of a bilayer cantilever micro-beam subjected to electrostatic force, mechanical shock and thermal moment. International Journal of Applied Mechanics, 3(03), 543-561.

181. **Rivlin, R. S.and Ericksen, J. L.,** (1997). Stress-deformation relations for isotropic materials. Collected Papers of RS Rivlin, 911-1013.

182. **Rudraiah, N.and Chandrashekara, G.**, (2012). Effects of couple stress on the growth rate of Rayleigh-Taylor instability at the interface in a finite thickness couple stress fluid. Journal of Applied Fluid Mechanics, 3(1), 83-89.

183. **Saad, M. A.,** (1985). Compressible fluid flow. Englewood Cliffs.

184. **Saffman, P. G., and Taylor, G. I.,** (1958). The penetration of a fluid into a porous medium or Hele-Shaw cell containing a more viscous liquid. Proceedings of the Royal Society of London. Series A. Mathematical and Physical Sciences, 245(1242), 312-329.

185. **Saville, D. A.,** (1970). Electrohydrodynamic stability: fluid cylinders in longitudinal electric fields. The physics of fluids, 13(12), 2987-2994.

186. Sezer, N., Atieh, M. A.,and Koç, M., (2019). A comprehensive review on synthesis, stability, thermophysical properties, and characterization of nanofluids. Powder technology, 344, 404-431.

187. Sharma, R. C.and Chand, S., (1999). The instability of streaming Walters' viscoelastic fluid B′ in porous medium. Czechoslovak journal of physics, 49(2), 189-195.

188. Sharma, R. C.and Chand, S., (2000). Hall effect on thermal instability of Rivlin-Ericksen fluid. Indian Journal of Pure and Applied Mathematics, 31(1), 49- 60.

189. Sharma, R. C.and Kango, S. K., (1999). Thermal convection in Rivlin-Ericksen elastico-viscous fluid in porous medium in hydromagnetics. Czechoslovak Journal of Physics, 49(2), 197-203.

190. Sharma, R. C.and Kumar, P., (1996). Effect of rotation on thermal instability in Rivlin-Ericksen elastico- viscous fluid. ZeitschriftfrNaturforschung a, 51(7), 821-824.

191. Sharma, R. C.and Kumar, P., (1997). Hydromagnetic stability of two Rivlin-Ericksen elastico-viscous superposed conducting fluids. Zeitschrift für Naturforschung A, 52(6-7), 528-532.

192. Sharma, R. C.and Kumar, P., (1997). Study of the stability of two superposed Walters'(Model B′) visco-elastic liquids. Czechoslovak Journal of Physics, 47(2), 197.

193. Sharma, R. C.and Kumar, P., (1997). Thermal instability in Rivlin-Ericksen elastico-viscous fluids in hydromagnetics. Zeitschrift für Naturforschung A, 52(4), 369-371.

194. Sharma, R. C., (1977). Thermal instability in compressible fluids in the presence of rotation and magnetic field. Journal of Mathematical Analysis and Applications, 60(1), 227-235.

195. Sharma, R. C., Kumar, P., and Sharma, S., (2001). Rayleigh-Taylor instability of Rivlin-Ericksen elastico-viscous fluid through porous medium. Indian J. Phys B, 75, 337-340.

196. Sharma, V.and Gupta, U., (2006). Stability of stratified elastico-viscous Walters'(Model B') fluid in the presence of horizontal magnetic field and rotation in porous medium. Archives of Mechanics, 58(2), 187-197.

197. Sharma, V., Kishor, K.and Rana, G., (2001). The instability of streaming Rivlin-Ericksen fluids in porous medium. Studia Geotechnica et Mechanica, 23(3-4), 83-93.

198. Sharp, D. H., (1984). An overview of Rayleigh-Taylor instability. Physica D: Nonlinear Phenomena, 12(1-3), 3-18.

199. Shibata, Y., and Tanaka, K., (2003). On the steady flow of compressible viscous fluid and its stability with respect to initial disturbance. Journal of the Mathematical Society of Japan, 55(3), 797-826.

200. Shrivastava, R. K.and Singh, K. K., (1988). Drag on a sphere oscillating in a conducting dusty viscous fluid in presence of uniform magnetic field. Bulletin of the Calcutta Mathematical Society, 80(4), 286-291.

201. Shukla, A. K., Awasthi, M. K.and Asthana, R., (2021). Rayleigh-Taylor instability at viscous gas-viscoelastic fluid interface with heat and mass transfer. Materials Today: Proceedings, 46, 10217-10220.

202. Sirwah, M. A., (2007). Nonlinear Kelvin–Helmholtz instability of magnetized surface waves on a subsonic gas–viscous potential liquid interface. Physica A: Statistical Mechanics and its Applications, 375(2), 381-400.

203. Sirwah, M. A., (2008). Non-linear temporal dynamics of two-mode interactions of magnetized flow. International Journal of Non-Linear Mechanics, 43(5), 416-436.

204. Spiegel, E. A.and Veronis, G., (1960). On the Boussinesq approximation for a compressible fluid. The Astrophysical Journal, 131, 442.

205. Srivastava, R. K., and Singh, K. K., (1988). Unsteady flow of a dusty elastic-viscous Rivlin-Ericksen fluid through channels of different cross-sections in the presence of time-dependent pressure gradient. Bull. Cal. Math. Soc, 80, 286-308.

206. Talwar, S. P., (1959). Hydromagnetic stability of a conducting, inviscid, incompressible fluid of variable density. Zeitschrift fur Astrophysik, 47, 161.

207. Tauber, W., Unverdi, S. O., and Tryggvason, G., (2002). The nonlinear behavior of a sheared immiscible fluid interface. Physics of Fluids, 14(8), 2871-2885.

208. Taylor, G. I., (1950). The instability of liquid surfaces when accelerated in a direction perpendicular to their planes. I. Proceedings of the Royal Society of London. Series A. Mathematical and Physical Sciences, 201(1065), 192-196.

209. Taylor, G. I., (1964).Disintegration of water drops in an electric field. Proceedings of the Royal Society of London. Series A. Mathematical and Physical Sciences, 280(1382), 383-397.

210. Tiwari, D. K., Awasthi, M. K., and Agrawal, G. S., (2012). Study on electrohydrodynamic capillary instability of viscoelastic fluids in presence of axial electric field. International Journal of Applied Mechanics, 4(03), 1250027.

211. Tomotika, S., (1935). On the instability of a cylindrical thread of a viscous liquid surrounded by another viscous fluid. Proceedings of the Royal Society of London. Series A-Mathematical and Physical Sciences, 150(870), 322-337.

212. Turkyilmazoglu, M.and Gajjar, J. S. B., (2000). Direct spatial resonance in the laminar boundary layer due to a rotating-disk. Sadhana, 25(6), 601-617.

213. Turkyilmazoglu, M., (2005). Lower branch modes of the compressible boundary layer flow due to a rotating-disk. Studies in Applied Mathematics, 114(1), 17-43.

214. Turkyilmazoglu, M., Cole, J. W., and Gajjar, J. S. B., (2000). Absolute and convective instabilities in the compressible boundary layer on a rotating disk. Theoretical and Computational Fluid Dynamics, 14(1), 21-37.

215. Turkylmazoglu, M., and Ruban, A. I., (1999). The absolute instability of thin wakes in an incompressible/compressible fluid. Theoretical and computational fluid dynamics, 13(2), 91-114.

216. Ueno, I., Ando, J., Koiwa, Y., Saiki, T., and Kaneko, T., (2015). Interfacial instability of a condensing vapor bubble in a subcooled liquid. The European Physical Journal Special Topics, 224(2), 415-424.

217. Usha, R.and Sahu, K. C., (2019). Interfacial instability in pressure-driven core-annular pipe flow of a Newtonian and a Herschel–Bulkley fluid. Journal of Non-Newtonian Fluid Mechanics, 271, 104144.

218. Valli, A.and Zajaczkowski, W. M., (1986). Navier-Stokes equations for compressible fluids: global existence and qualitative properties of the solutions in the general case. Communications in mathematical physics, 103(2), 259-296.

219. Vasu, B., Prasad, V. R., Bég, O. A., Aziz, A., and Prashad, R. D., (2010). Numerical analysis of magnetohydrodynamic nonlinear convection heat and mass

transfer from a sphere in a non-Darcian variable-porosity medium. Int J Appl Math Mech, 6, 64-111.

220. **Vinningland, J. L., Toussaint, R., Niebling, M., Flekkoy, E. G., and Maloy, K. J.,** (2012). Family-Vicsek scaling of detachment fronts in granular Rayleigh-Taylor instabilities during sedimentatinggranular/fluid flows. The European Physical Journal Special Topics, 204(1), 27-40.

221. **Von Mises, R., Geiringer, H.and Ludford, G. S. S.,** (2004). Mathematical theory of compressible fluid flow. Courier Corporation.

222. **Walters, K.**, (1962). Non-Newtonian effects in some elastico-viscous liquids whose behaviour at small rates of shear is characterized by a general linear equation of state. The Quarterly Journal of Mechanics and Applied Mathematics, 15(1), 63-76.

223. **Walters, K.,** (1962). The solution of flow problems in the case of materials with memory. J. Mecanique, 1(4), 479-486.

224. **Wang, J., Joseph, D. D.and Funada, T.,** (2005). Pressure corrections for potential flow analysis of capillary instability of viscous fluids. Journal of Fluid Mechanics, 522, 383-394.

225. **Wang, J., Joseph, D. D., and Funada, T.,** (2005). Viscous contributions to the pressure for potential flow analysis of capillary instability of two viscous fluids. Physics of Fluids, 17(5), 052105.

226. **Wang, X. T., Ning, Z.and Lu, M.,** (2020). Temporal instability analysis of a confined non-Newtonian liquid jet with heat and mass transfer. European Journal of Mechanics-B/Fluids, 84, 350-356.

227. Weber, C., (1931). Zumzerfalleinesflüssigkeitsstrahles. ZAMM-Journal of Applied Mathematics and Mechanics/Zeitschrift für AngewandteMathematik und Mechanik, 11(2), 136-154.

228. Xia, W. F., Ahmad, S., Khan, M. N., Ahmad, H., Rehman, A., Baili, J.and Gia, T. N., (2022). Heat and mass transfer analysis of nonlinear mixed convective hybrid nanofluid flow with multiple slip boundary conditions. Case Studies in Thermal Engineering, 32, 101893.

229. Yadav, D., Agrawal, G. S.and Bhargava, R., (2012). The onset of convection in a binary nanofluid saturated porous layer. International Journal of Theoretical and Applied Multiscale Mechanics, 2(3), 198-224.

230. Yadav, D., Agrawal, G. S.and Bhargava, R., (2013). Onset of double-diffusive nanofluid convection in a layer of saturated porous medium with thermal conductivity and viscosity variation. Journal of Porous Media, 16(2).

231. Yadav, D., Agrawal, G. S., and Bhargava, R., (2011). Thermal instability of rotating nanofluid layer. International Journal of Engineering Science, 49(11), 1171-1184.

232. Yadav, D., Bhargava, R.and Agrawal, G. S., (2012). Boundary and internal heat source effects on the onset of Darcy–Brinkman convection in a porous layer saturated by nanofluid. International Journal of Thermal Sciences, 60, 244-254.

233. Yadav, D., Bhargava, R., and Agrawal, G. S., (2013). Numerical solution of a thermal instability problem in a rotating nanofluid layer. International Journal of Heat and Mass Transfer, 63, 313-322.

234. Yadav, D., Bhargava, R., and Agrawal, G. S., (2013). Thermal instability in a nanofluid layer with a vertical magnetic field. Journal of Engineering Mathematics, 80(1), 147-164.

235. Yerushalmi, J., Katz, S., and Shinnar, R., (1970). The stability of steady shear flows of some viscoelastic fluids. Chemical Engineering Science, 25(12), 1891-1902.

236. Yu, F., Chen, Y., Liang, X., Xu, J., Lee, C., Liang, Q., and Deng, T., (2017). Dispersion stability of thermal nanofluids. Progress in natural science: Materials International, 27(5), 531-542.

237. Yu, H., and Livescu, D., (2008). Rayleigh–Taylor instability in cylindrical geometry with compressible fluids. Physics of Fluids, 20(10), 104103.

238. Yu, W., and Xie, H., (2012). A review on nanofluids: preparation, stability mechanisms, and applications. Journal of nanomaterials, 2012.

239. Zhao, X., Koh, S. J. A., and Suo, Z., (2011). Nonequilibrium thermodynamics of dielectric elastomers. International journal of applied mechanics, 3(02), 203-217.

240. Zhao, Z., Wang, P., Liu, N.and Lu, X., (2020). Analytical model of nonlinear evolution of single-mode Rayleigh–Taylor instability in cylindrical geometry. Journal of Fluid Mechanics, 900.

241. Zhou, Y., (2017). Rayleigh-Taylor and Richtmyer-Meshkov instability induced flow, turbulence, and mixing. I. Physics Reports, 720, 1-136.

242. Zhou, Y., (2017). Rayleigh-Taylor and Richtmyer-Meshkov instability induced flow, turbulence, and mixing. II. Physics Reports, 723, 1-160.